Geotechnical Extreme Events Reconnaissance Association
www.geerassociation.org

GEOTECHNICAL ENGINEERING RECONNAISSANCE OF THE 30 NOVEMBER 2018 M7.0 ANCHORAGE, ALASKA EARTHQUAKE

Version 2.1

Editors: Kevin W. Franke and Rich D. Koehler
DOI: doi:10.18118/G6P07F

Geotechnical Extreme Events Association
GEER Report GEER-059
January 2, 2019

Geotechnical Engineering Reconnaissance of the 30 November 2018 Mw 7.1 Anchorage, Alaska Earthquake

Version 2.1

GEER Team Co-Leaders: Kevin W. Franke (BYU) and Richard Koehler (UNR)

Contributing Authors (in alphabetical order):
Fikret Atalay (Georgia Tech University)
Christine Z. Beyzaei (Exponent)
Ashly Cabas (North Carolina State University)
Sam Christie (COWI North America)
Stephen Dickenson (New Albion Geotechnical, Inc.)
Kevin W. Franke (Brigham Young University)
Richard Koehler (University of Nevada, Reno)
Nicole Hastings (Brigham Young University)
Ian Pierce (University of Nevada, Reno)
Armin Stuedlein (Oregon State University)
Xiang Wang (University of California San Diego)
Zhaohui (Joey) Yang (University of Alaska Anchorage)
Chen ZhiQiang (University of Missouri-Kansas City)

Other Contributors (in alphabetical order):
Bryce Berrett (Brigham Young University)
Stephanie Dow (University of Alaska Anchorage)
Michael Freeman (Brigham Young University)
Tara Hutchinson (University of California San Diego)
Shawn Herrington (University of Missouri-Kansas City)
Falko Kuester (University of California San Diego)
Kannon Lee (University of Alaska Anchorage)
Eric Lo (University of California San Diego)
Gabriel Pierce (University of Alaska Anchorage)
Prativa Sharma (University of Missouri-Kansas City)

Table of Contents

Acknowledgements

The work of the GEER Association is based in part on work supported by the National Science Foundation through the Geotechnical Engineering Program under Grant No. CMMI-1266418. Any opinions, findings, and conclusions or recommendations expressed in this material are those of the authors and do not necessarily reflect the views of the NSF. The GEER Association is made possible by the vision and support of the NSF Geotechnical Engineering Program Directors: Dr. Richard Fragaszy and the late Dr. Cliff Astill. GEER members also donate their time, talent, and resources to collect time-sensitive field observations of the effects of extreme events.

We acknowledge and thank the University of Alaska Anchorage (UAA) for providing meeting space to our team. We also acknowledge the valuable assistance from and collaboration with the following organizations and companies (in no particular order): Port of Alaska, Anchorage Water and Wastewater Utility, State of Alaska Department of Transportation & Public Facilities, Anchorage Department of Building Safety, Wasilla Department of Public Works, Matanuska-Susitna Department of Emergency Services, Golder & Associates, Professional & Technical Services (PTS) Inc., Shannon & Wilson, the U.S. Geological Survey, the U.S. National Institute of Standards and Technology, the Earthquake Engineering Research Institute, the Structural Extreme Events Reconnaissance Network, and the Anchorage Geotechnical Advisory Commission. We particularly thank the following individuals for the assistance they provided our team and the information/data they shared (in alphabetical order): Kate Allstadt (USGS), Jacques Annandale (AWWU), Kyle Brennan (Shannon & Wilson), Casey Cook (Mat-Su Borough Emergency Services), Alex Grant (USGS), Peter Haeussler (USGS), William Hammond (University of Nevada, Reno, Nevada Geodetic Laboratory), Youssef Hashash (University of Illinois, Champaign-Urbana), David Hemstreet (AK Department of Transportation), Jim Jager (Port of Alaska), Randall Jibson (USGS), Dean Karcz (Professional & Technical Services, Inc.), Steven Karcz (Professional & Technical Services, Inc.), Elmer Marx (AK Department of Transportation), Paul Morrison (Alaska Native Tribal Health Consortium), Ross Noffsinger (Anchorage Department of Building Safety), Stephen Nuss (AWWU), Barrett Salisbury (Alaska Division of Geological & Geophysical Surveys), Jonathan Stewart (University of California, Los Angeles), Eric Thompson (USGS), John Thornley (Golder & Associates), Sharen Walsh (Port of Anchorage), Rob Witter (USGS), and Paolo Zimmaro (University of California, Los Angeles).

We acknowledge the time and consideration of the numerous residents of Anchorage and the surrounding communities. Your first-hand experiences and observations greatly improved our understanding of this event and added valuable perspective. Finally, we are grateful for constructive reviews by John Stewart of University of California, Los Angeles.

Executive Summary

A M7.1 earthquake occurred at 08:29 AM local time on November 30, 2018 at an epicentral distance of about 41.6 km to downtown Anchorage, Alaska (epicenter; Lat/Long: 61.346°, -149.955°). The intraslab event occurred due to normal faulting within the subducting Pacific plate at an approximate hypocentral depth of 40 kilometers beneath the ground surface. The initial release of ground motion data included records from 25 functional ground motion instrument stations which had recorded the earthquake. Most of these stations recorded peak ground accelerations (PGA) between 0.2 g and 0.3 g, with two isolated stations showing recorded PGA values greater than 0.5 g in the central and southeastern vicinities of Anchorage.

Between the dates of December 8 through 15, 2018, the Geotechnical Extreme Events Reconnaissance Association (GEER) deployed a multi-disciplinary Phase I team comprised of seven investigators to observe and document the significant geotechnical engineering impacts and lessons learned from this event. The GEER team collaborated closely with other engineering reconnaissance efforts including those led by the Earthquake Engineering Research Institute (EERI), the Structural Extreme Events Reconnaissance Association (StEER), the U.S. Geological Survey (USGS), and the Alaska Division of Geological & Geophysical Surveys (DGGS). The GEER team also benefited greatly from coordination and partnerships with the local geotechnical engineering community and the Municipality of Anchorage (MOA) Geotechnical Advisory Commission (GAC), state department of transportation engineers, Anchorage building officials and engineering service managers, municipal public works officials, National Institute of Standards and Technology (NIST) and Federal Emergency Management Agency (FEMA) officials, and various municipal emergency response coordinators. GEER deployed a Phase II team focused on remote sensing and geophysical data collection in spring 2019 (post snowmelt).

No fatalities were reported following the November 30 Anchorage earthquake, and initial damage assessments suggest that most infrastructure damage was non-structural. Nearly all significant embankment slope failures along highways and major arterials were repaired by the State of Alaska Department of Transportation & Public Facilities (AK DOT&PF) within one week of the event. In addition, deep intraslab earthquakes like those of the November 30 Anchorage event have historically produced smaller ground motion intensities and relatively insignificant infrastructure damage in developed regions of the world. However, despite these favorable observations and outcomes, the November 30 Anchorage earthquake should not be disregarded or classified as an insignificant event. The November 30 Anchorage earthquake is significant to the engineering community for the following reasons:

1. The November 30 Anchorage earthquake is one of the largest magnitude earthquakes to strike near a major U.S. city since the 1994 Northridge earthquake.
2. A significant number of co-seismic landslides and liquefaction ground failures have already occurred in Anchorage in recent history, most notably during the 1964 M9.2 Good Friday earthquake.
3. The Anchorage area currently has a relatively dense network of ground motion recording stations, including instrumented structures and deep vertical arrays.

4. Numerous challenging soil conditions exist in the region including relatively sensitive clays, liquefiable soils, soft organic soils, and a seasonally frozen crust that is 15-50 cm thick.
5. The November 30 Anchorage earthquake provides the opportunity to assess the effectiveness of seismic provisions in modern building code; the Municipality of Anchorage currently adopts and enforces the 2012 International Building Code (IBC).
6. Various types of geotechnical site improvements (e.g., deep soil mixing, deep dynamic compaction, and excavation and replacement) have been implemented across Anchorage over the past 50 years, allowing us to observe and document the seismic performance of these types of ground improvements.

Based on the observations from the GEER Phase I team and its collaborators, many significant lessons can be learned from the November 30 Anchorage earthquake, including:

1. In general, the earthquake generated ground motions below the current Anchorage design level. Only three instances of structural collapse were observed by the GEER Phase I team. This observation suggests that modern building code, when implemented properly, is generally effective in preventing structural collapse for ground motions equal to or less than the design ground motion.
2. It seems that the duration of strong shaking from the M7.1 event was not long enough to initiate substantial movements on the majority of the historic landslides from the 1964 M9.2 earthquake, including the slides at the Turnagain Heights and 4th Avenue. However, liquefaction appeared to have contributed to re-mobilization of the 1964 Potter Hill (Rabbit Creek) landslide. Investigators from the USGS were able to observe very small cracks forming at the head of the historic slides at the Turnagain Heights (no cracks were observed at the 4th Avenue slide) prior to the arrival of the GEER team and the substantial snowfall that occurred during the week of December 8. However, these cracks are believed to have developed in response to the ground oscillation from the November 30 event and are not believed to indicate a reactivation of the slides.
3. Although the Port of Alaska experienced some damage to its administration building, terminals, and experienced isolated instances of ground failure, the damage was limited in impact and Port operations were delayed for only a short period of time. Efforts to counter significant corrosion of terminal-supporting piles and fenders appeared to provide significant benefit during the earthquake.
4. While the majority of the damage that was observed in Anchorage and in the surrounding communities appeared to be non-structural, the isolated cases of structural damage that were observed by the GEER team appeared to be caused by geotechnical issues, particularly settlement of the foundation and/or slope deformations. Such cases of structural damage were also more commonly observed in residential structures and small commercial structures. Larger commercial or industrial structures generally performed well in the November 30 event.
5. Structural damage related to ground deformation and significant embankment deformations appeared to occur most frequently in areas where significant amounts of organic soils are located (e.g., swampy areas or peat bogs), or in areas of sloping ground.

6. While isolated instances of soil liquefaction were observed and confirmed by the GEER team within Anchorage, it was difficult to confirm liquefaction as the cause of observed ground deformations at many sites because of the snow cap covering the ground surface. Bearing capacity issues in organic soils produced damage similar to that observed with soil liquefaction. Phase II investigations conducted in the Spring 2019 (Appendix B) identified liquefied sand in a few locations.
7. While evidences of soil liquefaction including cracks, small sand boils, and significant settlements were observed within the footprint of several residential and small commercial structures, few if any of these evidences were observed in the free-field near these structures. Additionally, the majority of these observations occurred in swampy areas such as the Sand Lake or Jewel Lake neighborhoods of Anchorage. Given the common practice of over-excavation in organic soils and replacement with sand fill in these types of areas in Anchorage, it appears that soil liquefaction in improperly placed or insufficiently compacted granular fills may have contributed to the observed structural settlements.
8. Considering the structural settlements and slope deformations that were observed by the GEER team, the vast majority of these involved anthropogenic fills. In some cases (e.g., Vine Road embankment failure), the deformations occurred due to loss of shear strength in the underlying bearing soils. In other cases, it is not yet clear whether the deformations occurred within the fills themselves or in the underlying bearing soils.
9. The GEER team visited several sites in Anchorage with soil ground improvement, and all were observed to have performed well during the November 30 earthquake. However, it is important to note that many more sites without soil ground improvement were visited and were observed to also perform well.
10. In terms of resiliency, the combined local, state, and federal engineering response to the November 30 Anchorage earthquake is commendable. The GEER team deployed to Anchorage within eight days of the event. However, within the eight-day span between the earthquake and our team's arrival, all major highway embankment deformations had been repaired, utility services had been restored to nearly all customers, all highway and road bridges had been inspected, and structural repairs to many residences were already underway.

This Version 2.0 report expands on the Version 1.0 report. Principal findings have not changed from the Version 1.0 report, but additional information is presented here for several of the sites that were investigated by the Phase I team. A Phase II reconnaissance team was deployed to Anchorage in late April/early May 2019 for the specific purpose of collecting preliminary remote sensing and geophysical data immediately following snowmelt. A summary of the Phase II data is contained in Appendix B. All data and derivative models from the Phase II investigation are available to the public via NHERI DesignSafe at: https://www.designsafe-ci.org/data/browser/public/designsafe.storage.published//PRJ-2336/Phase2.

1.0 Introduction

The moment magnitude 7.1 (M7.1) Anchorage earthquake occurred on 30 November 2018 at 08:29 AM local time and caused widespread power outages, structural and non-structural damage to buildings, damage to roadways and railways, and closure of schools and businesses. The earthquake initiated below the southern Susitna lowlands (Lat/Long: 61.346°, -149.955°) approximately 11.3 kilometers north of downtown Anchorage at a hypocentral depth of 40 kilometers (Figure 1-1).

The earthquake was located within the subducting Pacific Plate and was the result of normal faulting along a north-south striking, moderately dipping, intraslab fault plane. This type of earthquake is common in the region and is similar to the M7.1 Iniskin earthquake that occurred in 2016. Although these types of deep, intraslab earthquakes are commonly associated with minor structural damage, the close proximity of the November 30 event to the Anchorage metropolitan area resulted in more severe damage that affected the City of Anchorage and the nearby communities of Wasilla, Houston, Palmer, and Eagle River. Despite significant impacts to infrastructure, loss of life did not occur.

The NSF-funded Geotechnical Extreme Events Reconnaissance (GEER) Association mobilized a multidisciplinary team to the affected region from 8 to 15 December 2018. Our team was comprised of seven experts in the fields of liquefaction, slope stability, geotechnical engineering, ground improvement, ground motions, and earthquake geology. Our team included co-leaders Kevin Franke (Brigham Young University) and Rich Koehler (University of Nevada, Reno), as well as members Armin Stuedlein (Oregon State University), Ian Pierce (University of Nevada, Reno), Ashly Cabas (North Carolina University), Zhaohui (Joey) Yang (University of Alaska Anchorage), and Christine (Zee) Beyzaei (Exponent, Oakland). Team members Sam Christie (COWI North America) and Stephen Dickenson (New Albion Geotechnical, Inc.) joined the team following the field reconnaissance to contribute specifically to the description of damage at the Port of Alaska due to their institutional knowledge. The team worked in close collaboration with local geotechnical engineering consultants, the Municipality of Anchorage Geotechnical Advisory Commission, students and researchers from the University of Alaska Anchorage, and the U.S. Geological Survey. The main objectives of the GEER team were to identify, observe, and document perishable data and assess general patterns of damage to better understand earthquake effects. This type of information is important for improving engineering design, informing future planning efforts, and reducing society's exposure to seismic risk. The 8 to 15 December GEER deployment has been classified as a Phase I deployment. A second GEER deployment (Phase II) focusing on remote sensing and geophysical data collection occurred in late April/early May 2019 (after the snowmelt), and included Rich Koehler (University of Nevada, Reno), ZhiQuang Chen (University of Missouri, Kansas City), Xiang Wang (post-doc at University of California, San Diego), Zhaohui (Joey) Yang (University of Alaska, Anchorage), Fikret Atalay (student at Georgia Tech), Nicole Hastings (student at Brigham Young University), and Bryce Berrett (student at Brigham Young University). All efforts and data collected by the Phase II team are reported in Appendix B.

The approach employed by the Phase I team was to inspect and document damage throughout the affected area using a combination of on-ground site mapping and aerial reconnaissance with state-of-science geomatics technology and photogrammetry. The combination of techniques resulted in a thorough characterization of damage and provided baseline data for innovative future research.

1.1. Summary of Earthquake

The M7.1 earthquake began at a hypocentral depth of about 40 kilometers and was associated with a moment release of 4.71e+19 N-m. Very strong shaking intensities (MMI VII) were experienced in the greater Anchorage, Eagle River, Wasilla, and Palmer areas with moderate to strong shaking intensities (MMI V-VI) felt throughout the Susitna Basin and northwestern Kenai Peninsula (Figure 1-1A). Assessment of aftershocks by the Alaska Earthquake Center (AEC) indicates that the rupture began in the subducting Pacific plate and ruptured upward and towards the north along a plane ~25-35 kilometers in length (Figure 1-1B). As of mid-March 2019, the AEC has reported over 9,000 aftershocks with about 40 events of magnitudes M>4.0 and the largest aftershock of M=5.7 (Figure 1-2). Analyses of the geodetic time series models for all the 24 hour sample rate solutions before and after the earthquake by the Nevada Geodetic Laboratory (NGL) using the GPS data processing framework of Blewitt et al. (2018) indicate north-south contraction and coseismic E-SE oriented horizontal displacements of about 2 cm in Anchorage (Figure 1-1C). The measured displacements extend farther towards the east, suggesting that the slip occurred on the shallower, down to the east nodal plane observed in the seismic data (William Hammond, NGL, pers. comm.). Thus, the available data suggests that the earthquake is best characterized as an intraplate normal faulting event.

1.2. Immediate Response and Preliminary Reconnaissance Efforts

The earthquake occurred in the early morning hours of November 30th (8:29 AM local time) as most of the region was beginning their daily routine and resulted in the immediate closure of many businesses and schools. Widespread power outages, water line shut-offs, and traffic congestion were some of the immediate impacts across the region in the hours after the event as residents tried to contact family and friends and make their way home to assess damages. Information of more severe damage to roadways and buildings began rapidly circulating throughout the area on social media and news outlets, prompting the USGS and DGGS to mobilize helicopter and ground surveys to evaluate the extent and severity of damage and evaluate geologic effects. The DGGS effort was primarily focused on assessing impacts to the Glenn Highway between Anchorage and Wasilla and the Seward Highway south of Anchorage. In addition to assessing impacts around population centers, the USGS documented extensive geologic effects in the surrounding areas including liquefaction and ground cracking at the mouth of the Little Susitna River and along the tidal flats of Knik Arm. Multiple types of mass failures along the Port Mackenzie Bluffs, the Eklutna and Eagle River valleys, and the bluffs along Turnagain Arm were also identified (Figure 1-3). New ground failure probability and landslide hazard maps were field-calibrated by the USGS (Thompson et al., 2019). These initial surveys proved invaluable to our team as snowfall began to cover evidence of ground deformation in the days immediately following the event. Upon arrival, our team was briefed by the USGS and DGGS, and we utilized their GPS locations and photographs of observed landslides and liquefaction phenomena to inform our field reconnaissance. A map showing the locations visited by the GEER team during the Phase I investigation is presented in Figure 1-4.

In addition to the USGS and DGGS, valuable preliminary information regarding post-earthquake damage assessment and site locations was obtained through collaboration and coordination with several organizations and groups (Figure 1-5). For example, our team communicated regularly with reconnaissance teams from EERI and StEER, participating in regular information sharing and coordination meetings organized by EERI. Local geotechnical engineering groups including the MOA GAC also met with and briefed our team on information they had obtained following the earthquake. Engineers from AK DOT&PF met with our team and educated us on the status of transportation infrastructure in the region. Our team was also referred to MOA building safety officials and public works officials/engineers, who subsequently collaborated with us and provided much valuable information regarding the distribution, type, and frequency of reported infrastructure damage. Based on the observations and recommendations from these local professionals, our team developed a list of priority sites to investigate during our deployment. This list of priority sites evolved during the week of our deployment as additional information was collected by us and our collaborators.

1.3. Remote Sensing Methods with Unmanned Aerial Vehicles

Two commercial off-the-shelf (COTS) UAV platforms were used in the Anchorage Phase I reconnaissance. We used the DJI™ Mavic 2 Pro quadrotor platform. The Mavic 2 Pro is equipped with a 4K video camera that has a 1” CMOS sensor, 77-degree field of view, 20 MB images, and a focal length of infinity. The platform weighs 907 grams, has a maximum flight time of 31 minutes (26 minutes typical), and offers the ability to hover and/or collect imagery from vertical faces such as steep rock cliffs or buildings. We also used a DJI™ Phantom 4 Pro quadrotor platform. The Phantom 4 is equipped with a 4K video camera that has a 1/2.3” CMOS sensor, 94-degree field of view, 12.4 MP images, and a focal length of infinity. The platform weighs 1.38 kg, has a maximum flight time of 28 minutes (19 minutes typical).

<u>Structure from Motion Photogrammetry Software</u>

One of the most common forms of UAV-based remote sensing involves the use of lightweight optical sensors and a computer vision technique called Structure from Motion (SfM) (Marr and Nishihara 1978; Snavely et al. 2008). For this particular study, the commercial SfM software program *ContextCapture* by Bentley Systems, Inc. was used.

The traditional workflow of these and most other commercial and open source SfM platforms includes:

- Tie Point Extraction – This step usually incorporates the SIFT (Scale Invariant Feature Transform) algorithms developed by Lowe (Lowe, 2004) or one of its variants to extract from each image a large number of homologous points (i.e., the sparse point cloud).

- Camera Orientation and Calibration – Using camera internal parameters (e.g., focal length, principal point, and distortions), the sparse point cloud is orientated in a local coordinate system (usually connected to the starting reference image) with a relative scale and asset.
- Bundle Block Adjustment – An adjustment is performed to the sparse point cloud to minimize location error. This is usually performed with the Levenberg-Marquardt (LM) method, which is an iterative technique that locates a local minimum of a multivariate function expressed as the sum of squares of several non-linear, real-valued functions.
- Dense Point Cloud Generation – Once the sparse point cloud has been developed, dense point cloud generation is initiated using the sparse point cloud as a “lattice” for the dense cloud. The techniques and algorithms used to develop the dense point cloud vary. However, most of these techniques and algorithms incorporate some variant of the Semi Global Matching approach proposed by Hirschmüller (2005; 2008).
- Output Development – The final 3D dense point cloud enables the development of products such as a DSM (Digital Surface Model), DEM, Orthophoto, and 3D mesh textured model.

For the Phase I field work, no ground control points or check points were surveyed because the Phantom 4 Pro UAV was using an onboard post-processing geo-location correction system (i.e., PPK). Unfortunately, the PPK system was malfunctioning in the field, possibly due to the cold temperatures. Therefore, models of sites from the Phase I reconnaissance generally have relatively poor accuracies, with horizontal and vertical 3D model accuracies of 1.3 meters or better based on our comparisons with limited field measurements. Improved models were developed as part of the Phase II reconnaissance (Appendix B).

Resulting 3D Models and Orthophotos

All 3D mesh textured models developed from *ContextCapture* can be viewed and explored online with any standard Internet browser using the free *Acute3D Web Viewer* add-in by Bentley Systems, Inc., which allows for basic retrieval of latitude, longitude, and elevation information from the model, as well as basic linear measurement between two points. All models developed from the Phase I reconnaissance mission can currently be accessed on the Internet at: http://prismweb.groups.et.byu.net/gallery2/alaska-2018/. These models have been uploaded and shared with the public on NHERI DesignSafe at: https://www.designsafe-ci.org/data/browser/public/designsafe.storage.published//PRJ-2336/Phase1.

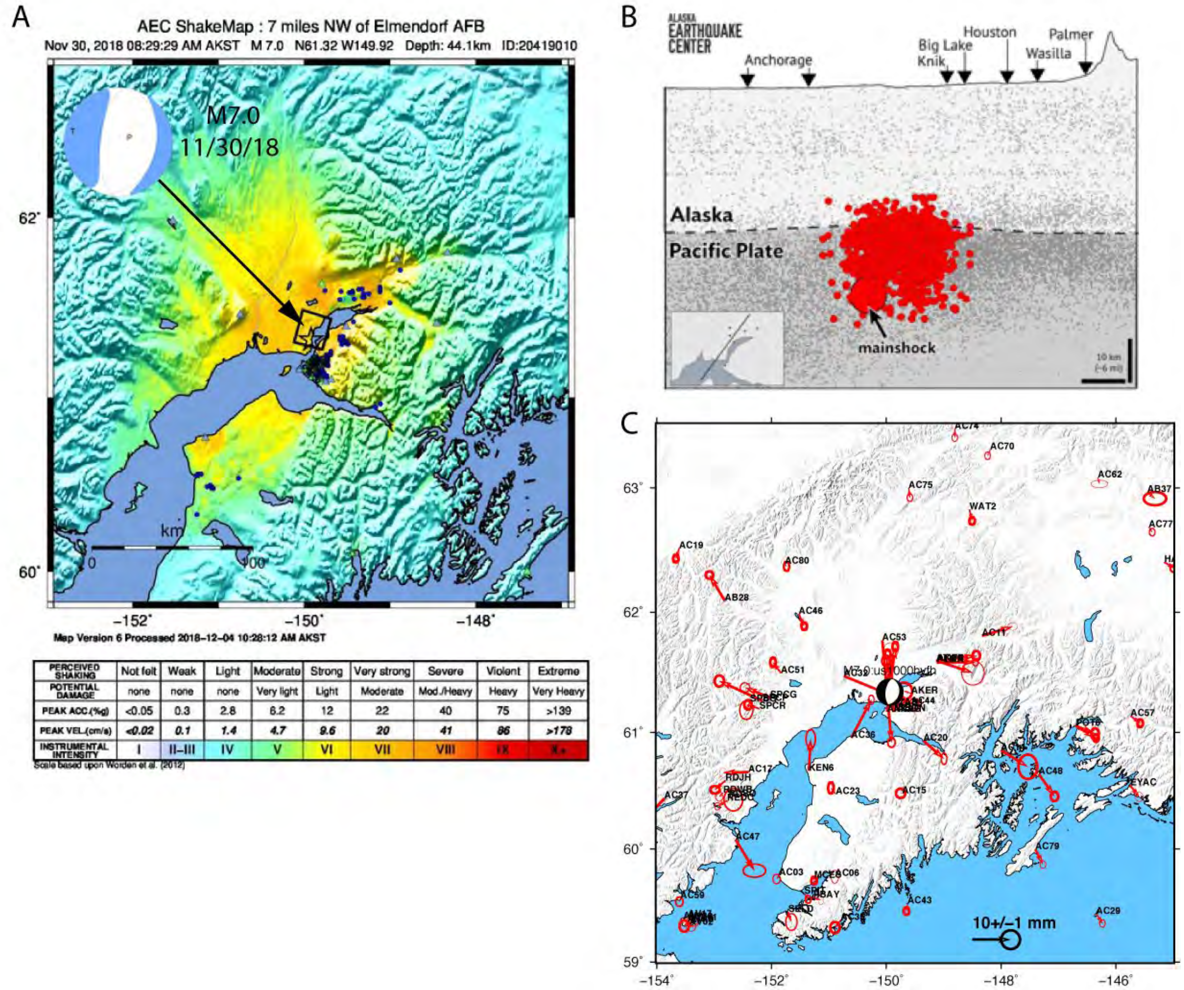

Figure 1-1. (A) Location of the epicenter, focal mechanism, and shaking intensities in the affected area (source: USGS), (B) a cross section of the epicenter and distribution of aftershocks (source: Alaska Earthquake Center), and (C) Assessment of geodetic displacement vectors provided by William Hammond of the Nevada Geodetic Laboratory.

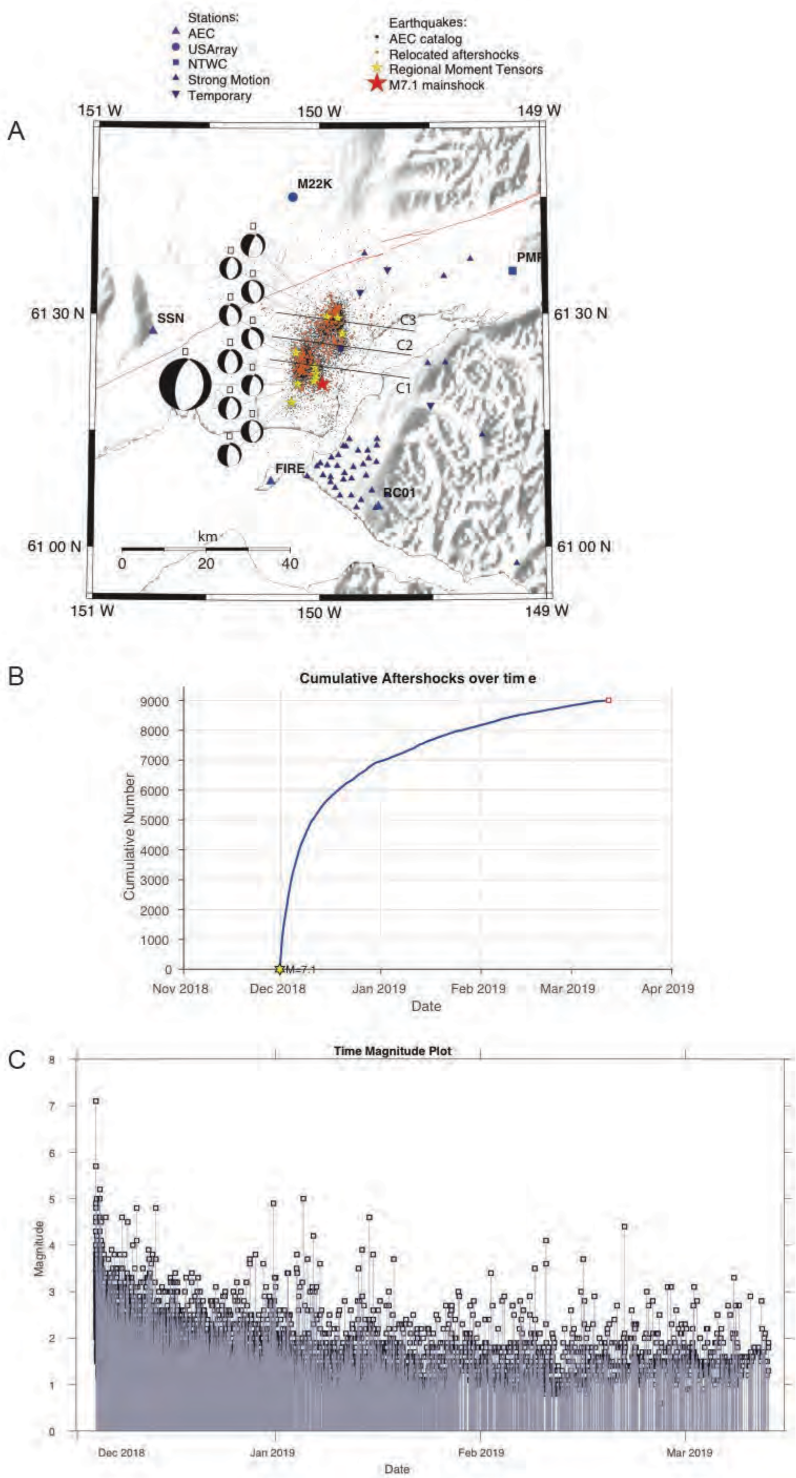

Figure 1-2. (A) Map of the epicentral region showing seismic stations, aftershock locations, and source mechanisms. (B) Cumulative number of aftershocks reported as of March 12, 2019. (C) Time magnitude plot of recorded aftershocks reported as of March 12, 2019. Images from West et al. (in prep.).

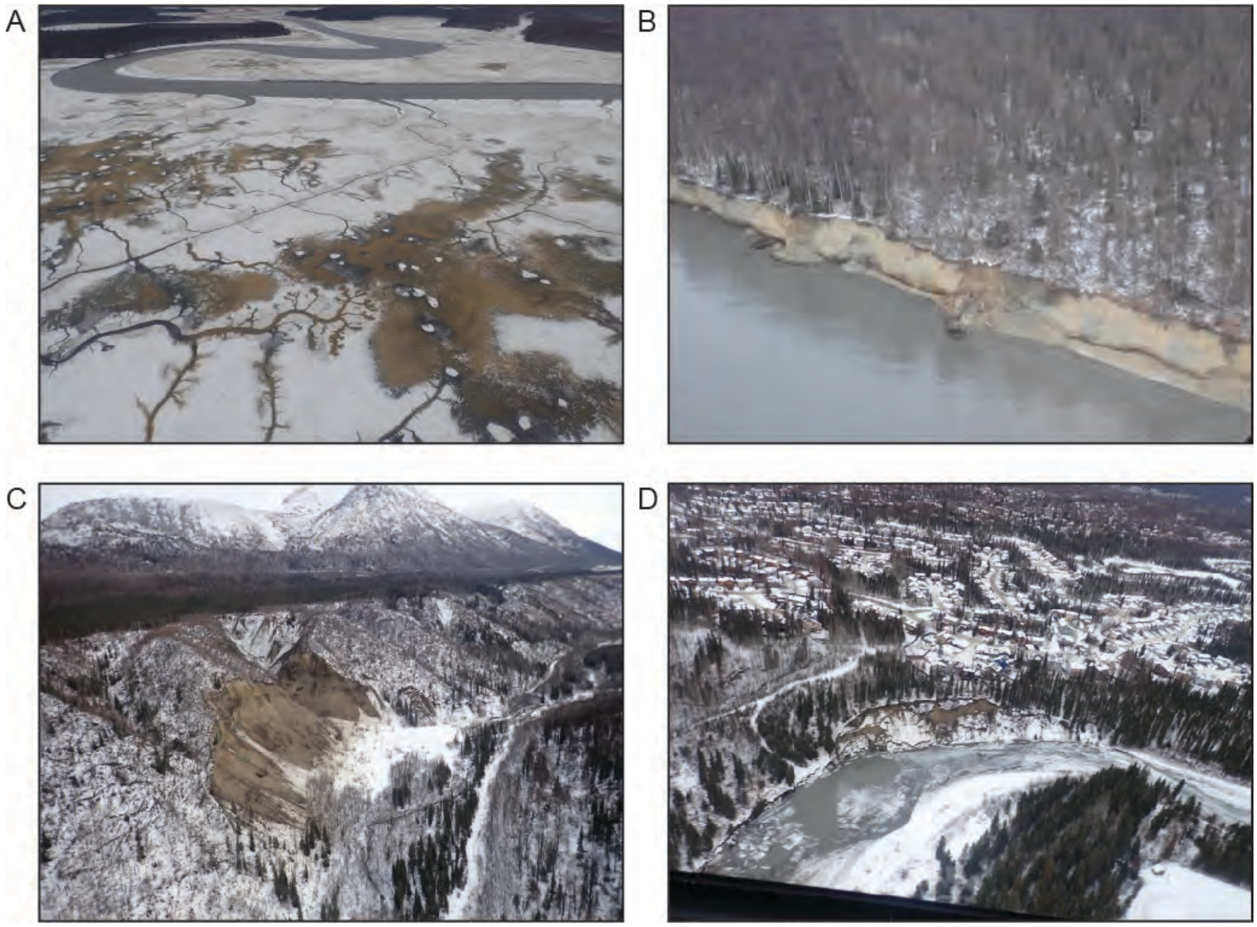

Figure 1-3. (A) Extensive liquefaction and ground cracking along the Little Susitna River floodplain (Lat/Long: 61.2792°, -150.3250°). (B) Mass failures along the Port Mackenzie Bluffs (Lat/Long: 61.4141°, -149.7978°). (C) Mass failure within the Eklutna River valley (Lat/Long: 61.4161°, -149.2062°). (D) Bluff failure along Eagle River (Lat/Long: 61.2972°, -149.5320°). Photos courtesy of Rob Witter.

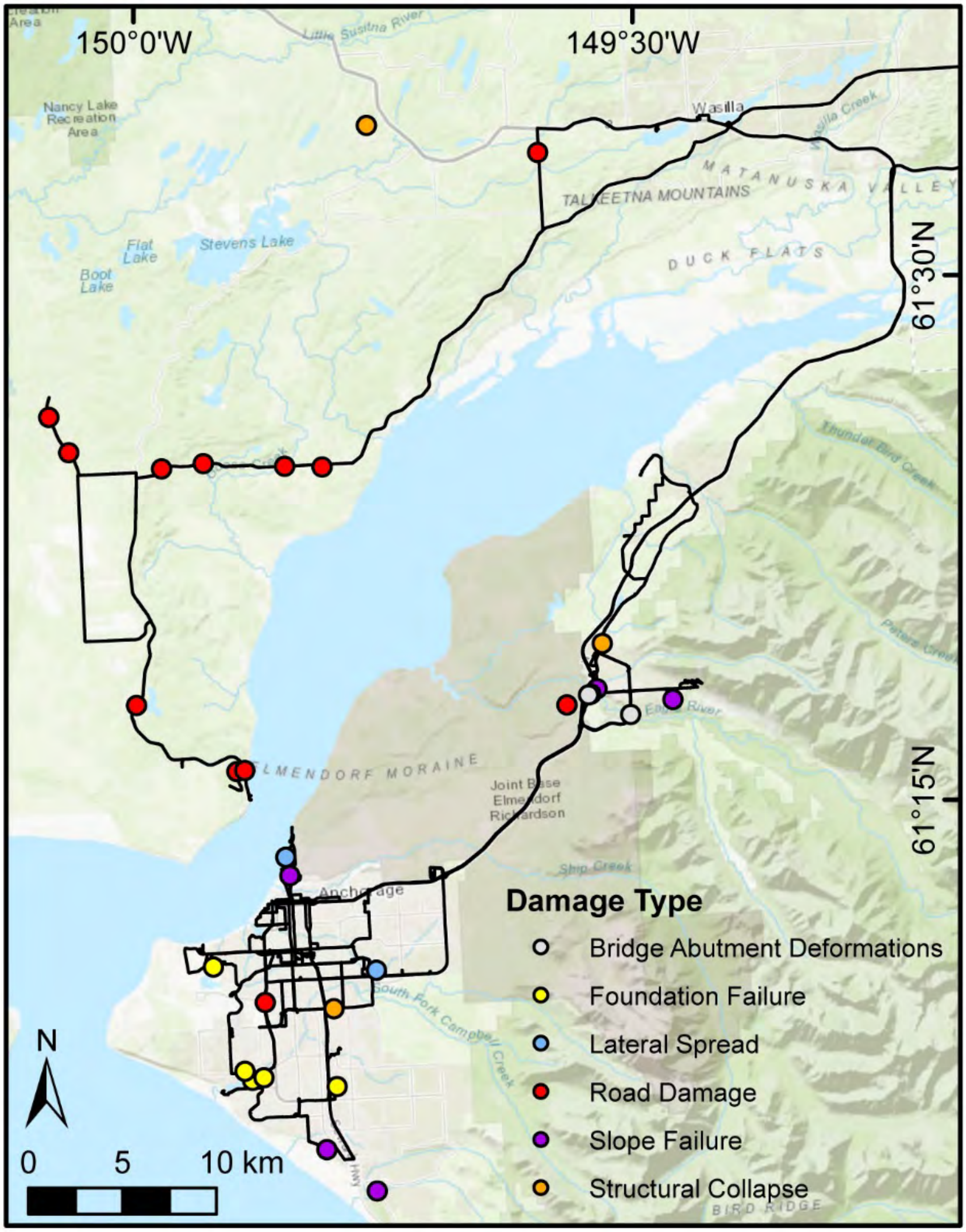

Figure 1-4. Map showing track lines (black) and locations of damage inspected by the GEER team (colored dots).

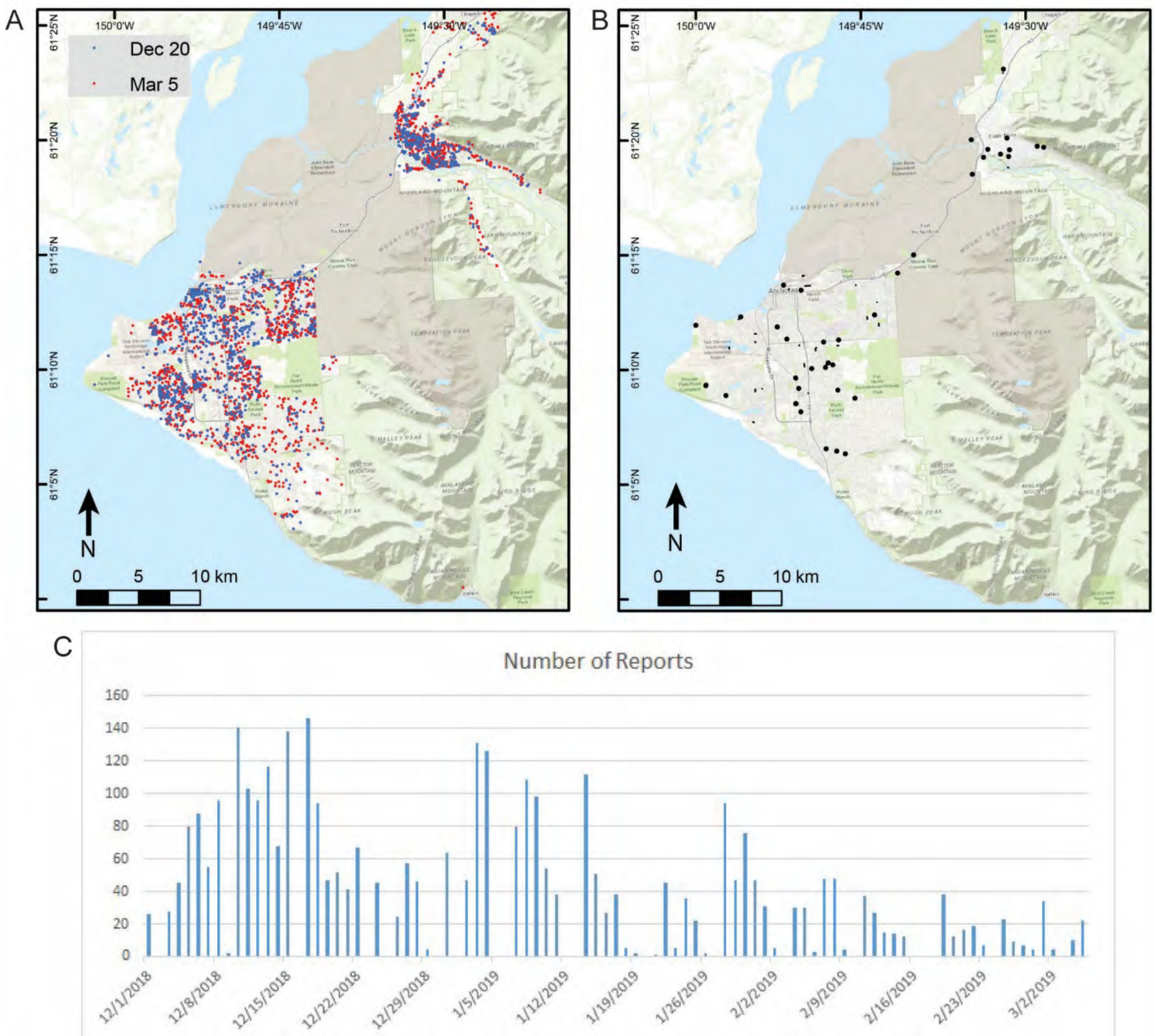

Figure 1-5. Maps of locations of reported damage in the vicinity of Anchorage including (A) damage reported by December 20, 2018 (blue dots) and damage reported by March 5, 2019 and (B) damage to Anchorage Water and Wastewater Utilities infrastructure. (C) Reported instances of damage through time. The total number of damage reports was 3,573 as of March 5, 2019. Damage distribution information provided by Casey Cook, Mat-Su Borough emergency manager, Ross Noffsinger, acting building official, Municipality of Anchorage, and Jacques Annandale, Anchorage Water and Wastewater Utilities.

2.0 Regional Tectonics, Seismicity, and the 1964 Great Alaska Earthquake

Tectonic deformation in south-central Alaska is driven by subduction of the Pacific Plate beneath the North American plate along the Alaska-Aleutian subduction zone (Figure 2-1) and has created the rugged Chugach Mountains and the Cook Inlet forearc basin. Seismicity includes events in the shallow crust, intermediate and deep interplate events along the shallowly dipping subduction interface, and intraplate events that represent internal deformation of the subducting Pacific Plate. Shallow crustal sources include fault-cored folds in upper Cook Inlet and the Castle Mountain fault which extends across the Susitna lowland north of Anchorage. Many earthquakes originating within the Pacific Plate are felt in Anchorage every year. Significant events include the 2016 (M7.1) Iniskin earthquake and the 2014 (M6.3), 1999 (M5.2), and 1991 (M6.3) events.

The Alaska-Aleutian subduction zone was the source of the 1964 M9.2 Great Alaska earthquake, which ruptured over 500 miles of the plate interface and was associated with up to 82 feet of horizontal displacement. The 1964 earthquake caused major ground shaking and landslide damage in Anchorage and generated a destructive tsunami that devastated coastal communities in Prince William Sound. Similar events are thought to have occurred nine times in the last 5,000 years with recurrence intervals ranging between 333 and 875 years (Carver and Plafker, 2008). Although a repeat of a M>9 1964-type rupture is not likely in the near future, the subduction zone is capable of generating frequent M>8 events.

The 1964 Great Alaska earthquake occurred along the Alaska-Aleutian subduction zone at 5:36 PM local time, Friday, March 27, 1964 with a magnitude of M9.2, the second largest earthquake ever recorded. The amplitude ground motions were greatest in areas of saturated, unconsolidated deposits, the duration of strong shaking exceeded 4 minutes, and widespread damage occurred throughout an area of about 50,000 square miles in south-central Alaska (Plafker, 1969). Vertical ground displacements on the seafloor generated a destructive tsunami that caused casualties and damage throughout Prince William Sound and Kodiak Island, and effected coastal communities as far away as California.

Although Anchorage is located over 120 km northwest of the epicenter from the 1964 event, strong ground motions destroyed many buildings and damaged nearly all multistory buildings. Considerable damage in Anchorage resulted from ground cracking, liquefaction-induced lateral spread displacement, and differential settlement in alluvium and artificial fills (Hansen et al., 1966). Lateral spread displacement of marine silts along the coastal bluffs resulted in the failure of the Turnagain Heights neighborhood, which extends over one square kilometer, destroying 75 homes.

The scientific importance of the 1964 earthquake is eloquently summarized by West et al. (2014): “Advances in earthquake geology related to the investigations of the event include validation of the theory of plate tectonics, increased understanding of earthquake rupture mechanics and fault geometry, understanding of tsunami source mechanisms, and recognition of the types of secondary earthquake processes that affect the built environment. The effects and lessons learned from the 1964 earthquake have contributed to the development of building codes in

Anchorage that exceed the Uniform Building Code, establishment of advisory commissions on geologic hazards, and development of seismic monitoring and warning systems."

Damage from the November 30, 2018 earthquake, although less severe than was experienced in 1964, followed similar patterns in terms of the types and locations of ground failures and the type of infrastructure impacted. Thus, although the non-trivial economic and societal impacts of the 2018 earthquake are still being evaluated, community awareness, preparedness, and planning contributed to the resilience of the affected area.

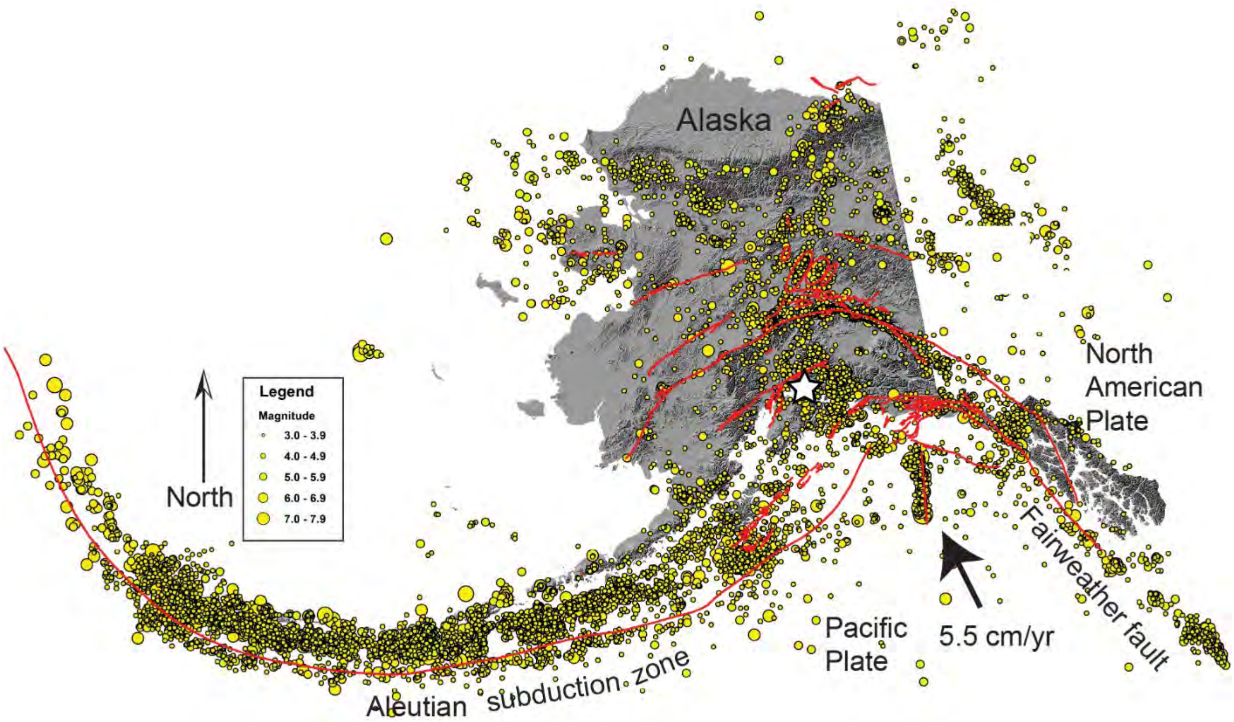

Figure 2-1. Regional hillshade map of Alaska showing the regional tectonic setting. Red lines show active faults taken from the Quaternary fault and fold database of Alaska (Koehler, 2013; Koehler et al., 2012). Yellow circles show crustal seismicity (M>3.0) from 1980-2011 from the Alaska Earthquake Center. Approximate epicenter of the 30 November 2018 earthquake and the city of Anchorage shown by white star. Relative rate (~5.5 cm/yr.) and direction of convergence between the Pacific and North American plates shown by black arrow

3.0 Regional Geology

3.1. Bedrock and Quaternary geology, Upper Cook Inlet

Mesozoic crystalline igneous and metamorphic rocks comprise the basement bedrock in the region. These rocks are overlain by weakly consolidated clastic sedimentary rocks of Tertiary age that are up to 3,900 meters thick (Figure 3-1). Late Quaternary deposits in the region include extensive glaciomarine deposits, glacial moraines, ice-stagnation deposits, and alluvium associated with proglacial fluvial systems, and extensive swamps and peat bogs (Reger and Updike, 1993). The Quaternary depositional package is up to 1,200 meters thick in the lower Susitna River area (Reger and Updike, 1993). Surficial geologic units in Anchorage primarily consist of glaciomarine Bootlegger Cove formation and glacial deposits, as will be described in Section 3.2. Surficial deposits are saturated across much of the region and are largely susceptible to liquefaction.

3.2. Surficial Geology, Anchorage area

The Quaternary geology of the Anchorage vicinity is the result of several major glaciations. The stratigraphy and timing of their deposition is detailed in Miller and Dobrovolny (1959) and Reger et al. (1995). The oldest glacial deposits are associated with the Eklutna glacier and include till and outwash deposits that are exposed north of the Eagle River Flats along the Knik Arm bluff. Deposits associated with the Knik glaciation are variably exposed throughout the Anchorage area and include lateral and ground moraines, pitted outwash, glaciofluvial and ice-contact deposits, and glaciomarine clay known as the Bootlegger Cove formation. The Bootlegger Cove formation is one of the more extensive deposits in the area and underlies the Susitna Basin, Anchorage, and the region to the south of the city. The Bootlegger Cove formation consists of glaciomarine clay, silty clay, and silty fine sand with variable amounts of medium grained sand and gravel (Updike, 1984). Major destructive landslides originated in the Bootlegger Cove formation during the 1964 earthquake. The youngest glacial deposits are associated with the latest Pleistocene Naptowne glaciation, overly deposits of the Knik glaciation, and include sorted and unsorted glacial drift, well preserved moraines, kame fields and kame terraces, and outwash.

Inspection of the surficial geologic map in Figure 3-1 indicates that Holocene alluvial fans bury glacial deposits over much of northwest Anchorage including downtown. Glaciomarine deposits are the dominant surficial unit in the midtown area. Undifferentiated late Pleistocene glacial deposits are exposed along the eastern part of the Anchorage Bowl along the base of the Chugach Mountains and in the vicinity of the airport. The Bootlegger Cove formation is exposed along the coastal bluffs from the vicinity of the Port of Anchorage to the airport and within the lower Campbell Creek drainage. A narrow northeast trending band of glaciodeltaic deposits is exposed southeast of Campbell Creek in south Anchorage.

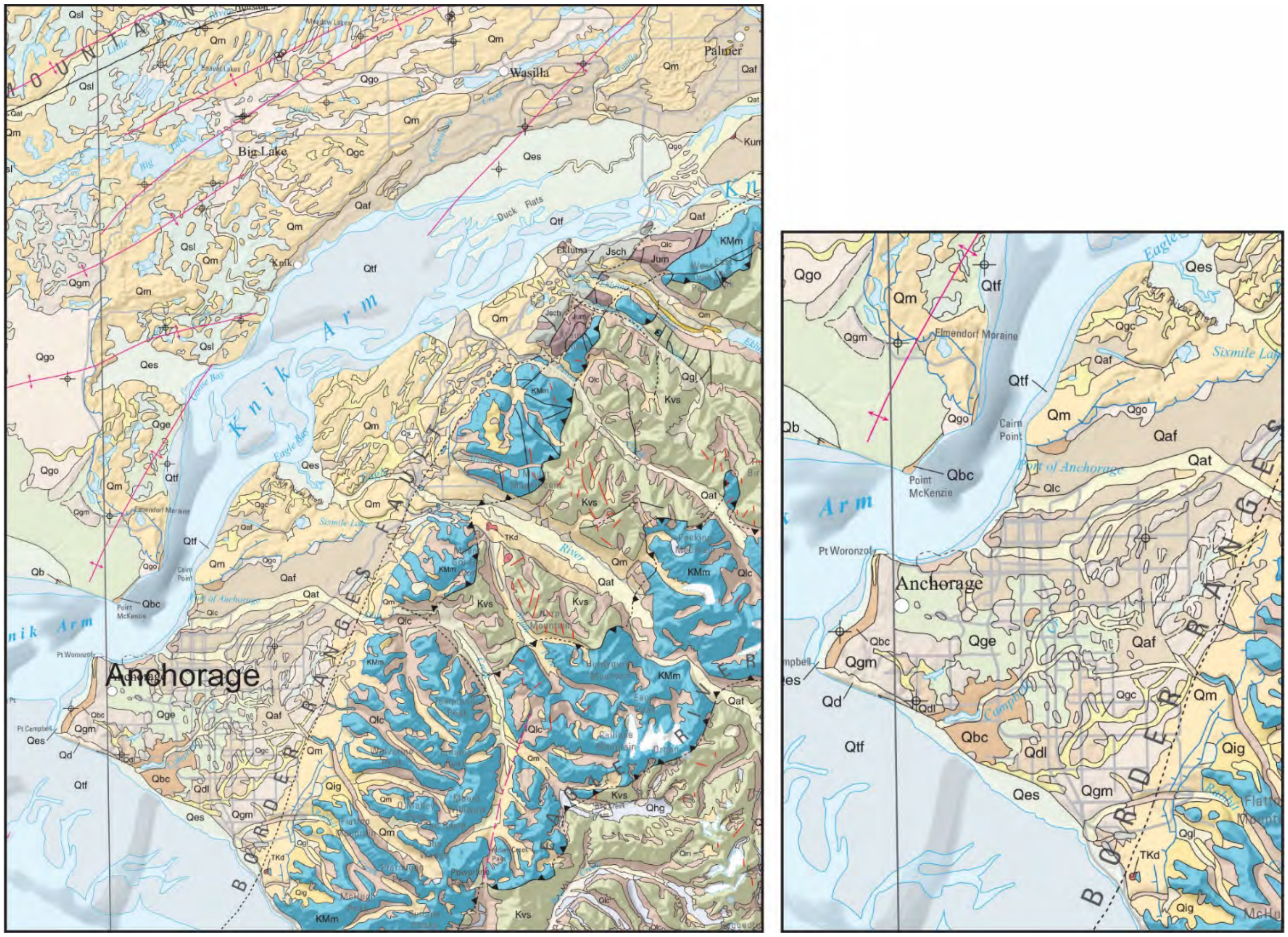

Figure 3-1. Part of the geologic map of the Cook Inlet region (Wilson et al., 2012). Main area affected by the earthquake (left) and close up view of Anchorage (right).

4.0 Ground Motions

4.1. Seismic Network in Anchorage

The seismic network in the metropolitan area of Anchorage is operated and maintained by the USGS (through their National Strong Motion Project, NSMP), and by the Alaska Earthquake Center (AEC). The latter operates seismic monitoring stations across the state of Alaska and their data center is located at the Geophysical Institute on the University of Alaska Fairbanks campus (UAGI). Data from these networks are made publicly available online (https://strongmotioncenter.org/cgi-bin/CESMD/iqr_dist_DM2.pl?iqrid=us1000hyfh and https://earthquake.alaska.edu/network). At the time this report was prepared, the Center for Engineering Strong Motion Data (CESMD) had released ground motions from the mainshock recorded at more than 80 sites, including instrumented high-rise buildings (i.e., structural arrays) located in different areas of Anchorage (e.g., Atwood building, close to the Delaney Park downhole array with seven sensors down to a depth of 61 m; the BP building; the Frontier Building; and the Hilton Hotel). Table 4-1. presents the station name and location corresponding to sites with available recordings at the CESMD website and epicentral distances (R_{epic}) less than 100 km (last updated March 12 2019). Recording stations visited by the GEER team are also indicated in Table 4-1. Available information regarding National Earthquake Hazards Reduction Program (NEHRP) site classes and shear wave velocity measurements are provided and discussed in subsequent sections of this report. Appendix A provides the complete table with all available stations in the CESMD (last updated March 12 2019).

Figure 4-1 depicts the coverage of the seismic network available in the region impacted by the 2018 Mw 7.1 Anchorage earthquake. The density of stations creates a unique opportunity to investigate further the impacts of this event. On December 9th the GEER team met with local geotechnical engineering consultants and researchers from the USGS. We learned that recorded motions from some CESMD and AEC stations were still being processed. Considering this information, the GEER team decided to focus reconnaissance efforts on stations where reliable data were recorded or knowledge of damage nearby was available.

4.2. Site conditions in Anchorage

Anchorage, Alaska, is built on the edge of a deep sedimentary basin at the foot of the Chugach Mountains, 7-km deep around 150 km southwest of Anchorage, and more than 1 km thick in the western side (Boore 2004, Hartman et al., 1974). Our understanding of the site conditions in the basin has been advanced through an integration of the geology of the area and available shear-wave velocity (V_s) measurements. Measurements of V_s at 36 sites in the basin from Nath et al., 1997 and Dutta et al., 2000 led to the National Earthquake Hazards Reduction Program (NEHRP) site class contour maps shown in Figure 4.2 and the identification of four distinct lithological units (Fig. 4.2.a): glaciofluvial deposits in the area classified as site class D (DGF), Bootlegger Cove formation (DBC), glaciofluvial deposits in the area classified as site class C (CGF), and glacial drift (CGD). As seen in Figures 4.2.b, c, and d, most areas in Anchorage are considered NEHRP Site Classes C or D. The C/D class was defined by Martirosyan et al. (2002) as an intermediate between NEHRP Site Class C and D when the average V_S in the top 30 m (V_{s30}) is between 320 and 410 m/sec.

The aforementioned information was used in the present study to infer site conditions at the recording stations presented in Table 4-1. Measured V_s values from previous studies are only available at nine stations (i.e., K203, K204, K208, K209, K210, K211, K212, K213, and K215), and those are provided in Table 4.1. Figure 4.3 depicts a subset of the recording stations provided in Table 4-1 and located in the Anchorage basin, along with the NEHRP contours proposed by Martirosyan et al. (2002) for reference purposes.

The strong impedance contrast present in the basin as a result of the combination of low velocity sediments overlying the metamorphic bedrock is ideal for the amplification of seismic waves (Boore, 2004). Previous site response studies in the region (e.g., Martirosyan et al. 2002, Dutta et al. 2003) have found significant ground motion amplification in the basin with respect to a reference rock site nearby Chugah Mountains (i.e., Station K216). "Although the detailed site-specific findings differ amongst the studies, they all find on average that the largest site amplifications are on the lower-velocity class D sites, with average amplifications around 3 at low frequencies (0.5–2.5 Hz) and around 1.5 at higher frequencies (3.0–7.0 Hz)" (Boore 2004).

Boore (2004) documented site effects from the 2002 M_w 7.9 Denali earthquake in Alaska. Comparisons of peak ground acceleration, velocity and displacement from stations on softer soils versus the assumed reference rock station (i.e., K216) revealed an increase in peak amplitude intensity measures for stations on the sedimentary basin. It must be noted that recorded motions from station K216 have been found to be affected by amplifications at frequencies larger than 7 Hz (Martirosyan and Biswas, 2002; Martirosyan et al., 2002). Moreover, station K216 has not been well-characterized in terms of subsurface conditions (including no V_s measurements at the site). As a result, Boore (2004) presented evaluations of site effects using the average response of ground motions recorded at stations classified as Site Class C as reference.

As seen in Figure 4-2, there is an apparent systematic spatial distribution of site classes in the Anchorage metropolitan area. Boore (2004) developed maps of site amplification in the sediments to the west of the Chugach Mountains, relative to the geometric mean of motions on class C sites (Figure 4-4) for four different frequencies (i.e., 0.2, 1, 5, and 14 Hz). The amplifications were smoothed over short frequency ranges around the aforementioned frequencies (Boore 2004). In general, these maps show an increase in amplification toward the west for low-frequency motions. Of special interest is the trend for the 0.2 Hz motions, which roughly corresponds to increasing depth to bedrock (Boore 2004). The spatial variations at higher frequencies may be due to local variations in near-surface geology, as described by Dutta et al. (2001), Martirosyan et al. (2002, 2004), Nath et al. (2002), and Dutta et al. (2003). Amplifications near the Chugah Mountains in Figure 5.4 for a frequency of 14 Hz do not seem to be controlled by geologic features, but rather by observations at a single station (Boore, 2004). In addition, Boore (2004) found site amplification from the 2002 Denali ground motions extends to periods of at least 10 sec.

Other site response studies in the area also reported increased amplifications from the foothills of the Chugach Mountains to the western, deeper part of the basin. Martirosyan et al. (2002) computed spectral ratios from 114 seismic events recorded at 22 weak-motion stations (WM) and 46 earthquakes recorded at 19 strong-motion (SM) stations in Anchorage. The free-field instruments from the WM network were operated only for about six months, and 114 earthquakes with local magnitudes between 1.5 and 5.5. were recorded. The SM network with 22 stations has been operational since 1995.

There are four WM stations that were placed within 150 m from a SM station; their locations are provided in Table 4.2. Unfortunately, during the time when both networks were operational, only five weak motion events triggered some of the instruments in the SM network. Martirosyan et al.

(2002) also reported the “drilling of a special purpose borehole of 9 m depth located close to the sites An01 and K2-16”, which indicated the presence of approximately 4 m thick weathered and fractured metamorphic rock. These authors hypothesized that the weathered layer with unknown spatial extent is the “result of repeated freezing and thawing of the in situ formations”.

Spectral ratios computed by Martirosyan et al. (2002) using both networks are presented in Figure 4-5, where variations in the site response of the multiple stations considered within the basin is evident. In general, spectral ratios increase in the western region of Anchorage where the basin also reaches greater depths.

4.3. Shear wave velocity measurements in Anchorage

Dutta et al. (2000) estimated the spatial distribution of shear wave velocity in the metropolitan area of Anchorage as part of a seismic microzonation study. They used V_s measurements from Nath et al. (1997), which were based on Rayleigh waves and a stochastic inversion scheme at 36 sites. Of the 36 sites in that study, only 15 corresponded to strong ground motion stations, and 7 were referred to as calibration sites (identified with a “C” in Table 4-3), where downhole V_s measurements were available. The depth range of the V_s measurements by Nath et al. (1997) covered approximately from 0 to 50 m. Moreover, additional geotechnical information was available at the calibration sites, such as SPT blow counts. The remaining sites are denoted with the letter “S” in Table 4-3. Locations and V_{s30} values are also provided in Table 4-3. The locations of the calibration sites and the complete 36 sites with velocity measurements are provided in Figure 4.6. Unfortunately, none of the available downhole measurements corresponded to the location of strong ground motion recording stations. Calibration sites C-04, C-05, and C-06 seem close to K202 recording station, and the resulting V_s profiles from the downhole tests are available in Nath et al (1997). Other stations located near calibration sites include K203 (close to C-02), and K206 (close to C-03). Nath et al. (1997) reported an overall good agreement between the V_s measurements at the calibration sites, except for C-05 and C-07. At C-05, the surface wave method yielded higher average velocity than the downhole method in the 0-25 m depth range, whereas lower values were obtained by the surface wave method at depths greater than 25 m. At the C-07 site, the layering estimated by the surface wave method did not match the layering obtained from the downhole measurement (Nath et al. 1997).

Dutta et al. (2000) also proposed a different lithology for the site class C and D areas (see Fig. 4-2a), indicating that portions of the basin with predominantly site class D soils “along the Knik Arm in west Anchorage with low V_{s30} values coincide with areas of high ground failure susceptibility observed after the 1964 Great Alaska earthquake”. The four groups proposed based on lithology were the following: glacial drift (GD), non-cohesive (SS) and cohesive (SC) facies of the Bootlegger Cove formation, and glaciofluvial deposits (GF) and are further described in Table 4-4. These authors also found that the aforementioned formations increase in thickness from the east (i.e., Chugach Mountains) to the west side of Anchorage. The corresponding V_s profiles for each lithologic unit are depicted in Figure 4-7.

Shear wave velocity measurements estimated with array measurements of microtremors have also been conducted in the metropolitan area of Anchorage. Dutta et al. (2007) found that engineering rock with a V_s>750 m/s lies at a depth of approximately 40 m in the eastern part of the basin, and around 100 m and 150 m deep at southcentral and western parts, respectively. This estimated depth to bedrock is in reasonable agreement with the general dip of the basin. Figure 4-8a provides the location of nine sites where the aforementioned V_s measurements were performed. Three V_s profiles are also provided: in the western side of Anchorage (C3, Fig. 4-8b), in the north-central part of the basin on-shore of Knik Arm (B3, Fig. 4-8c), and in the eastern area along the foothills of the Chugach Mountains (B1, Fig. 4-8d).

Interestingly, velocity reversals were found in some of these sites as shown in Figure 4-8c. “Below the engineering basement, a well-developed low-velocity zone (LVZ) with V_s values in the range of 900–1040 m/s is found to be present in the eastern as well as along the Knik Arm side in the western part of the basin at a depth of 200 m and 900 m, respectively. Moreover, the central part of the basin is associated with a weakly developed LVZ below the engineering basement depth. In the rest of the basin, the V_s values increase gradually with depth” (Dutta et al. 2007). Unfortunately, Dutta et al. (2007) also reported poor resolution of their kernels at the B3 site below 1000 m. The proper identification of the lateral and vertical extent of this potential LVZ would be key to understand the site response at many locations in the Anchorage basin. Further geophysical testing in the eastern as well as along the Knik Arm side in the western part of the basin is likely necessary to characterize such a geological feature.

4.4. Observations of Damage near Ground Motion Recording Stations

As reconnaissance efforts from the GEER team started, a list of ground motion recording stations (and the corresponding recorded ground motions available in December 2018) was downloaded from the CESMD website, and their locations were cross-matched with identified infrastructure with observed damage. The latter information resulted from a preliminary list of relevant sites developed during the GEER team’s first meeting with the local geotechnical engineering and engineering seismology community. Additional lists of damaged buildings (i.e., yellow- and red-tagged buildings) were also shared by the Municipality of Anchorage. At the time of field reconnaissance, the GEER team identified 40 stations with reliable data (from the CESMD website, the AEC website, and the USGS ShakeMap). Of those 40 stations, 14 had records available on the CESMD website. During the Phase I reconnaissance efforts, the GEER team visited more than 30 sites in the vicinity of those 14 stations.

Version 1 of this GEER report (released on December 31 2018) included information about ground motion characteristics from the mainshock, which is now updated in the following section. However, the documentation of relevant observations of damage near strong ground motion recording stations is still summarized herein. Figure 4-9. shows the location of selected stations relative to the epicenter of the November 30 Anchorage earthquake, Shakemap PGA and Modified Mercalli Intensity (MMI) contours.

Response spectra corresponding to the two horizontal components from the mainshock recorded at station NSMP 8027 are provided in Figure 4-10. Station NSMP 8027 is located in the C/D NEHRP site class transition zone shown in Figure 4-3. The polarization in the ground motion is evident as the HNE component is stronger over a wide range of spectral periods. The GEER team visited this station, which is located inside a warehouse immediately to the north of the Fish and Game building (Lat/Long: 61.1609,-149.8894). Settlement of nearly one foot was observed at one of the corners at the Fish and Game building. This settlement occurred within 200 ft of the instrument (Figure 4-11).

Station K223 (Lat/Long: 61.2338,-149.8675) was the closest operating station (with available recorded data by the time of completion of this Version 2 report) to the mainshock epicenter. It is located in the site class D zone shown in Figure 4-3. CESMD reported a PGA value of 0.27 g at that station.

Stations NSMP 8036 (Lat/Long: 61.1779, -149.9657), and NSMP 8038 (Lat/Long: 61.2184, -149.8829) were also near damaged infrastructure and observed ground failures. Station NSMP 8036 at the Department of Interior, Office of Aviation Services is located within 1 km from the Coast International Inn (Lat/Long: 61.1752, -149.9475), where structural damage to the first floor rendered the building red-tagged (i.e., deemed not safe to be occupied). At the time of inspection by GEER members, a significant portion of this two-story building, where walls had shifted and separated from the foundation, was closed. Information regarding the foundation design was not available. Figure 4-12 provides photos of the damaged walls as well as the pseudo-spectral accelerations obtained from the recorded motions nearby at station 8036. Largest values of PSA correspond to an oscillator period of approximately 0.2 sec.

Station 8038 (Lat/Long: 61.2184, -149.8829) is near the Port of Alaska (Lat/Long: 61.2304, -149.8846), which makes the corresponding recorded ground motions key information to assess the performance of this critical facility during a large magnitude seismic event. Members of the GEER team identified a slope failure adjacent to the port during their inspection of the port facilities. Due to difficulties accessing this area from the port, other members of the GEER team documented the slope failure from the top in a public park. Photos depicting key features of the slope failure are shown in Figure 4-13, including a scarp of about 50 cm. It is possible that other significant cracks had been covered by the snow by the time of our inspection.

The GEER team also visited strong motion recording stations located near sites that performed well during this event, including six buildings in the Alaska Native Tribal Health Consortium (ANTHC, Lat/Long: 61.1827, -149.8034) campus. Multiple buildings with different foundation types and ground improvement techniques implemented are all located within the ANTHC, and their performance during the mainshock of the 30 November Anchorage earthquake is described in later sections of this report. Figure 4-14. shows response spectra corresponding to the two horizontal components from the mainshock recorded at station NSMP 8030 (Lat/Long: 61.1795,-149.8058). Recording station NSMP 8030 is preliminarly characterized as a NEHRP site class C, according to the contour maps provided by Martirosyan et al. (2002) shown in Figure 4-3. Also, note the lack of polarization of the recorded ground motions in comparison with the response observed at station NSMP 8027 in Figure 4-10.

Minimal damage was observed in the vicinities of station NSMP 8037 (located at the NOAA Weather Facility, Lat/Long: 61.1563, -149.9850). The GEER team visited a residential complex on the gravel pit by the Sand Lake area and minimal settlement was observed in terms of settlement. It is important to note that the snow made it difficult to identify relevant geotechnical features during our reconnaissance efforts, including surficial expressions of liquefaction triggering.

The highest PGA reported from this event was recorded near Rabbit Creek at station RC01, with an epicentral distance of 30.9 km and classification of NEHRP site class C based on NEHRP contour plots in Figure 4-3. A PGA of 0.66 g was recorded in the HNE component obtained from the mainshock at RC01 (Lat/Long: 61.089, -149.739), and the corresponding response spectra are shown in Figure 4-15. The GEER team visited Rabbit Creek and found a large scarp approximately 2 to 3 m high (shown in Figure 4-15). Multi-Spectral Analysis of Surface Waves (MASW) was conducted at 12 sites during GEER's Phase II investigation including surveys at sites K211, K215, 8027, 8036, 8038, 8037, K209, K203, K220, 2100 Minerva Way (not a station), 8047, 8021. Data from these surveys are contained in Appendix B.

4.5. Ground Motion Characteristics

This section focuses on strong ground motion records from the mainshock obtained less than 100 km away from the source (see Table 4-1). The records were processed by the CESMD using USGS processing protocols (i.e., Jones et al. 2017). Some stations managed by the Alaska Earthquake Center (AEC) were originally recorded using 50 samples per second (sps). Ground motions recorded at these 34 AEC stations were resampled to 200 sps prior the USGS processing, and were filtered above 20 Hz. The remaining ground motions recorded from this event were filtered above 40 Hz. Appendix A provides a list of stations with original data recorded at 50 sps as provided by CESMD. Selected recorded acceleration histories and response spectra (5% damping) are provided in Figures 4-16 and 4-17 for the western, central and eastern sides of the Anchorage basin. These acceleration histories and response spectra are grouped by their location in the Anchorage basin to facilitate the interpretation of ground motion characteristics. Shallower depths to bedrock (~40 m) are characteristic of the eastern side. The strong and shallow impedance contrast between the metamorphic rocks and the overlying softer sediments has been found representative of stations located in the eastern side, such as K212 (Figure 4-7) and the study site B1 with V_s profile shown in Figure 4-8d. Such profile may explain the strong ground shaking observed in that region, but further subsurface characterization is required to better understand potential site effects. In fact, the highest PGA values were recorded at stations RC01 in Rabbit Creek and K215, both located on the eastern side of Anchorage. Ground shaking intensity in the central region is generally lower compared to the eastern region, but station NSMP 8027 appears to have experienced some amplification with respect to the record at NSMP 8030 located at a stiffer site and comparable epicentral distance. Directionality effects are not evident in the selected subset of motions (except for station NSMP 8027) as observed in Figure 4-18, which depicts the corresponding response spectra.

Stations RC01 and K215 have no direct measurement of the depth to bedrock, but previous studies have suggested bedrock can be shallow and associated with high spectral ratios (Martirosyan et al. 2002). Station NSMP 8047, a site class C, represents an interesting case study as it recorded a PGA equal to 0.4g but it is located near NSMP 8030 which recorded a PGA of only 0.29g. Boore (2004) identified a zone of high site amplification (see Figure 4-4) and station K220 with recorded PGA of 0.33g is located in such zone. Additionally, on the eastern side of Anchorage's basin, station NSMP 8037 recorded a PGA of 0.36g, but the GEER team observed only minimal damage in structures located nearby.

The systematic observation of site effects in the Anchorage basin documented by previous studies (e.g., Martirosyan et al. 2002, and Boore 2004), motivated preliminary analyses evaluating site effects on the recorded motions from the M_w 7.1 November 30 2018 mainshock near Anchorage. Figure 4-19 and 4-20 provide a comparison between records from station NSMP 8037, site class D (estimated), and station K209, site class C (V_{s30}=582 m/s). Both stations have epicentral distances of approximately 21 km, however, station NSMP 8037 is located on the far west of the basin, while station K209 is located on the eastern side. Peak amplitude parameters such as PGA are larger at the softer soil site (i.e., station NSMP 8037). Similarly, intensity measures such as Arias intensity and the cumulative absolute velocity are larger at NSMP 8037.

Significant duration is calculated using the normalized cumulative squared acceleration between the Husid plot, H(t), 5 and 75 percentiles (Somerville et al. 1995), which we refer to as $D_{5\text{-}75}$. Additionally, we compute the normalized cumulative squared acceleration between H(t)=5-95%, after Trifunac and Brady (1975), which we refer to as $D_{5\text{-}95}$. As seen in Figure 4-19, significant duration increases for the softer site (NSMP 8037) compared to station K209 for the HNN components. However, the expected increase in duration for soil sites is not evidenced in the HNE direction as shown in Figure 4-20.

Another example of potential site effects is provided in Figures 4-21 and 4-22. Characteristics of records at station K220, which was identified by Boore (2004) as one of the stations located in the area of highest site amplification in the basin (see Figure 4-4) are compared to recordings at station K203. Station K203 is a site class C, with a V_{s30} of 474 m/s, while station K220 is a site class D (estimated) located at the western end of Anchorage. Epicentral distances are comparable (i.e., 18 km for K203 and 22 km for K220). More detailed subsurface characterization at these sites can elucidate some of the sources of differences in ground motion intensity measures observed.

Polarization of ground motions was observed in records from multiple stations, as evidenced in Figure 4-23. The subset of recording stations shown is located on the eastern side of the basin and all the stations have epicentral distances of approximately 20 km (except for K215 with an epicentral distance of 30.9 km).

4.6. Comparison with Building Code Design Spectra

With the dense seismic network and strong local community of engineers, the 2018 Anchorage earthquake provides the opportunity to assess the effectiveness of seismic provisions in modern building codes. The Municipality of Anchorage currently adopts and enforces the 2012 International Building Code (IBC), although it must also be noted that some of the surrounding communities have opted out of inspections for building code compliance. Figure 4-24 compares spectra for the recorded motions with the 2012 IBC design spectra at several sites visited by GEER and discussed in the previous sections. In general, the event seems to have generated ground motions below current Anchorage design level, although at some stations the peak of the recorded motion spectrum (in one or both components) does exceed the design code plateau. At NSMP 8027, which exhibits stronger directionality, the design spectrum essentially envelopes the HNE component. Further evaluations of the recorded motions and comparisons with building code implementation may provide additional insights and the opportunity to evaluate how the building code is implemented and enforced throughout Anchorage and the surrounding communities.

4.7. Comparison to Ground Motion Models

Ground motion models for subduction tectonic environments are compared in this section to the observed motions from the M_w 7.1 30 November 2018 Alaska earthquake. Considering that at the time of completion of this report there are still two possible fault planes associated with the M_w 7.1 event according to the USGS (i.e., east-dipping 30 or west-dipping 60), an assessment of the aftershocks from West et al. (*in prep*) is used to select an assumed depth to the top of the rupture. Their aftershocks analyses suggest at least two distinct clusters, where “the southern cluster aligns along a west-dipping trend, and the northern cluster aligns along a steeply-dipping east plane" (West et al. *in prep*). The shallowest aftershocks are located at 22 km deep, however 95% of them occurred at depths between 48 and 30.5 km (West et al. *in prep*). Thus, 30 km is assumed as a reasonable estimate for the top of the rupture. Figure 4-25 presents the Youngs et al. (1997) ground motion model estimations of PGA, for a soil site, M_w 7.1 intraslab earthquake with a focal depth of 46.7 km (https://earthquake.usgs.gov/earthquakes/eventpage/ak20419010/executive). Values of PGA corresponding to two recorded horizontal components (as provided by CESMD) are plotted for comparison purposes.

The ground motion model by Atkinson and Boore (2003) was also implemented and compared with recorded motions from the M_w 7.1 2018 November Alaska earthquake. Figures 4-26a and 4-26b provide this comparison for stations classified as NEHRP Site Class C and D, respectively. Figure 4-27 includes all sites and provides estimated PGA median values for a Site Class C. The recorded values of PGA are in reasonable agreement with the estimations from both ground motion models (except for longer rupture distance and the Youngs et al. 1997 model).

A more recent ground motion model for subduction zones, the updated BC Hydro 2018 model (PEER, 2018) is now available. Data from Alaskan earthquakes were not included in the development of this model due to an unusual distance scaling observed in those records, as shown in Figure 4-28. Additional investigation of ground motion characteristics is key to improve our understanding of source, path, and site contributions to ground motion characteristics in the Alaska region.

4.8. Timing of Liquefaction Triggering

The binary classification system for liquefaction triggering case studies, based on the presence of surficial evidence (e.g., sand boils) or lack thereof does not provide information on the timing of liquefaction triggering. The latter has been proposed as a "missing dimension in liquefaction hazard evaluation" (Kramer et al. 2016).

Time-frequency analyses by means of the Stockwell-Transform (Stockwell, 1996) can be used to evaluate the evolutionary changes in frequency content of a given ground motion. If sudden and dramatic changes in a ground motion frequency content can be identified at a site underlain by liquefiable soils, the timing of liquefaction triggering can be estimated. Such an estimation provides a new kind of case histories that can inform current empirical models of liquefaction triggering.

Currently, only 45 liquefaction case studies include estimates of the timing of liquefaction triggering (Kramer et al. 2016). The M_w 7.1 2018 Anchorage, Alaska earthquake provides a unique opportunity to add more liquefaction-influenced ground motions to the existing database. In fact, ground motions from the mainshock recorded at K211 and NSMP 8027 stations have been preliminarily identified as good candidates for time-frequency analysis and the estimation of timing of liquefaction triggering. Future investigation of these ground motions can prove meaningful to improve the liquefaction hazard assessment of the region.

4.9. Recommendations for future research

Further subsurface characterization in the Anchorage basin is imperative. Geotechnical investigations (i.e., borings or CPTs) should be performed in conjunction with geophysical testing.

The GEER team recommends the following sites for future geophysical and geotechnical investigations:

- Reference rock site: Chugach Mountains recording station K216

- Recording stations near critical facilities: NSMP 8038 near Port of Alaska (especially because the snow prevented the identification of other cracks in the ground/detailed characterization of the ground failure)

- Recording stations close to observed damage: NSMP 8036

- No liquefaction site: several possibilities (select site with no surface evidence of liquefaction, near recording station, on liquefiable soil, with structure) NSMP 8037?

- Possible liquefaction site: NSMP 8027 - Dept. of Fish and Game Building (settlement observed, but no ejecta)

- Definite liquefaction site: 1271 W 82nd Ave. (ejecta documented by resident, sample provided, particle size analysis performed at the University of Alaska Anchorage – described later in this report)

- Recording stations with multiple recorded events and the November 30 2018 mainshock

- Recording stations near (or at) sites with previous measurements of V_s: K214, K207, K212, K204.

Table 4-1. Recording stations with available records from the mainshock and R_{epic}<100 km.

Network	Station Number	Station Name	Latitude (N)	Longitude (W)	R_{epic} km	Visited by GEER	NEHRP Site Class	V_{s30} (m/s)
UAGI	K223	AK:Anchorage;Gvt Hill Elem Sch	61.234	149.868	13.4	**Y**	D	-
NSMP	2716	AK:Anchorage;Hilton Hotel	61.219	149.892	13.7	**Y**	D	-
NSMP	8043	AK:Anchorage;Port Access Br	61.222	149.885	14.4	N	D	-
NSMP	8038	AK:Anchorage;FS 01 (Central)	61.218	149.883	14.8	**Y**	D	-
NSMP	8040	Anchorage - R B Atwood Bldg	61.215	149.893	15.1	**Y**	D	-
NSMP	8045	AK Anchorage - VAMC	61.233	149.744	15.8	N	C	-
NSMP	8023	Anchorage - Football Stadium	61.205	149.876	16.3	N	C/D	-
NSMP	8041	AK:Anchorage;Turnagain ELMN	61.194	149.947	16.9	N	D	-
NSMP	8016	AK:Anchorage;BP Bld	61.192	149.864	16.9	**Y**	C/D	-
NSMP	8042	AK:Anchorage;Frontier Bld	61.188	149.884	17.2	N	C/D	-
NSMP	8011	Anch - Russian Jack Spr St Pk	61.209	149.786	17.8	N	C	-
NSMP	8007	AK:Anchorage;Intl Arpt	61.182	149.997	17.8	N	C	-
UAGI	K203	AK:Anchorage;St Christo Epi Ch	61.22	149.745	18	N	C	474
NSMP	8036	AK:Anchorage;DOI OAS	61.178	149.966	18.7	**Y**	D	-
UAGI	K208	AK:Anchorage;Spenard Rec Ctr	61.176	149.922	19	N	D	274
UAGI	K204	AK:Anchorage;Signature Flt Sup	61.176	150.012	19.2	N	D	309*
NSMP	8047	AK:Anchorage;USGS ESC	61.189	149.802	19.4	**Y**	C	-
NSMP	8028	AK:Anchorage;Coll Gate Elem	61.193	149.782	19.5	N	C	-
NSMP	8029	AK:Anchorage;Tudor Elem Sch	61.174	149.85	20	N	C	-
NSMP	8030	Anchorage - Police HQ	61.179	149.806	20.2	**Y**	C	-
NSMP	8027	AK:Anchorage;St Fish&Game	61.161	149.889	20.9	**Y**	C/D	-
UAGI	K209	AK:Anchorage;Scenic Prk Bib Ch	61.185	149.747	21.1	N	C	582
NSMP	8037	Anchorage - NOAA Weather Fac	61.156	149.985	21.2	**Y**	D	-
UAGI	K221	AK:Anchorage;St James Ortho Ch	61.152	149.951	21.6	N	D	-
NSMP	8025	Anchorage - BS Lutheran Ch	61.147	149.894	21.6	N	C/D	-
UAGI	K220	AK: Anchorage;Kincaid Park	61.154	150.055	22.1	N	D	-
UAGI	K211	AK:Anchorage;HQ Fire Dept #12	61.149	149.858	22.5	N	C	394*
UAGI	K212	AK:Anchorage;BLM	61.156	149.793	22.9	N	C	514
UAGI	K217	AK:Anchorage;Chugiak FS	61.396	149.516	24.1	N	-	-
UAGI	K210	AK:Anchorage;Mears Jr HS	61.129	149.931	24.2	N	D	269
NSMP	8021	AK:Anchorage;Klatt Elem Sch	61.113	149.91	26.1	**Y**	D	-
UAGI	K213	AK:Anchorage;ASD Operation Ctr	61.113	149.859	26.5	N	C/D	354
UAGI	K222	AK:Anchorage;Chapel by the Sea	61.088	149.837	29.5	N	C	-
UAGI	RC01	Rabbit Creek AK USA	61.089	149.739	30.9	N	C	-
UAGI	K215	AK:Anchorage;Rabbit Creek FS10	61.086	149.752	30.9	N	C	412
UAGI	SSN	Susitna AK USA	61.464	150.747	44.1	N	-	-
UAGI	K218	AK:Anchorage;PTWC	61.593	149.133	51.5	N	-	-
UAGI	KNK	Knik Glacier AK USA	61.413	148.459	80.1	N	-	-
UAGI	CAPN	Captain Cook Nikiski, AK, USA	60.768	151.154	91.1	N	-	-
UAGI	SAW	Sawmill AK USA	61.807	148.332	100	N	-	-
UAGI	PWL	Port Wells, AK	60.858	148.333	102.7	N	-	-

measurements made at old locations published first in Dutta et al. (2000), and then updated after relocation of the stations on Martirosyan et al. (2002).

**measurements made at old locations published first in Dutta et al. (2000), and then updated after relocation of the stations on Martirosyan et al. (2002)*

Table 4-2. Locations of a subset of close-by weak (temporal) and strong (permanent) motion stations analyzed by Martirosyan et al. (2002).

Strong Motion Station Number	Latitude (N)	Longitude (W)	Weak Motion Station Number	Latitude (N)	Longitude (W)	Station-to-station distance (m)
K201	61.235	149.869	An15	61.235	149.87	100
K212	61.156	149.792	An05	61.156	149.794	130
K206	61.191	149.822	An12	61.191	149.824	145
K216	61.099	149.685	An01	61.098	149.687	-

Table 4-3. Site locations of shear wave velocity (β) measurements by surface wave method (after Dutta et al. 2000). The average β provided in the last column correspond to V_{s30} estimates.

Site Code	Longitude (°W)	Latitude (°N)	Average β (m s^{-1})
K2-01	149.8681	61.2345	239
K2-02	149.8215	61.2243	366
K2-03	149.7176	61.2185	474
K2-04	150.0143	61.1786	309
K2-05	149.9108	61.1998	284
K2-06	149.8216	61.1920	491
K2-07	150.0030	61.1603	270
K2-08	149.9186	61.1776	274
K2-09	149.7436	61.1851	582
K2-10	149.9268	61.1285	269
K2-11	149.8691	61.1570	394
K2-12	149.7911	61.1560	514
K2-13	149.8546	61.1130	354
K2-14	149.7778	61.1406	524
K2-15	149.7500	61.0865	412
C-01	149.7441	61.2376	448
C-02	149.7175	61.2296	398
C-03	149.7966	61.1818	491
C-04	149.8216	61.2171	239
C-05	149.8271	61.2118	303
C-06	149.8531	61.2195	227
C-07	149.8938	61.2148	256
S-07	149.8973	61.1546	313
S-22	149.8050	61.1121	504
S-25	149.9048	61.1133	428
S-36	149.7671	61.1211	421
S-38	149.7631	61.2146	448
S-39	149.8316	61.0980	514
S-43	149.7953	61.2031	451
S-44	149.9498	61.1528	277
S-48	149.8453	61.1746	520
S-49	149.9471	61.1950	265
S-55	149.7845	61.2200	408
S-66	149.8295	61.1313	445
S-69	149.8726	61.1700	376
S-73	149.8895	61.1968	404

Table 4-4. Lithologic units identified in the metropolitan area of Anchorage (modified after Dutta et al., 2000).

Lithologic Unit	Description	Representative Vs profile	Depth (m)
GD	Heterogeneous undifferentiated till with silt and clay along the foothills of Chugach Mountain	K214	30
SS	Silts and sands near the central part of Anchorage	S-07	30
SC	Glacioestuarine silt and clay in south-central Anchorage	K207	25
GF	Sand and gravel with variable spatial distribution	K212 and K204	25-30

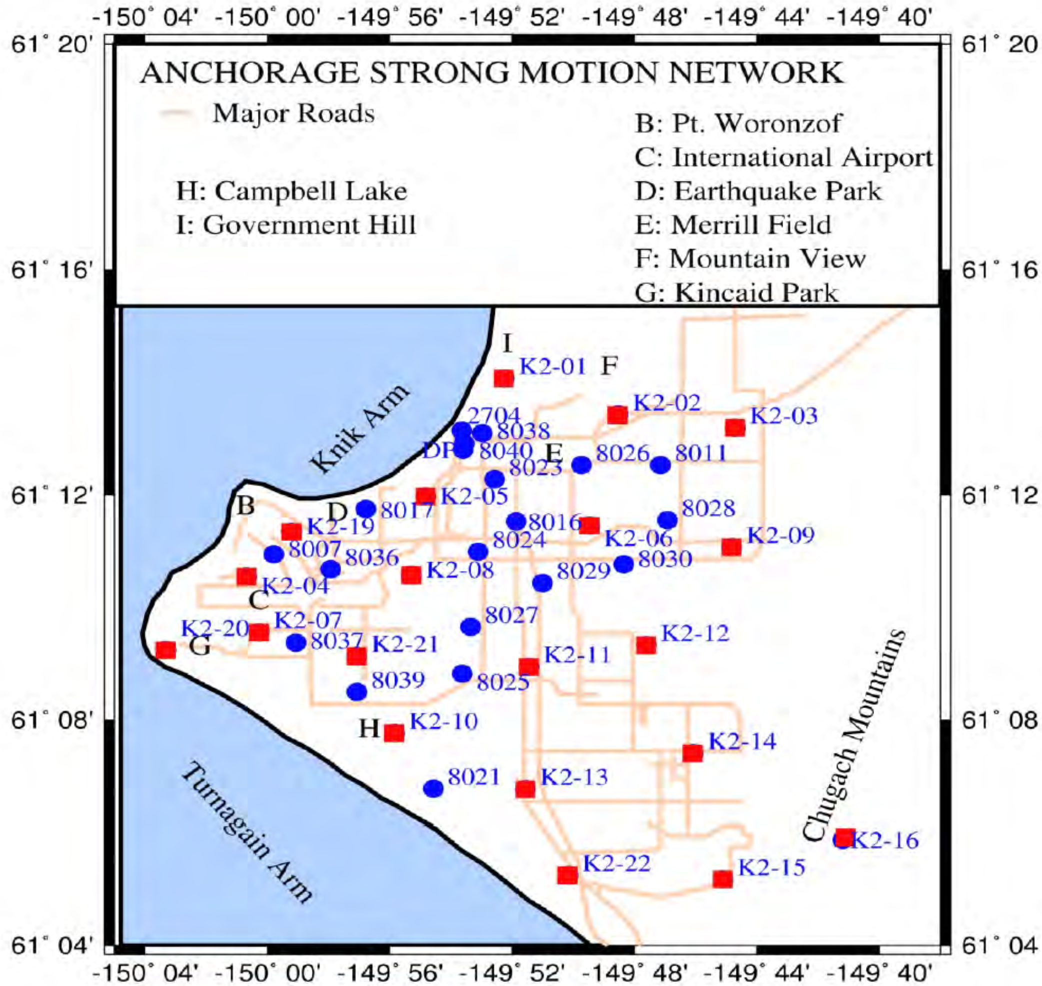

Figure 4-1. Anchorage Strong Motion Network. Red squares indicate free-field recording stations operated by the University of Alaska, and blue circles indicate USGS stations (after Dutta and Yang, 2010).

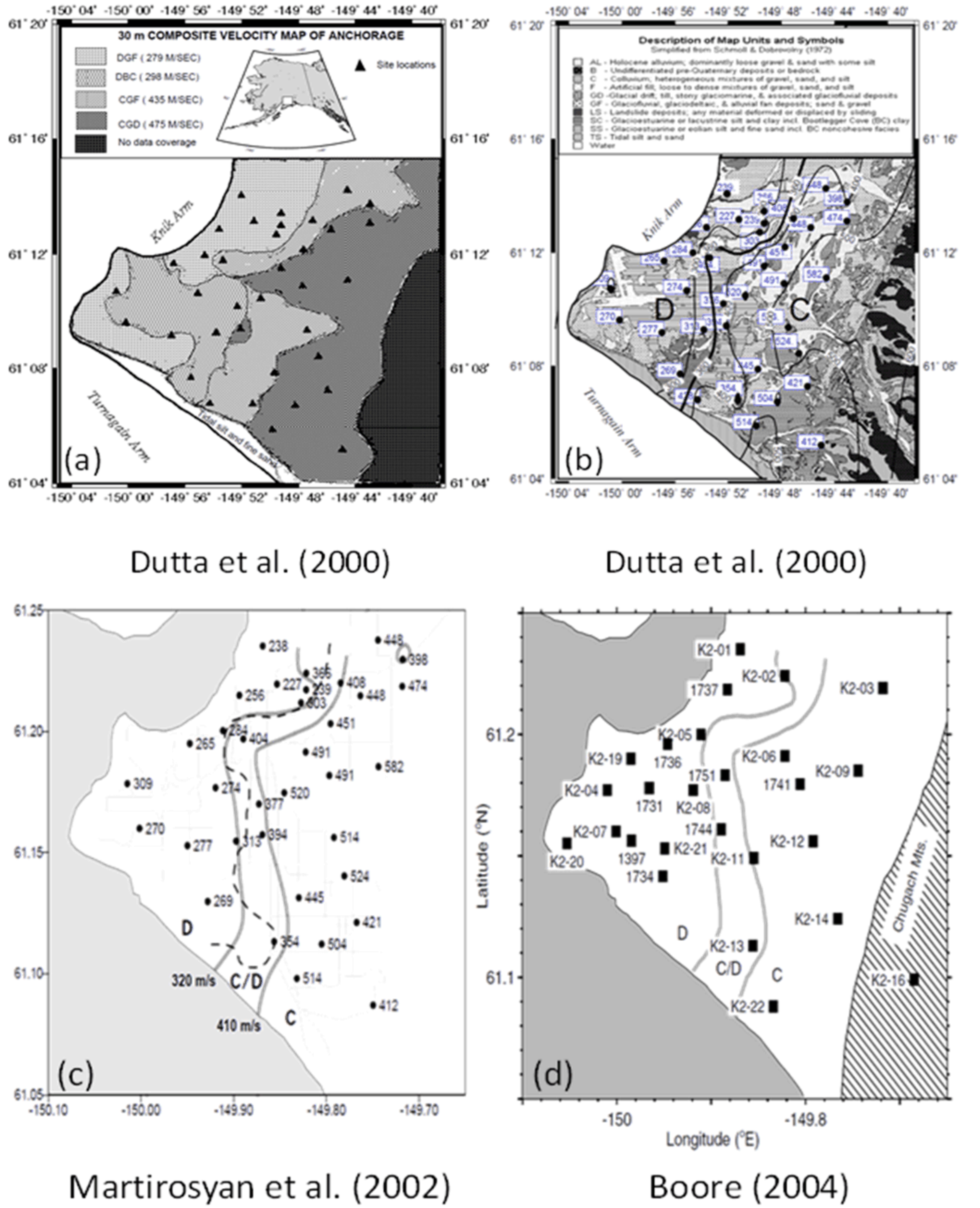

Figure 4-2. Site conditions in the Anchorage basin: (a) four distinct lithological units including glaciofluvial deposits, the Bootlegger Cove formation, and glacial drift, (b) measured V_s values at 36 sites, (c) NEHRP site class contours, and (d) assumed site conditions at recording stations based on location with respect to the site class contours.

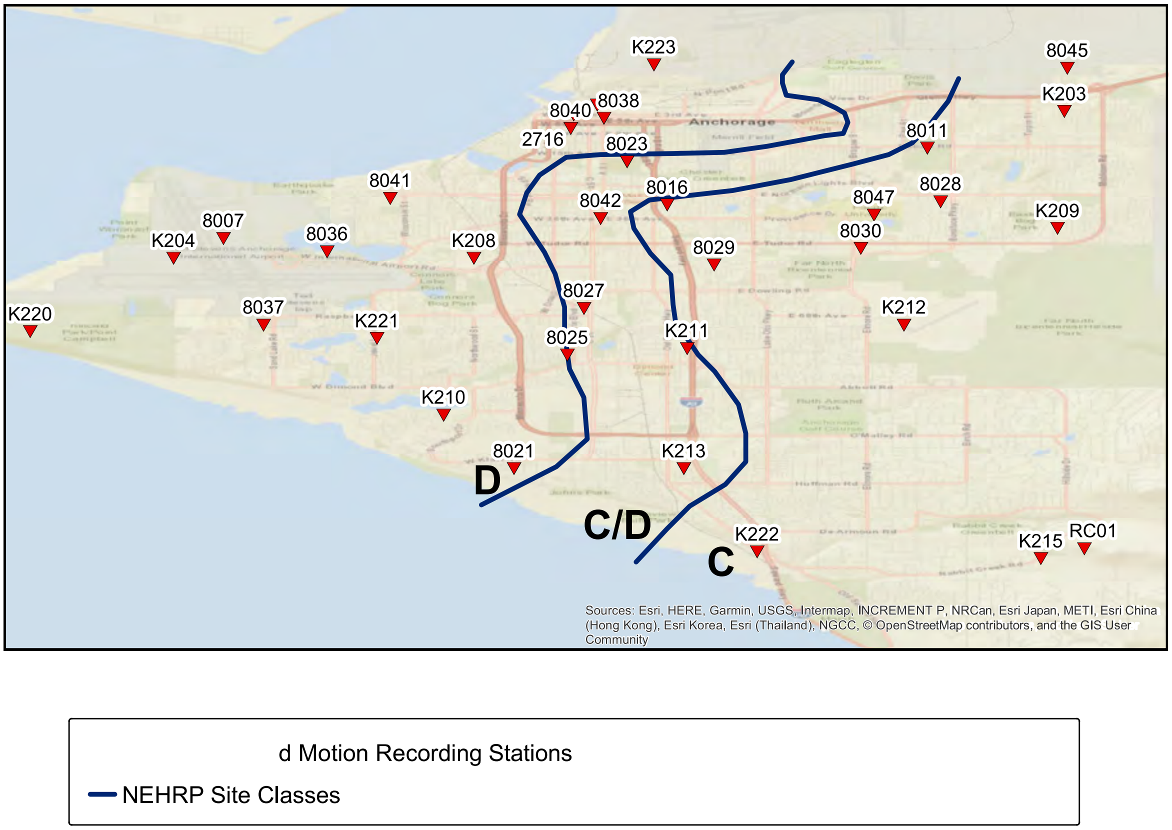

Figure 4-3. Location of strong ground motion stations in the metropolitan area of Anchorage and NEHRP contours proposed by Martirosyan et al. (2002).

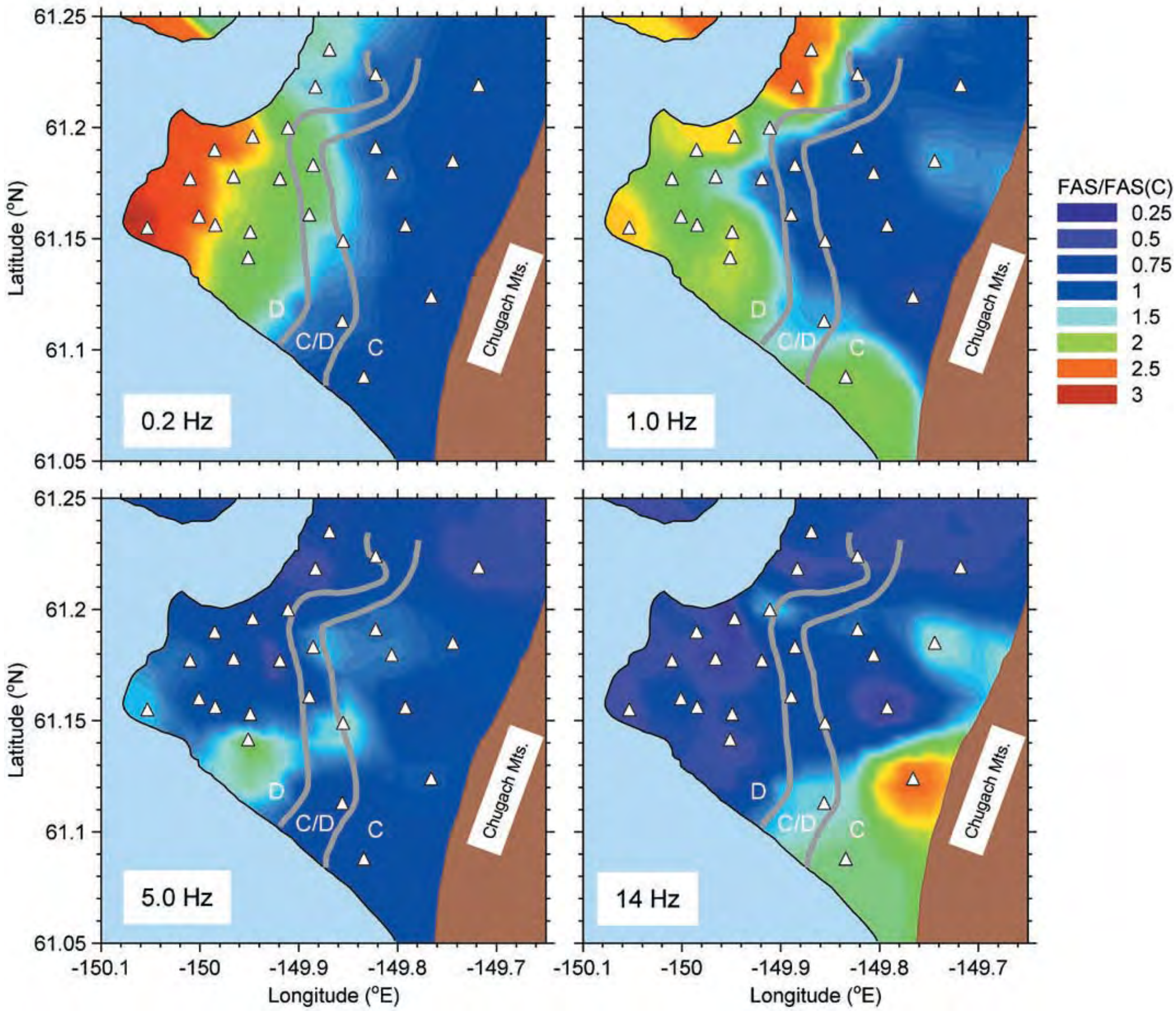

Figure 4-4. Maps of site amplification in the sediments to the west of the Chugach Mountains, relative to the geometric mean of motions on class C sites (brown area shows the location of the Chugach Mountains; after Boore, 2004).

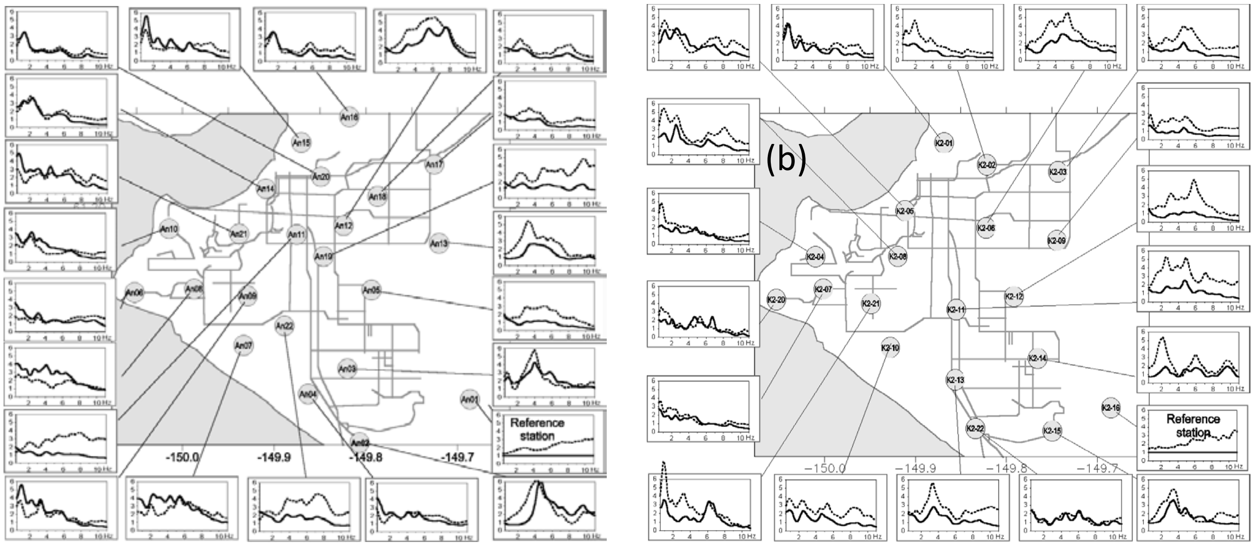

Figure 4-5. Spectral ratios at (a) weak and (b) strong motion stations as a function of frequency. The solid lines depict spectral ratios, while the dashed lines represent the results based on horizontal-to-vertical spectral ratios (HVR) methods also conducted by Martirosyan et al. (2002).

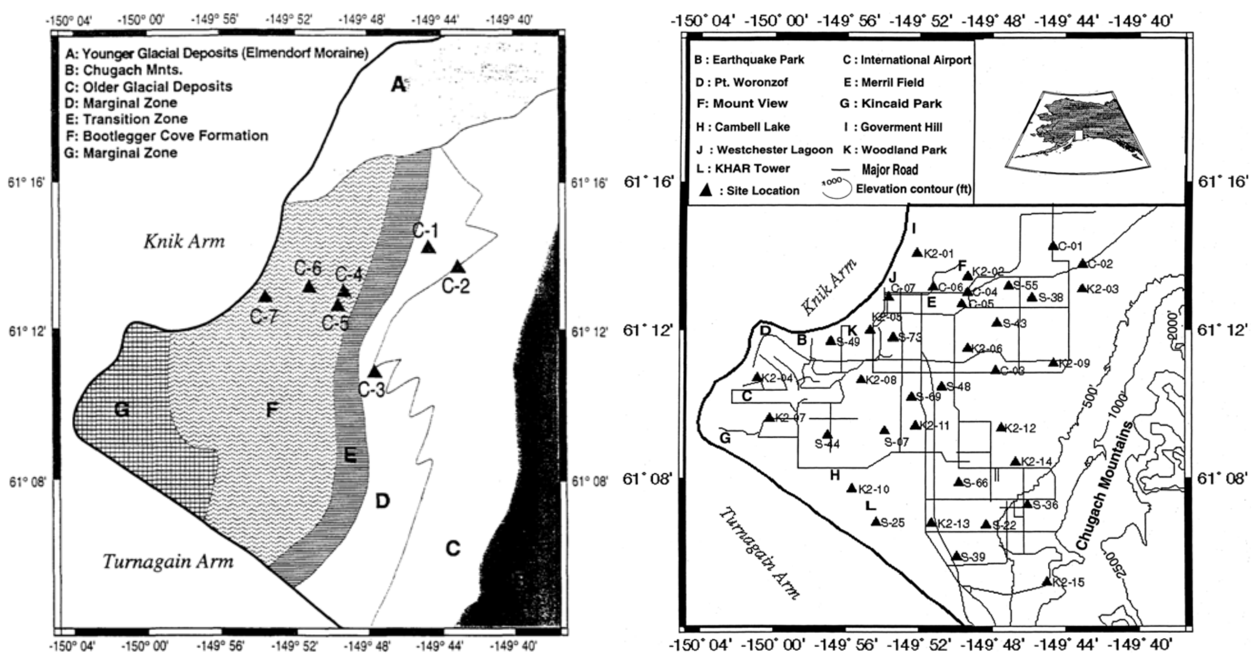

Figure 4-6. Location of the (a) seven calibration sites (after Nath et al., 1997), and (b) 36 sites with shear wave velocity measurements from surface wave methods (after Dutta et al., 2000).

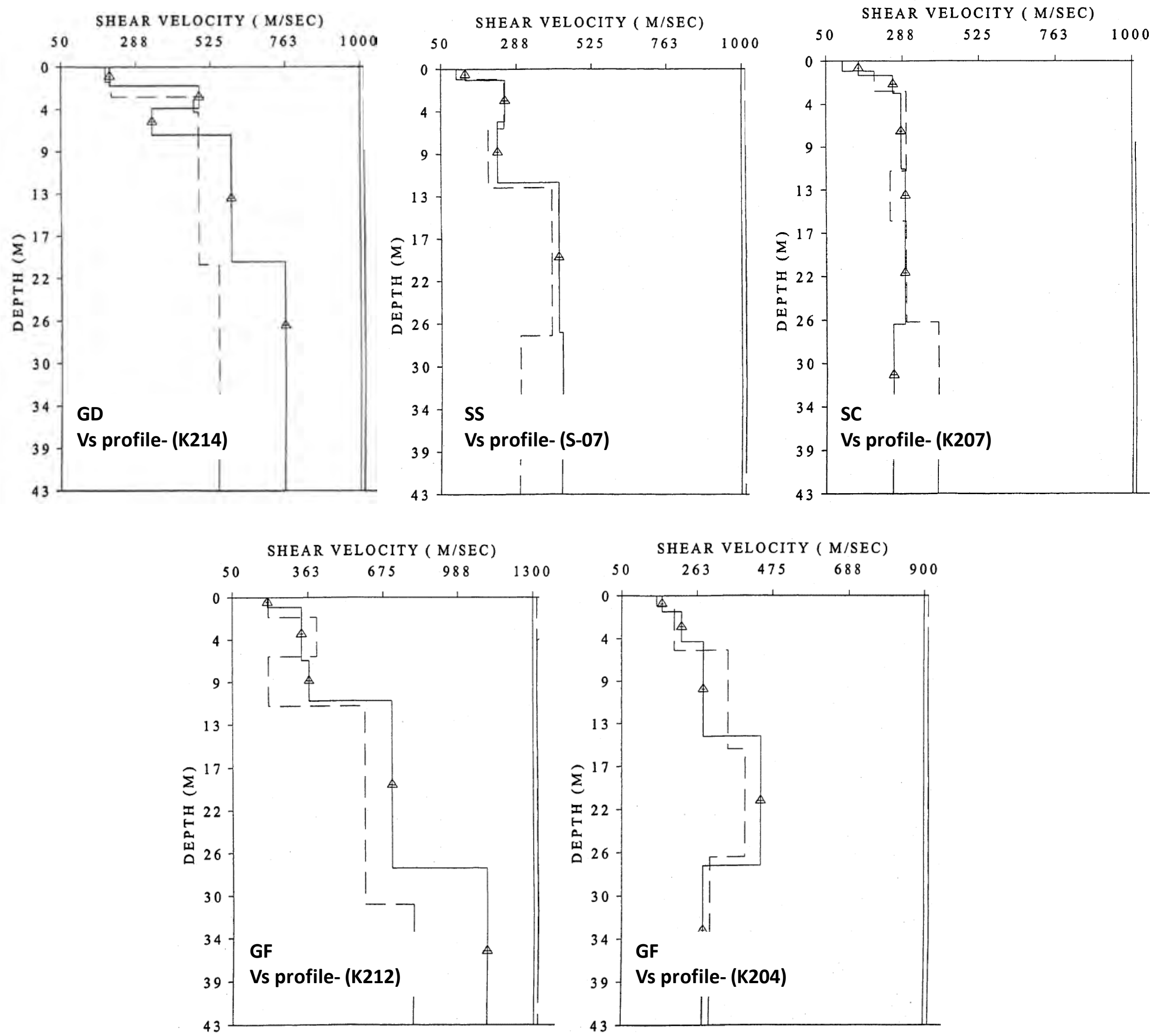

Figure 4-7. Shear wave velocity at four representative lithologic units in the Anchorage basin (modified after Dutta et al., 2000).

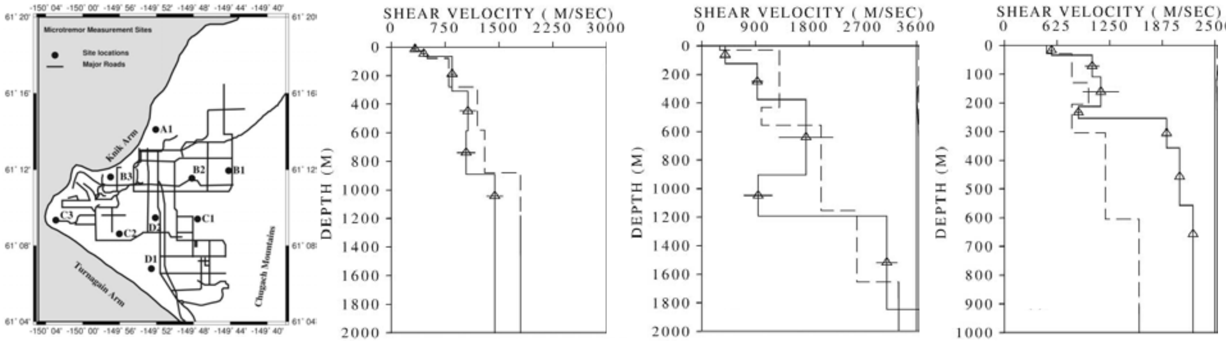

Figure 4-8. (a) Location of sites with V_s estimations using array measurements of microtremors (after Dutta et al., 2007); (b), (c), and (d) profiles of V_s at selected sites (modified after Dutta et al. 2007). The initial V_s profile is shown in the dashed line, and the best-fit V_s model is shown using a solid line. The triangles indicate the depth at which the resolving kernel was computed, and horizontal bars indicate the standard deviation of the best-fit model.

Figure 4-9. Location of selected stations (triangles) in the network, and Did You Feel It (DYFI) ShakeMap stations (circles). Modified after ShakeMap produced for this event by the USGS (https://earthquake.usgs.gov).

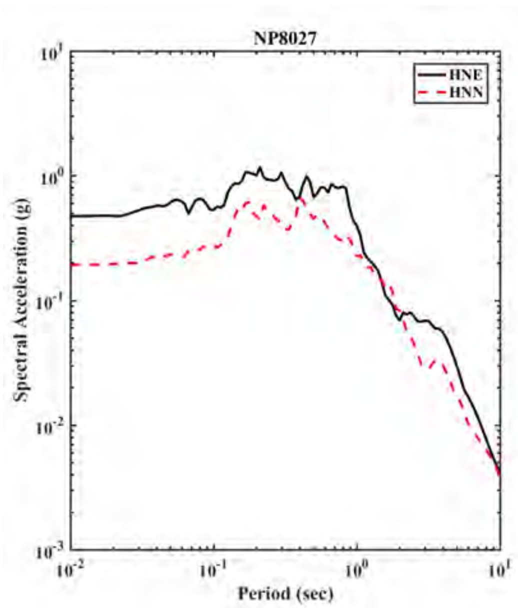

Figure 4-10. Pseudo-acceleration response spectra (5% damping) for two horizontal components recorded at NSMP 8027 (Lat/Long: 61.1609°, -149.8894°).

Figure 4-11. Settlement observed near recording station NSMP 8027 (Lat/Long: 61.1609°, -149.8894°).

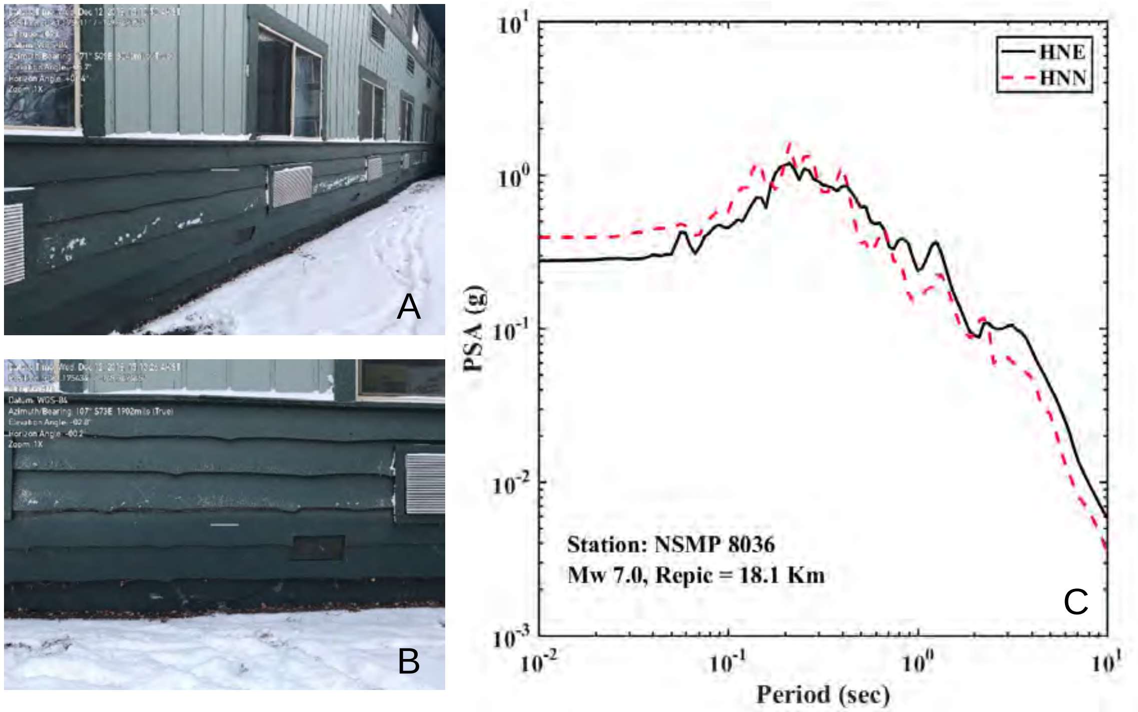

Figure 4-12. Damage observed at the Coast International Inn (Lat/Long: 61.1752°, -149.9475°), A) Shifted walls on the first floor, B) closer view of the deformation, and C) Pseudo-acceleration response spectra (5% damping) for two horizontal components recorded at station 8036 (Lat/Long: 61.1779°, -149.9657°).

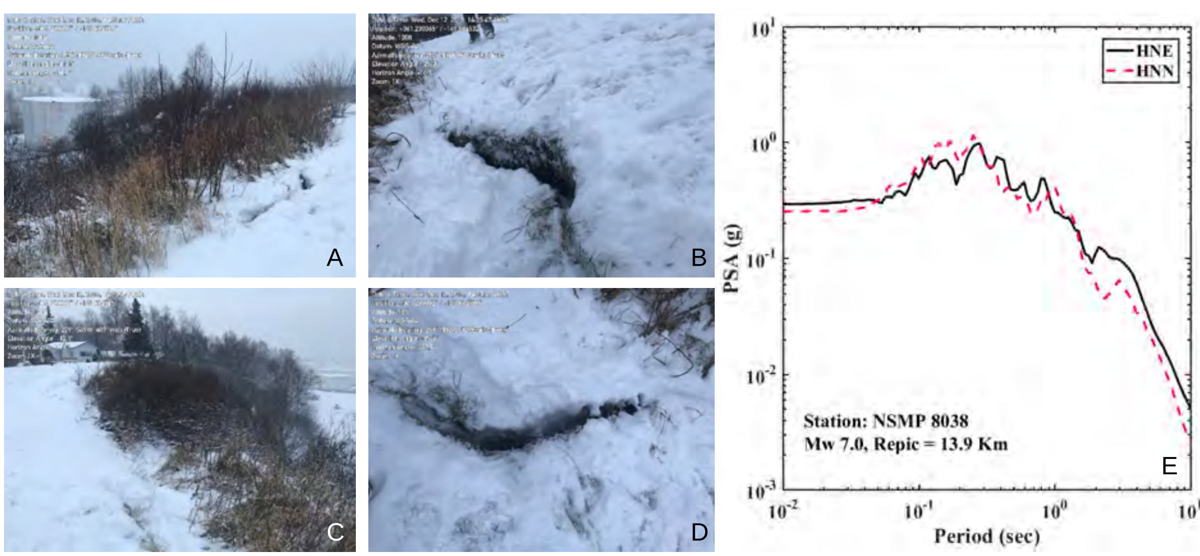

Figure 4-13. Slope failure adjacent to the Port of Alaska (Lat/Long: 61.2304°, -149.8846°); (A through C) an overall view of the slope and port facilities; (B) the 50-cm scarp; (D) a crack at this site with a width of approximately 20 cm; and (E) the pseudo-acceleration response spectra (5% damping) for two horizontal components recorded at the nearby station, NSMP 8038 (Lat/Long: 61.2184°, -149.8829°).

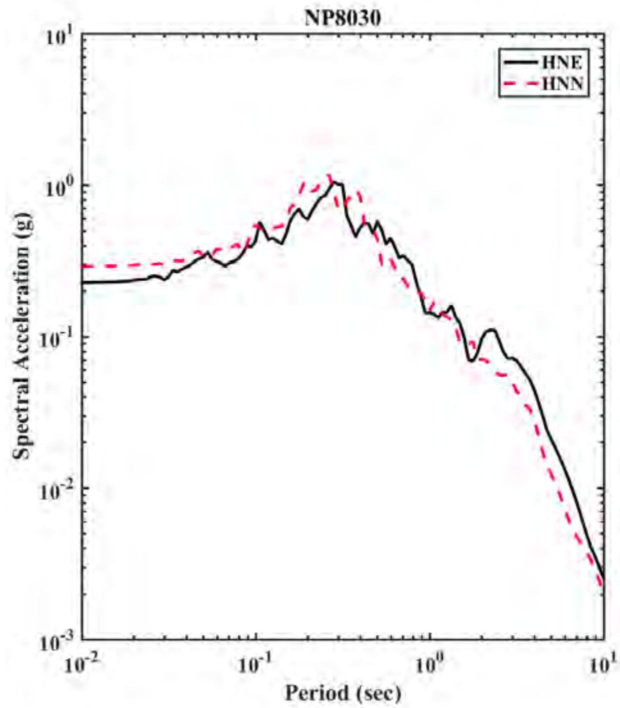

Figure 4-14. Pseudo-acceleration response spectra (5% damping) for two horizontal components recorded at station NSMP 8030 (Lat/Long: 61.1795°, -149.8058°).

Figure 4-15. Damage observed at Rabbit Creek near the RC01 recording station. Pseudo-acceleration response spectra (5% damping) for two horizontal components recorded at station RC01 (Lat/Long: 61.089°, -149.739°).

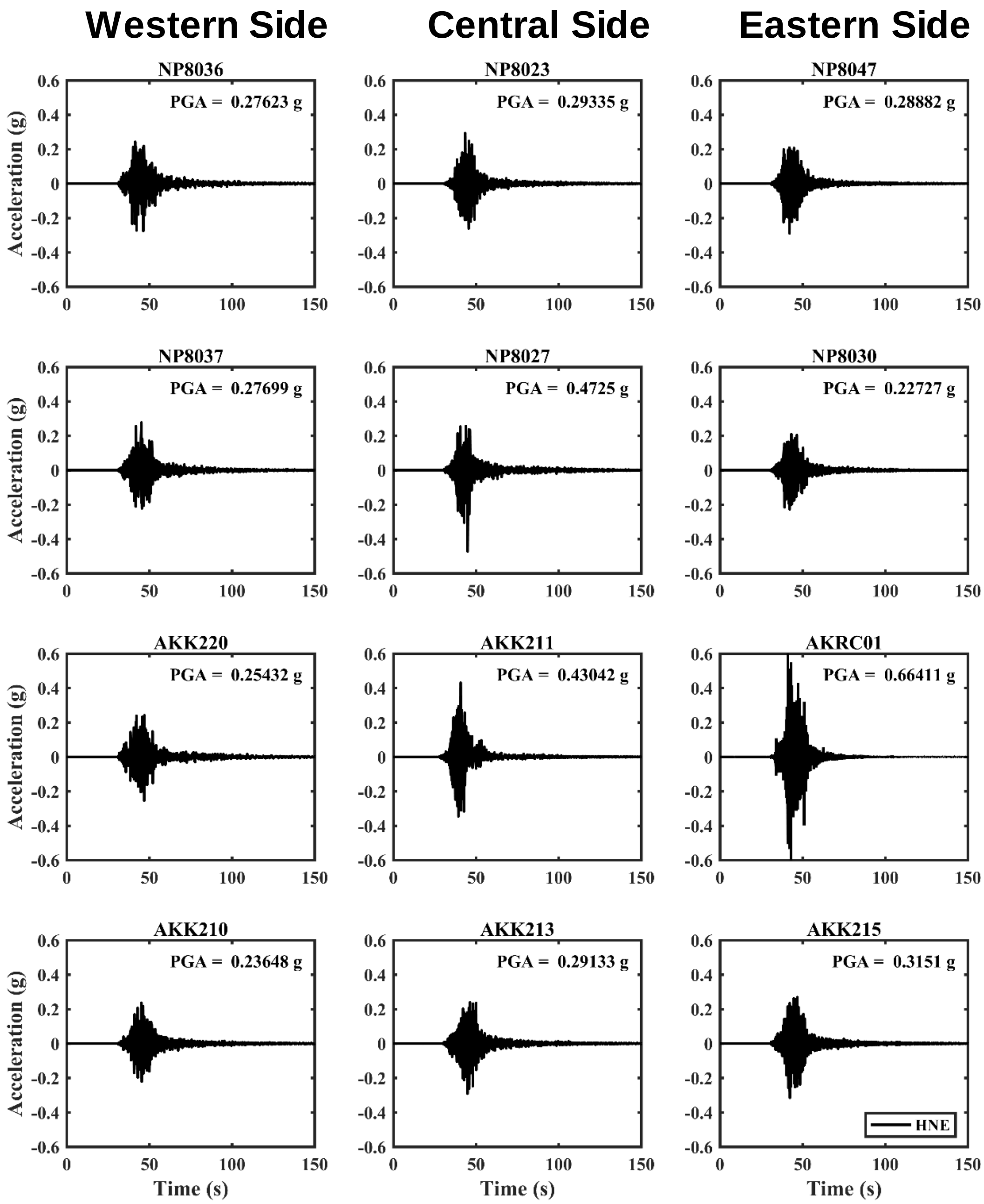

Figure 4-16. Acceleration time series at 12 stations located in west, central and east sides of the Anchorage basin. Only HNE components are shown.

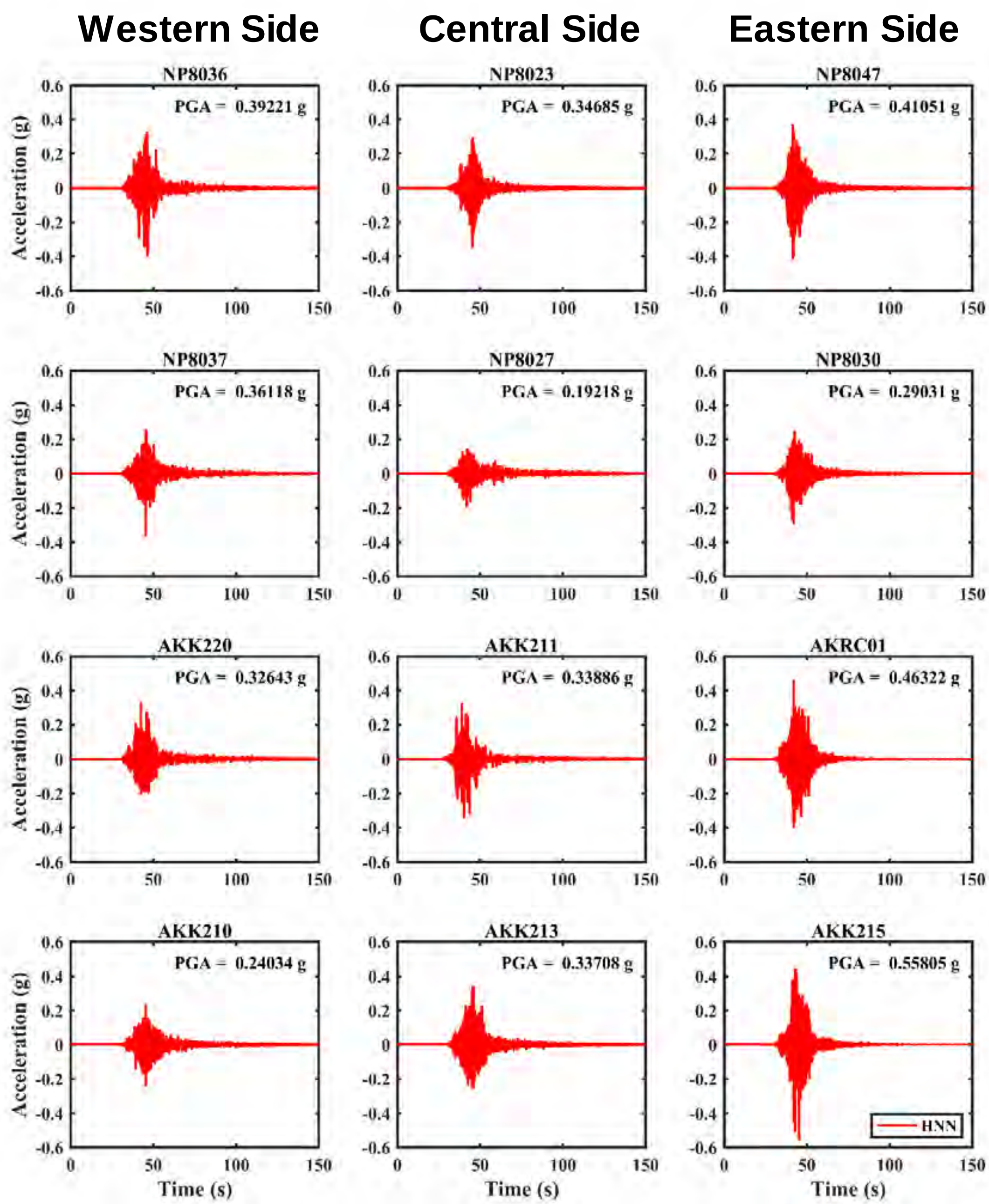

Figure 4-17. Acceleration time series at 12 stations located in west, central and east sides of the Anchorage basin. Only HNN components are shown.

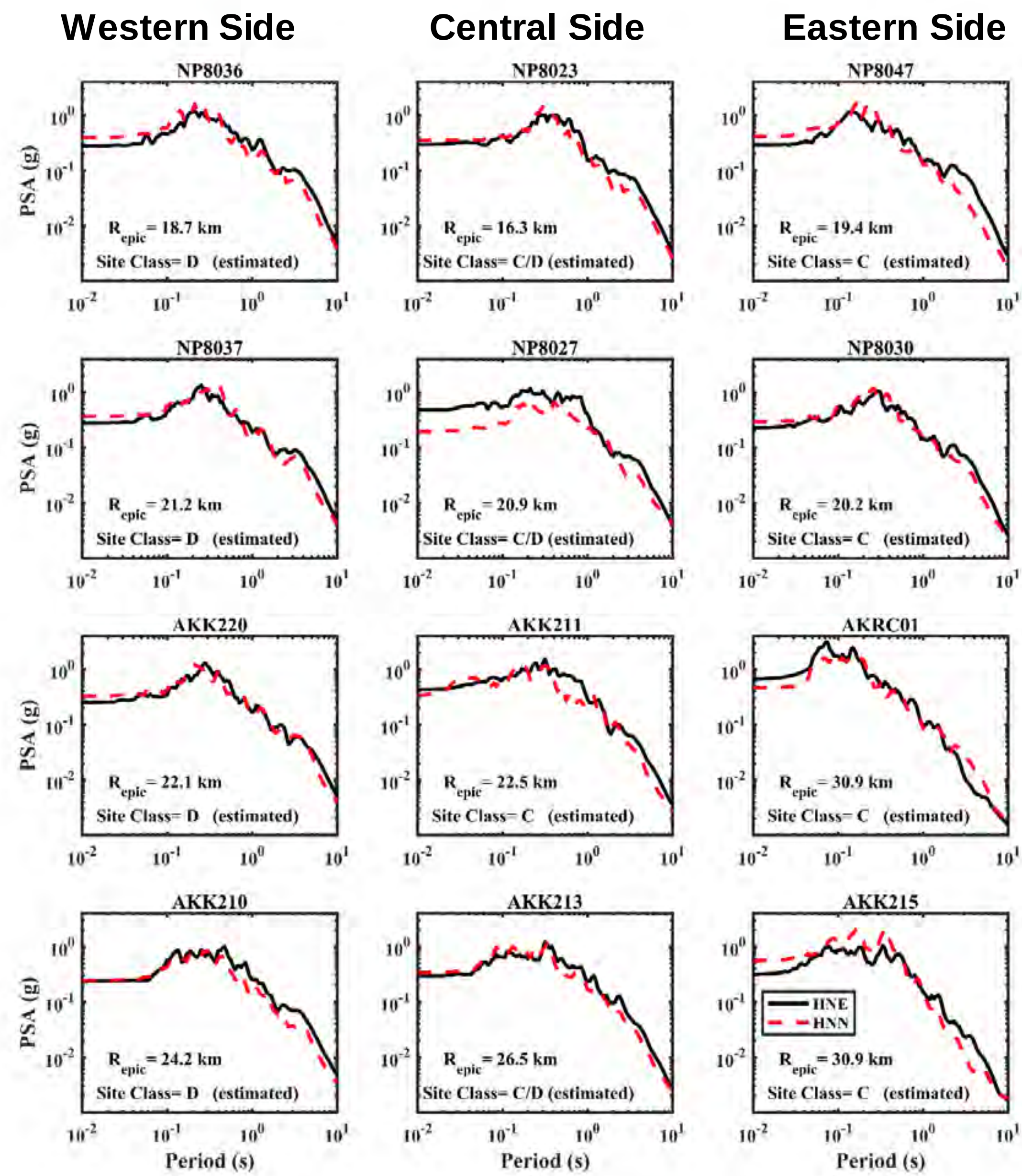

Figure 4-18. Pseudo-acceleration response spectra (5% damping) for 24 horizontal components recorded at stations located in the western, central and eastern sides of the Anchorage basin.

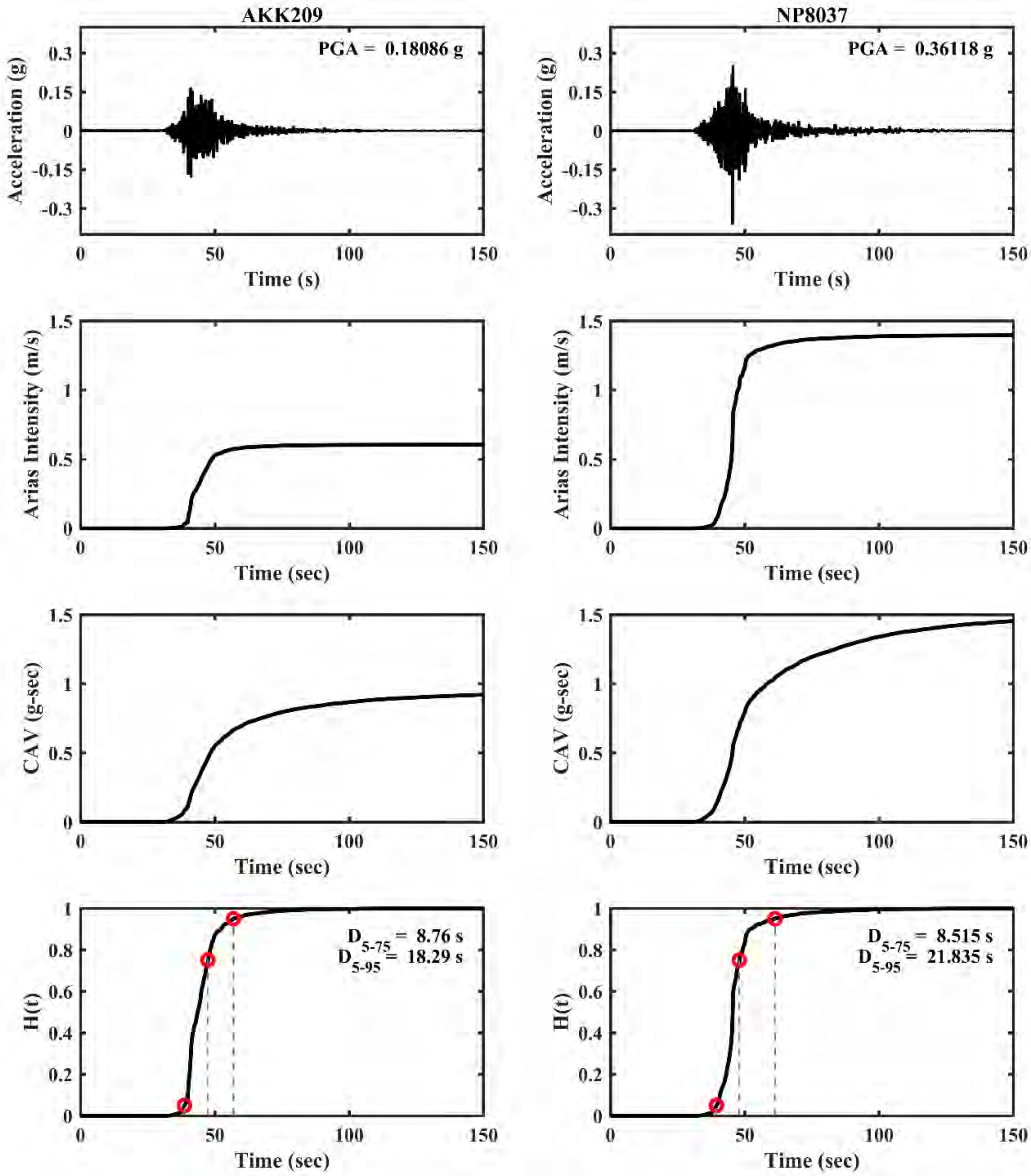

Figure 4-19. Comparison of intensity measures at stations 8037 (site class D) and K209 (site class C) corresponding to the HNN horizontal component.

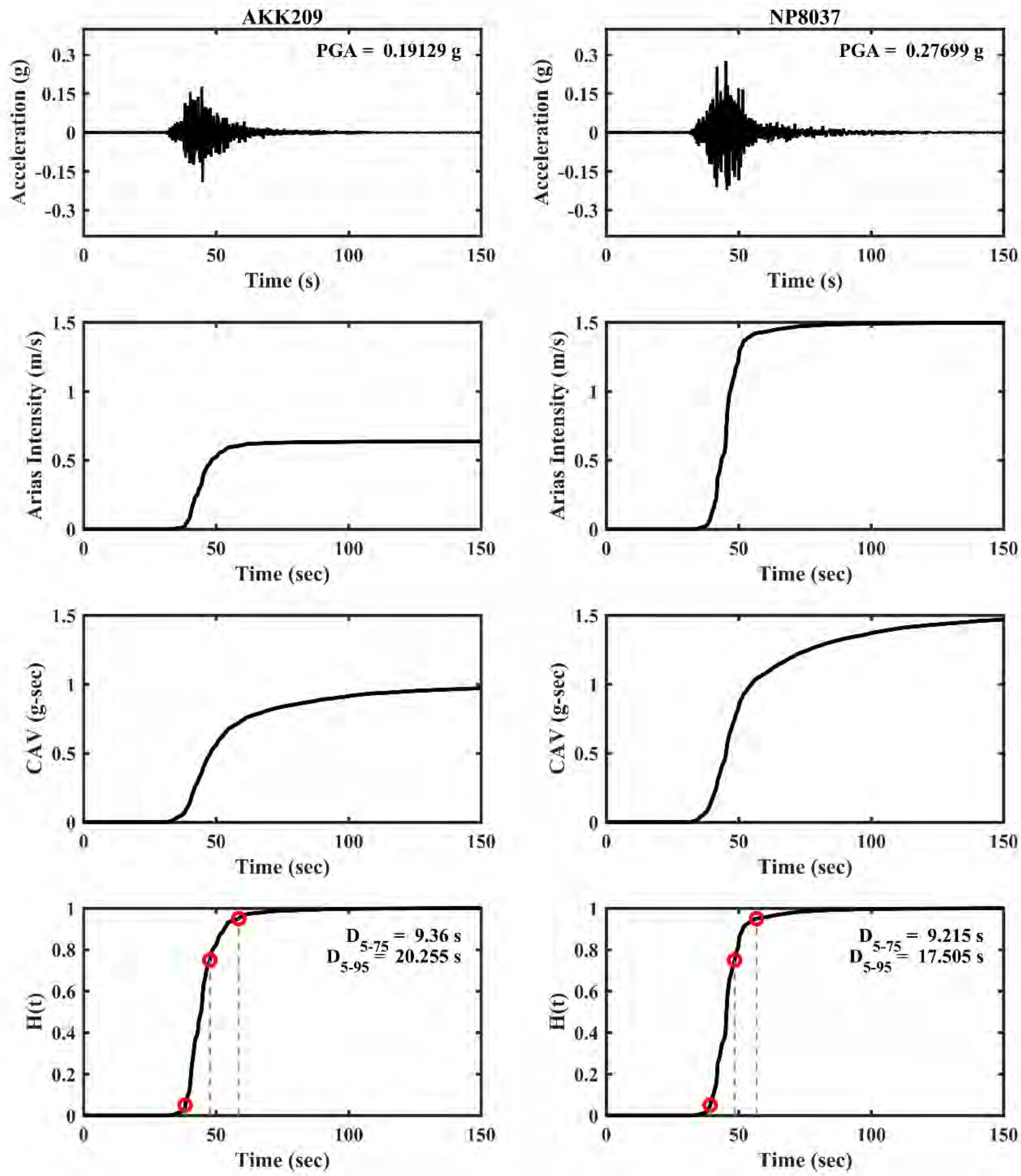

Figure 4-20. Comparison of intensity measures at stations 8037 (site class D) and K209 (site class C) corresponding to the HNE horizontal component.

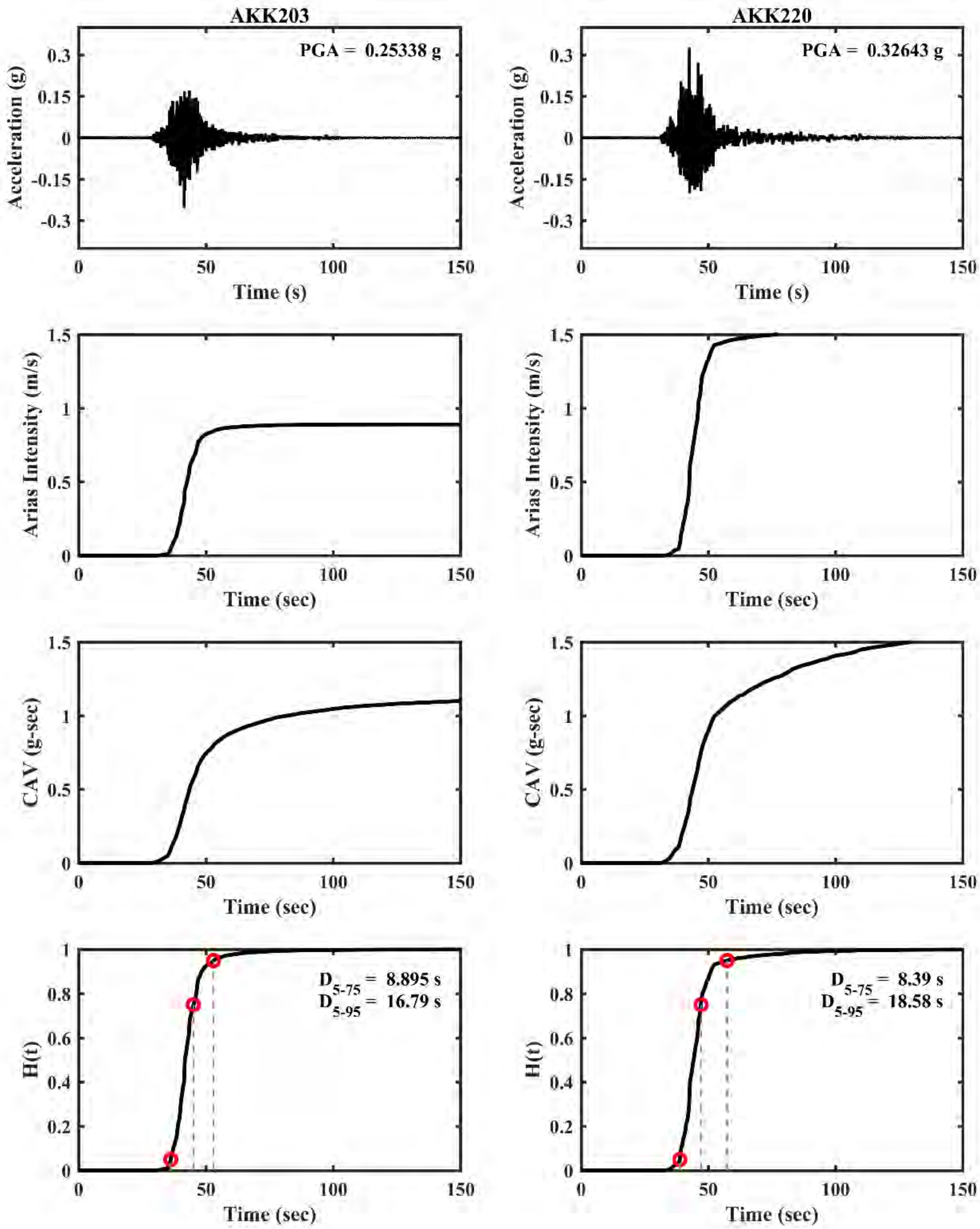

Figure 4-21. Comparison of intensity measures at stations K220 (site class D) and K203 (site class C) corresponding to the HNN horizontal component.

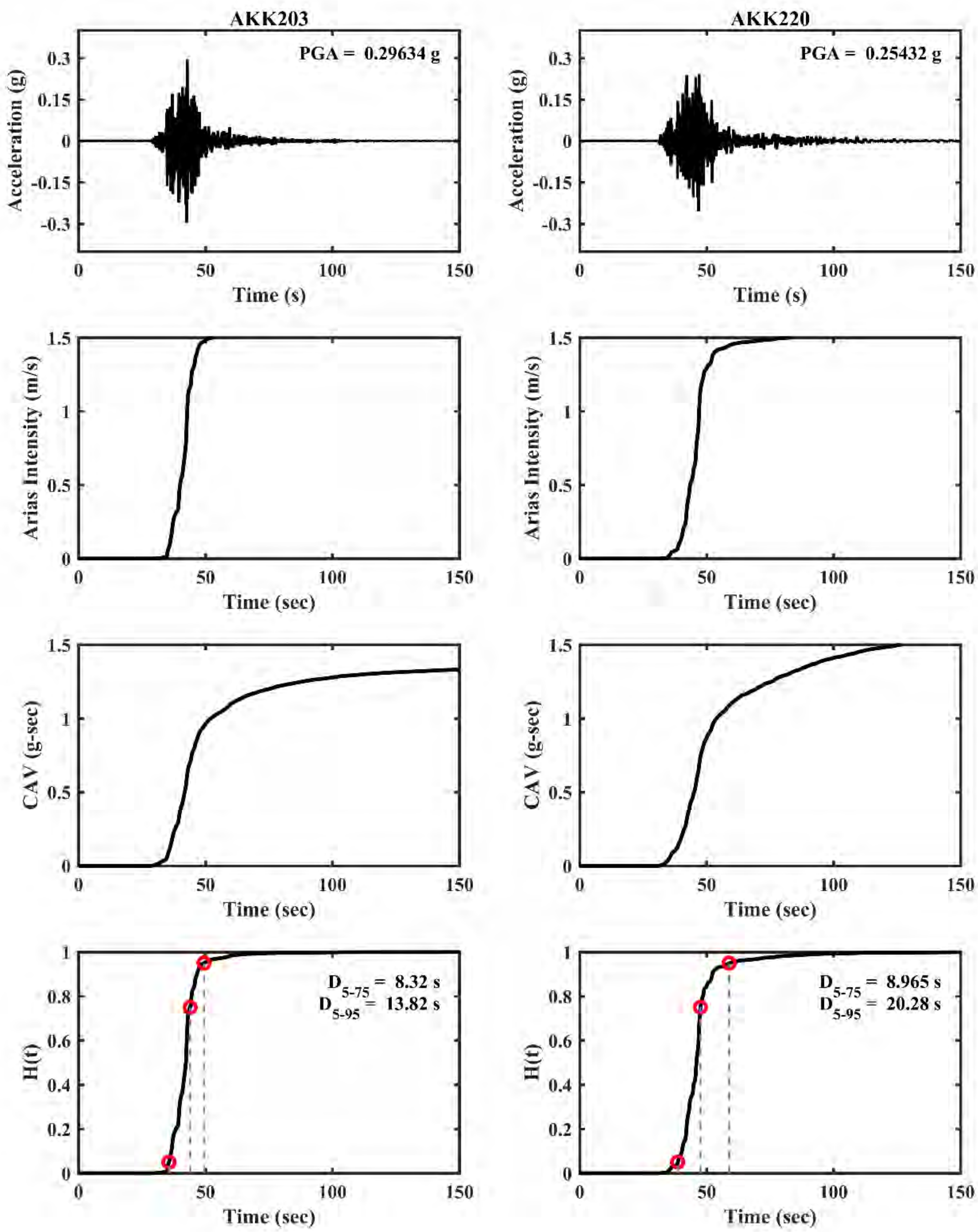

Figure 4-22. Comparison of intensity measures at stations K220 (site class D) and K203 (site class C) corresponding to the HNE horizontal component.

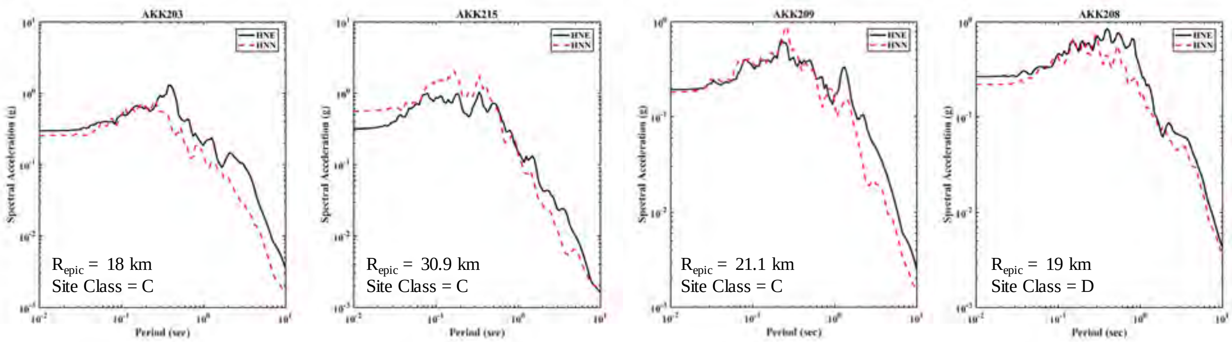

Figure 4-23. Pseudo-acceleration response spectra (5% damping) for eight horizontal components recorded at stations where directionality effects were observed.

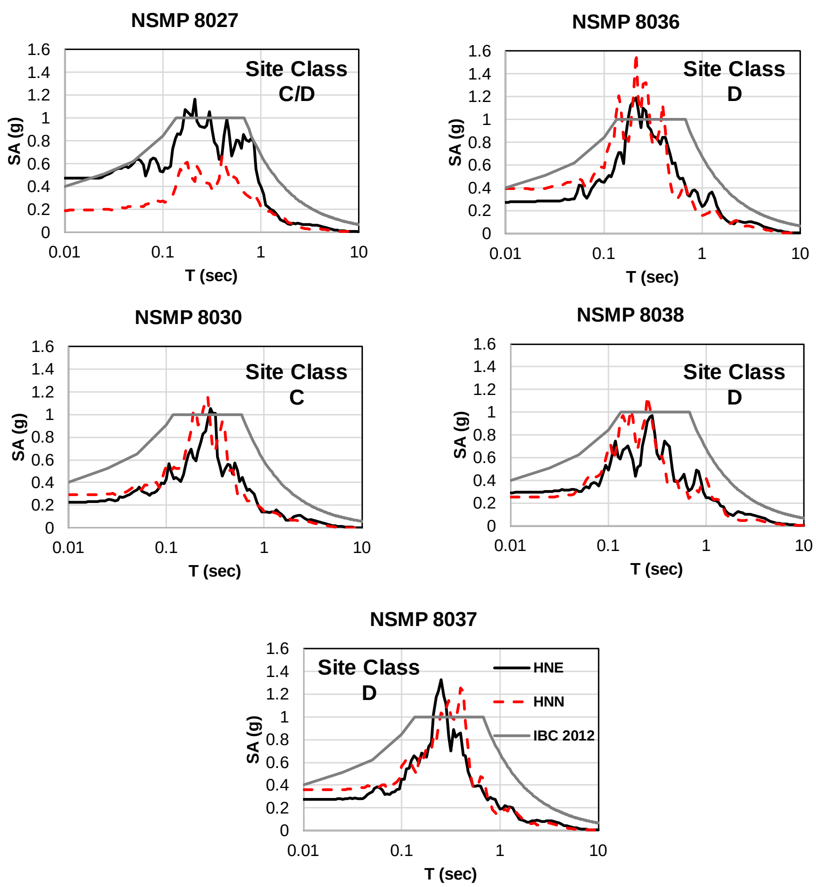

Figure 4-24. Comparison between design spectra and pseudo-acceleration response spectra (5% damping) for ten horizontal components recorded at stations visited by the GEER team in December 2018.

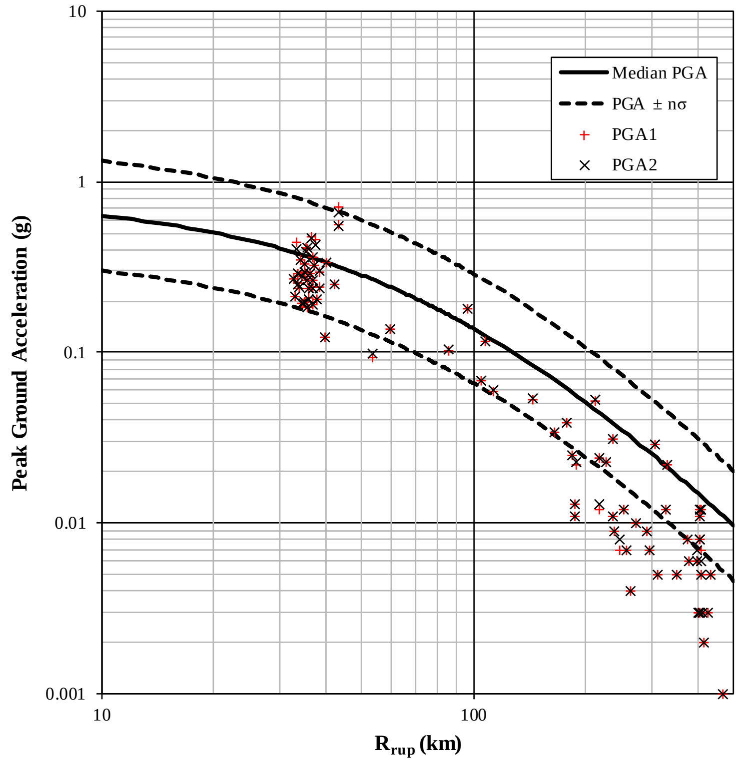

Figure 4-25. Comparison between Youngs et al. (1997) PGA estimations and observed ground motions from the M7.1 2018 November Alaska earthquake.

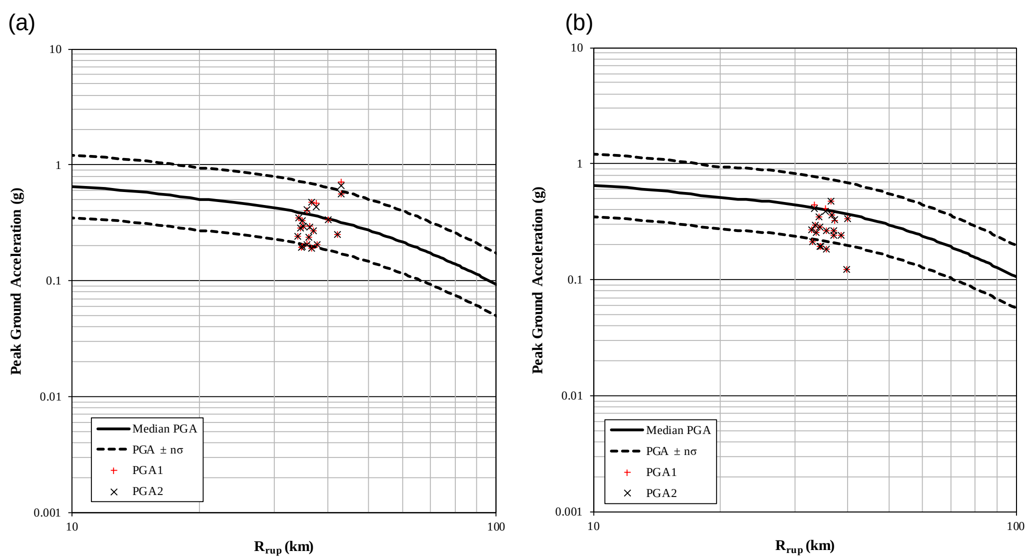

Figure 4-26. Comparison between Atkinson and Boore (2003) PGA estimations and observed ground motions from the M7.1 2018 November Alaska earthquake for (a) site class C, and (b) site class D. Only recorded motions at stations with a known or estimated NEHRP site class are shown in this figure.

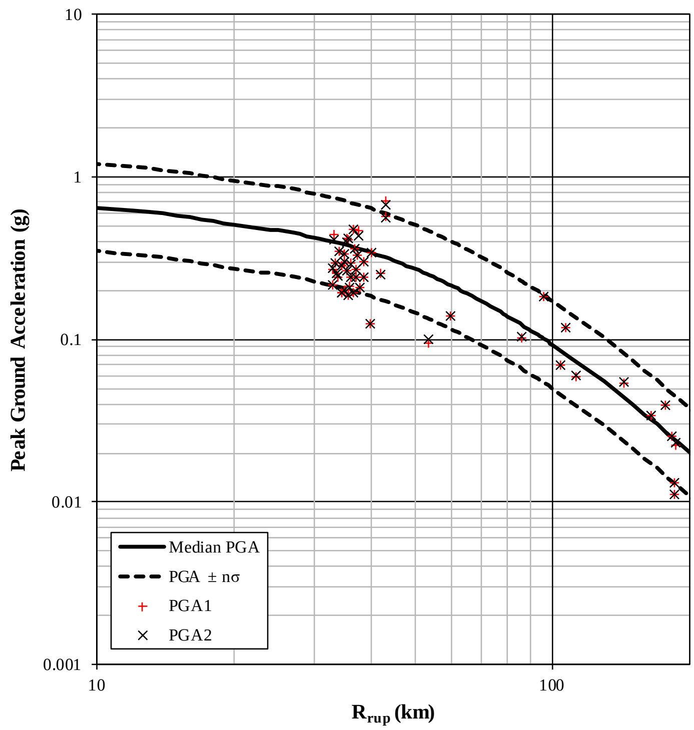

Figure 4-27. Comparison between Atkinson and Boore (2003) PGA estimations and observed ground motions from the M7.1 2018 November Alaska earthquake.

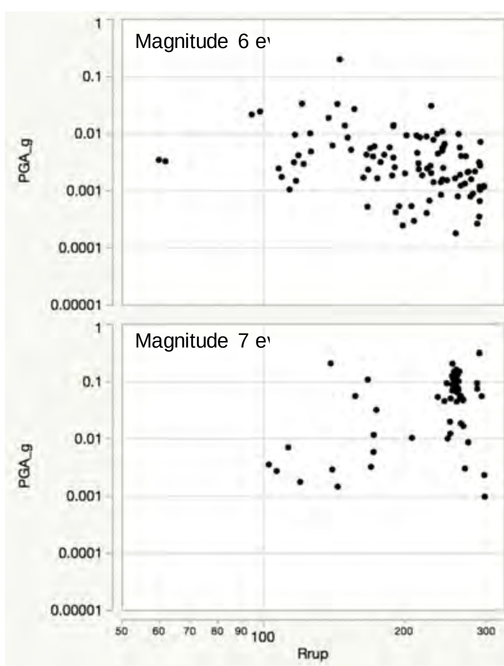

Figure 4-28. Distribution of PGA with rupture distance for the $M_w > 6$ events in the Alaska database (modified after Abrtahamson et al., 2018).

5.0 Summary of GEER Phase I Team Observations

Coordination with local officials resulted in more than 500 sites of reported damage (see Figures 1-4 and 1-5). In an attempt to learn from this earthquake, our team categorized the damage types that were reported and assigned particular emphasis to the following categories (in no particular order): highway embankment slopes and bridges, ground improvement sites, sites with various foundation types adjacent to one another, ground motion recording station sites (particularly sites with potential evidence of liquefaction nearby), historic landslide sites, sites of critical infrastructure (e.g., railroad embankments, ports), sites with potential landslide impacts to infrastructure, and sites with potential liquefaction impacts to infrastructure. Our team coordinated our daily activities based on these emphasized categories of damage, but also documented other types of significant damage that were encountered along the way.

It is important to clarify the challenging field conditions that existed during our Phase I deployment. Shortened arctic daylight hours limited our effective field time to the hours of 9:00am to 4:30pm each day. Two significant snow storms during our deployment covered the ground with more than 20 cm of snow, making the observation of surficial evidence of liquefaction and small ground deformations very challenging. During this reconnaissance, our team therefore needed to rely heavily on pre-snow observations made by other reconnaissance teams prior to our team's arrival (see Acknowledgements).

5.1. Buildings

Overall, buildings in Anchorage and surrounding communities performed well during this earthquake event. Observed damage in commercial buildings was relatively minor. More significant damage was observed primarily in residential and small commercial structures. Much of the observed damage appeared to occur due to localized liquefaction and settlement in the granular fills placed directly beneath these types of structures. Observed residential/small commercial building damage in Anchorage was not extensive but seemed to occur in pockets throughout the swampy/marshy parts of the city. Damage to residences in the Eagle River community appeared to occur primarily from seismic slope deformations.

This section provides brief descriptions of selected building sites that were investigated. Because the types of damages were similar at many sites, not all building sites that were visited are summarized and reported here.

5.1.1. Residential Damages

The majority structural damages observed during the Phase I GEER reconnaissance occurred in residential and small commercial buildings. The observed damage appeared to occur due to liquefaction-induced effects and ground failure in non-saturated fill soils, particularly settlement (Figure 5-1). Interestingly, these effects seemed to occur only beneath the structures themselves and not in the free field. Also interesting was the pattern of observed damage. For example, we would observe that one or more adjacent structures within a particular cul-de-sac would show similar evidence of liquefaction-induced damage (e.g., settlements of 1-20 cm, tilting, occasional sand boils in the crawl space, and cracking). However, the remaining structures in the cul-de-sac, often within meters of the damaged structures, would show no evidence of structural damage.

5.1.2. Alaska Native Tribal Health Consortium (ANTHC) Campus, Anchorage

The Alaska Native Tribal Health Consortium (ANTHC, Lat/Long: 61.1827°, -149.8034°) was visited by our team on Monday December 10, 2018. Paul Morrison of ANTHC escorted GEER members through the interior of buildings at 3900 Ambassador Drive and 4000 Ambassador Drive that suffered damage as described below. ANTHC also gave permission for our team to observe and document exterior conditions at these two locations and several other buildings on campus (4115 Ambassador Drive, 4141 Ambassador Drive, 4001-4043 Tudor Centre Drive, and 4315 Diplomacy Drive) which did not have any reported damage, except for minor nonstructural damage.

Facility operations at ANTHC were relatively uninterrupted. Electrical power system redundancies allowed power to continue throughout and after the event without the use of the backup generator. Surgeries and procedures were paused during the event but were resumed and completed after the event.

5.1.2.1. 3900 and 4000 Ambassador Drive, Anchorage

3900 and 4000 Ambassador Drive (Lat/Long: 61.1821°, -149.8066° and 61.1828°, -149.8061°) are founded on steel pipe piles ranging in length from 12 to 15 m with diameters of 325 or 610 mm and installed with one, two, or three piles per building column. Damage to the interior of 3900 Ambassador Drive appeared limited to the entryway (sliding glass doors and access doors in the front vestibule were damaged, and settlements on the order of 10-22 mm were observed). Walls and door entryways resting on the slab-on-grade placed in between pile caps and providing access to offices along the exterior of the northeast corner also experienced settlement and tilt ranging from 5-10 mm and 1.2-3.1 degrees, respectively. Settlement of sloped fill immediately outside the building at these locations reached magnitudes of up to 100 mm, indicating that the ground loss of soil supporting the interior slabs resulted in movement relative to the pile caps. Damage to the interior of the adjacent (and internally-connected) 4000 Ambassador Drive building manifested in terms of loss of serviceability of some doorways and cracking of drywall along the eastern margin of the building. Along the eastern exterior of the building, an unconnected brick deck structure that had previously experienced settlement and lateral movement exhibited further movement downward and outward toward the pond to the east as a result of the earthquake (Figure 5-2). This outward lateral movement manifested over the length of the building exterior and joined at the concrete walkway and stairs separating this building and 3900 Ambassador Drive.

5.1.2.2. 4115 Ambassador Drive, Anchorage

4115 Ambassador Drive (Lat/Long: 61.1841°, -149.8043°) is founded on shallow foundations overlying ground improved by deep dynamic compaction. An inspection of the building exterior by the GEER Team revealed little signs of damage. A short portion of the exterior concrete walkway adjacent to the northeast corner of the building exterior and approximately 6 m in length appeared to have settled 5 to 15 mm relative to the wall. A portion of this walkway supported HVAC or similar type of equipment.

Inspections of the building exteriors at the following locations also revealed little signs of damage:

- 4141 Ambassador Drive (piles)
- 4001 Tudor Centre Drive - Patient Housing at ANMC (excavate+replace, shallow foundations)
- 4043 Tudor Centre Drive - North Parking Structure (trash fill, shallow foundations)
- 4315 Diplomacy Drive - Hospital (shallow foundations, staging area for old asphalt plant)

5.1.3. Department of Fish and Game Building, Anchorage

The Alaska Department of Fish and Game Building (333 Raspberry Rd, Anchorage; Lat/Long: 61.1593°, -149.8879°) showed signs of significant stress from settlement beneath the south wing of the building. The two-story wood frame structure is shaped as an “L.” Ground cracking was observed within about three meters of the structure, and the ground had visibly settled up to 16 cm directly along its east side. Employees in the building reported interior settlements “of about 1 foot (25 cm),” though those claims could not be substantiated by our team because that portion of the building had been evacuated and was closed to all non-essential personnel. Figure 5-3 shows the type of damage that was externally visible at the Department of Fish and Game building. No surface evidence of liquefaction was visible beyond about three meters from the building, suggesting that these observed effects may have been limited to beneath the building footprint.

The observed settlement, indicating possible liquefaction, at the Department of Fish and Game Building is particularly significant because a ground motion recording station (NP 8027) is housed in a small warehouse next to the building, within about 30 meters of the observed damage.

5.1.4. Jamestown Drive, Anchorage

A series of condominium units (Lat/Long: 61.12951°, -149.84587°) were associated with significant settlement of up to 30 cm (Figure 5-4). Cracks extending across the front driveways of the units were about 7 cm wide and up to 23 cm deep. Fine sand was ejected onto the surface along deformation cracks. During the GEER team inspection, construction crews were using a vacuum truck to remove foundation materials from below the garage of one unit, presumably to backfill with more stable materials.

5.1.5. Houston Middle School, Houston

Initial inspection of the red-tagged Houston middle school (Lat/Long: 61.58634°, -149.77191°) indicated that there was limited evidence of damage to the exterior of the building, generally limited to minor cracking and dislodgement of several facade bricks from walls and the tops of columns (Figure 5-5). However, after discussions with the Mat-Su Borough emergency manager it was learned that the school had suffered extensive structural damage to the ceiling and the interior of the building and was not expected to reopen. Large chunks of concrete were reported to have fallen through the interior ceilings, and critical structural supporting elements inside the building were reported to have failed. Our team was not allowed inside the building due to safety concerns.

5.1.6. Downtown Eagle River

Extensive non-structural damage was observed throughout the main business district of Eagle River (Figure 5-6). Many businesses had broken windows and extensive water damage from broken water pipes. One building, including Garcias Cantina (Lat/Long: 61.32774°, -149.57280°), was associated with separation of support columns from the ground. Most of the support columns were cracked at their bases. Structural damage was also observed at an Eagle River pawn shop (Lat/Long: 61.33401°, -149.56367°) where the tilt-up cinder block walls panels had rotated out and interior ceiling was partially collapsed inward. The walls had been braced and repairs were underway when our team was onsite.

5.2. Bridges

In general, our Phase 1.0 reconnaissance team observed relatively little problems with bridges. By the time of our deployment, all AKDOT bridges in the region had already been inspected by AKDOT personnel, and areas of potential problems had been identified. Nearly all documented bridge problems involved settlements and lateral movements in the approach fill at one or both of the abutments, resulting in compression of the bridge deck and slight rotation at the affected abutments.

Our team inspected and confirmed all of the bridge problem sites communicated to us by AKDOT. All of these bridges were operational at the time of our Phase 1 deployment. This section summarizes our observations from a few of these bridge sites.

5.2.1. West Dowling Road Bridge, Anchorage

Members of our team visited the W. Dowling Rd. Bridge (AKDOT Bridge No. 2273, Lat/Long: 61.1655°, -149.8977°) on 10 and 12 December 2018 to observe the post-earthquake condition. Observations made by the team were supplemented by AKDOT inspection photos shared with the team by David Hemstreet, State Foundation Engineer of AKDOT. This three-year old bridge is a single span, 61 m long and 30 m wide steel box girder bridge and serves as an overpass of Arctic Boulevard and tracks owned by Alaska Railroad (Figures 5-7 and 5-8). The abutments are of the cantilever retaining wall type and founded on shallow foundations with dimensions of 7.3 m in width and 29.9 m in length, with the approach fill retained using mechanically-stabilized earth (MSE) walls. The bridge arcs to a heading southwest from the northeastern approach of W. Dowling St. with an approximate radius of 300 m. A large (approximately 10 to 12 m) culvert/tunnel (AKDOT Culvert No. 4100) retained by the MSE wall and accommodating two lanes of traffic on the western on-grade spur of W. Dowling Road lies immediately southwest of the overpass and under the southern approach fill.

General subsurface conditions for the site consist of 2 m of fill overlying 2 m of peat, then 5 m of loose to medium dense, non-plastic to low plasticity silt (with uncorrected SPT blow counts ranging from 5 to 15 bpf), transitioning to medium stiff to very stiff sandy silt, silt with sand, silt, and occasionally silty clay to 33 m depth, underlain in turn by very dense, glacially overridden gravel identified as glacial till (Yamasaki et al., 2015). Where exhibiting plasticity, the uppermost loose and soft silt layer was characterized with plasticity indices of 3 and 4, and water contents larger than the liquid limit. A sample boring and penetrometer log from the site is presented in Figure 5-9, where the penetrometer resistance is equal to the number of blows required to drive a steel rod with diameter of 64 mm a distance of 0.30 m with a 1.51 kN automatic hammer falling 0.76 m.

Design concerns ranged from static global stability and consolidation settlement during construction of the 12 m tall, cantilevered wall abutments and MSE wall approaches to seismic stability and settlement performance. Following consideration of a range of foundation alternatives at the site, wet soil mixing was selected for ground improvement of the peat and liquefaction-susceptible silt deposit with bridge abutments supported on shallow foundations (Yamasaki et al., 2015). Deep soil mixing (DSM) consisted of 2.44 m diameter columns arranged to form shear panels (i.e., secant-type walls) with 90% area replacement ratio under the spread footings supporting the skewed bridge abutments and 50% area replacement ratio in front of and behind the abutments (Figure 5-10). The DSM shear panels extended 10.7 m in width beyond the front of each abutment footing, and 9 m beyond the sides and behind each abutment footing. The design depth of treatment was 6 m below Elevation 29.87 m (98 ft, Figure 5-10). Compacted aggregate base course was specified to bear on top of DSM with a thickness of approximately 1.8 m to the bottom of the footing at Elevation 31.7 m (104 ft, Figure 5-10). Figure 5-11 presents an aerial photograph of the site under construction, with installation of the DSM columns for the West abutment underway, and the spread footing formed and poured at the East Abutment.

Post-earthquake inspections revealed a range of light damage; however, overall, the bridge and approaches performed well. Guardrails spanning expansion joints appeared slightly buckled at the extreme fiber of the strong direction, and light I-Sections supporting guard rails appeared to have buckled flanges and webbing (Figure 5-12).

Expansion joints appeared to have exhibited pounding with shear cracks observed along the northeast abutments and a relative permanent displacement parallel to the joint of approximately 25 mm (Figure 5-13). Spalling and/or delamination of concrete for several shear keys along both abutments indicated transverse interaction of the bridge deck and superstructure with the abutment substructure (Figure 5-14; Escamilla, 2018). Expansion bearings visible to the AKDOT inspection team appeared fully extended with little capacity for future relative movements: this indicates that the abutments may have moved closer to one another. Measurements of abutment tilt by our team showed that the southwestern abutment wall tilted away from the approach a maximum of 1.1 degrees on its eastern edge reducing to 0.4 degrees on its western edge. The northeastern abutment exhibited less tilt, with zero tilt along its western edge to 0.4 degrees away from the approach (and towards the span) along its eastern edge. These observations were consistent with the loss of expansion of the superstructure noted by AKDOT.

Minor spalling was observed at the abutments and MSE wall fascia panels. MSE wall panels retaining fill over and adjacent to the large culvert rotated towards the culvert on both sides of the culvert and approach fill and exhibited movements characterized by panel gap closure and extension of up to 75 mm, and tilt of up to 4.2 degrees (Figures 5-15 and 5-16). Several bearing pads exhibited unloading or loading, depending on the direction of tilt of the fascia panels.

No ground failure or signs of large differential soil movements were observed at the bridge approaches and abutments. A minor slope failure on the southern face of the eastern approach was noted, exhibited spreading-type cracks 100 mm wide and characterized by vertical scarp faces 300 mm tall. Planted saplings exhibited significant rotation commensurate with the slope failure (Figure 5-17).

5.2.2. Glenn Highway Bridges, Eagle River

The Glenn Highway is the primary land transportation route between Anchorage and the communities/cities located to the north. This highway includes two parallel bridges over the Eagle River (Lat/Long: 61.310746°, -149.578015°).

5.2.2.1. Northbound Bridge

The northbound Glenn Highway Bridge is a relatively new multi-span reinforced concrete bridge supported by multi-column reinforced concrete bents. The north abutment of the bridge has a 1:1 reinforced soil spill slope, and the abutments of the bridge are skewed.

Abutment movements at the southern abutment of the northbound bridge (Lat/Long: 61.310222°, -149.577127°) were observed and documented. These movements included settlement of 20-30 cm in spill slope (Figure 5-18) and unknown minor lateral movements that appeared to mobilize passive earth pressure behind the skewed abutment face. These earth pressures initiated minor rotation of the abutment (1-3 cm). Large (44 cm H-Piles) were exposed in the settlement-induced gap below the abutment stem wall. Inspection of the columnar bents supporting the bridge revealed minor to no damage. One 2cm-wide crack was observed around a large bent foundation indicating mobilization during the earthquake, but no concrete spalling.

No damage was observed at the northern abutment of the northbound bridge.

5.2.2.2. Southbound Bridge

The southbound Glenn Highway Bridge is an older multi-span reinforced concrete bridge. Reinforced concrete girders rest on flexible bearing pads and are visible for inspection. Inspection of the southern abutment revealed evidences of soil deformation at the abutment. No gap existed between the ends of the girders and abutment wall. Settlements of up to 3 cm were measured in the spill slope in front of the abutment. The bearing pads supporting the girders showed straining and deformations of up to 3 cm (Figure 5-19). Minor cracking and downslope movement were visible in the spill slope soils, but it was unclear if those cracks developed from the earthquake or prior movements due to static loads.

No damage was observed at the northern abutment of the southbound bridge.

5.2.3. Briggs Bridge, Eagle River

Members of our team visited the three-span, 186.3 m long Briggs Bridge (Lat/Long 61.298490°, -149.539713°) spanning the Eagle River south of the town bearing the same name on 11 December 2018 to inspect the approaches, abutments, and wingwalls (Figure 5-20). This bridge is a steel girder and truss diaphram-type structure and appears to have been constructed in 1990. The wearing surface of this bridge lies approximately 23 m above Eagle River at mid-span. Piers 2 and 3 (Figure 5-20) are supported on pile caps containing a combination of vertical (21 total, 3 x 7) and battered (74 total, two sets of 2 x 16 along longitudinal axes and two sets of 3 x 7 along transverse axes), steel HP12 and HP14 pile sections (Figure 5-21). The 35 m wide bridge abutments (stepped to match superelevation of wearing surface; Figure 5-22) consists of typical stem wall-abutments founded on two rows of HP12 sections (inner piles battered to resist overturning, outer piles vertical).

Subsurface conditions were explored with borings and penetrometers typical of Alaska geotechnical practice. Penetrometer soundings provide a penetrometer resistance defined as the number of blows required to drive a steel rod with diameter of 64 mm a distance of 0.30 m with a 1.51 kN automatic hammer falling 0.76 m. Subsurface conditions at the south abutment were explored prior to approach fill embankment construction and consisted of 4 m of medium dense silty sand and very stiff sandy silt, over 3 to 5 m of very stiff to hard sandy silt and silt, with transition to 3.5 m of silt, clayey gravelly sandy silt and silty sandy gravel with cobbles along the east end of the abutment, over the basaltic greenstones of the McHugh Complex Rock (depth of 11 m at the east rising to 7.5 m to the west). At the north abutment, shallow borings in the native, pre-construction slope revealed medium stiff to hard silt and medium dense to very dense sand, silty sand, gravelly sand, and silty sandy gravel to depths of 6 m. Penetrometer resistance ranged from 19 to 90 blows per 0.3m and terminated at depths ranging from 3.5 to 5.5 m. A nearby, downslope boring indicated 10 m of very dense silty sandy gravel with cobbles and boulders, over interlayered deposits of hard and very dense sandy silt and silt and silty sandy gravel to the termination depth of the boring (48.5 m). Subsurface conditions at Pier 2 consisted of interbedded very stiff to hard silt and sandy silt and sandy gravel and sandy silty gravel to a depth of 20 m, over the McHugh Complex Rock. Subsurface conditions at Pier 3 consisted of a deep deposit of very dense silty sandy gravel with occasional interbeds of clayey silt, sandy silt, and sand to a depth of 38 m, over the McHugh Complex Rock. Groundwater elevations varied with topographical features and was generally identified 1 to 6 m below the ground surface elevation.

The reconnaissance team made several observations regarding the seismic performance of the Brigg's bridge and approaches. The side slopes along the eastern edge of the north abutment approach fill exhibited an approximately 0.3 to 0.45 m vertical scarp, running north-south parallel to the highway, and accompanying downhill movement (Figure 5-23). The sloped fill against the southeastern edge of the abutment stem/pile cap moved outward 75 to 100 mm, increasing towards the east and the wrap-around side slope (Figure 5-24). Numerous tension cracks were noted along the bare soil slope mantling the southern portion of the north abutment under the bridge girders. Slope movements of 100 to 150 mm south (Figure 5-25), and 65 mm west (Figure 5-26), were observed adjacent to the western edge of the north abutment, with settlement of the soil slope relative to the piled abutment on the order of 100 mm at the southern edge and 200 mm along the western edge above the stem wall. The abutment itself appeared to have translated slightly to the east and settled on the order of 12 to 75 mm, as demonstrated by several tilted bolts and hex nuts hung well above the girder bearing plates (Figure 5-27). Numerous existing vertical cracks within the abutment stem wall appear indicated signs of recent movement, likely associated with the strong ground motion of the 30 November earthquake. Tilt of the northern abutment was observed equal to 1.2 and 1.8 degrees backwards (towards the approach fill) on the western and eastern sides, respectively.

At the south abutment, surrounding soil conditions were obscured by ice and snow. Evidence of soil movement or cracking was not observed beneath the bridge when moving from the east to west side. The bolt on the west side was in a vertical position while the bolt on the east side was observed to have tilted inward toward the abutment. Looking north from the south abutment, minor slope failures were observed at the north abutment and extending west in slopes along the river.

5.3. Utilities

A meeting between members of our team and Stephen Nuss, an official with Anchorage Water and Wastewater Utility, occurred on December 13, 2018. At the time of that meeting, 171 AWWU assets had been inspected. Of all those assets that were inspected, only three were assigned yellow tags to identify need for repair. At the time of our meeting, 50 breaks in water and sewer lines had been identified. 28 of those breaks were identified by the end of November 30, the day of the earthquake. Failures in water pipes were limited to locations where pre-existing weaknesses existed. For example, locations of unrestrained pipes, shackled points that were heavily corroded, valves with corroded gray iron bolts on the bonnets, or older cast iron pipes. Two of the problem areas occurred due to "geotechnical failure" in the slopes west of the Briggs Bridge in Eagle River and at Turnagain Heights. Detailed locations of these reported geotechnical failures were not provided to our team at the time of our meeting. Failures in sewer pipes continue to be more difficult to locate. AWWU must rely on reports of backed up sewage lines in residents' homes to identify areas of potential breaks or damage. Between 1977 and 1999, AWWU extensively used ductile iron for its piping. More recently, AWWU uses AWW-C900 PVC for its piping due to its corrosion and chemical resistance, its combination of rigidity and flexibility, its cost, and its size compatibility with ductile iron.

A meeting between members of our team and Archie Giddings, director of Wasilla Department of Public Works occurred on December 11, 2018. It was communicated to our team that only two water line breaks had occurred in the system, and they had already been identified and repaired. Wasilla incorporates a pressurized sewer system, which makes it easier to identify leaks in the system. As of December 11, no known leaks were identified in the pressurized sewer system.

Wasilla incorporates high density polyethylene (HDPE) for all of its water and sewer piping. The two identified breaks in the water line occurred at fused joints in the piping.

No gas line breaks were identified in Anchorage or surrounding communities. However, localities of other damage to Anchorage Water and Wastewater Utilities infrastructure are shown on Figure 1-5B. At the time of this writing, specific details on the nature of these damages were not available.

5.4. Slopes and Embankments

5.4.1. Anchorage Area

5.4.1.1. Rabbit Creek Landslide Complex, Anchorage

Collaborators from the USGS indicated that they had observed significant sliding in the vicinity of Rabbit Creek, located in southeast Anchorage next to the Cook Sound. Our team visited and confirmed the landsliding (Lat/Long: 61.0912°, -149.8470°). These slides along the coastal bluffs in the vicinity of Rabbit Creek are associated with bluff cracking, multiple individual small slide blocks, and appear to extend for kilometers in both directions along the bluffs. The larger landslide complex was associated with southwest directed translational failure of weak glaciodeltaic deposits. Headscarps were observed to range from 2-4 meters high and encroached within 50 meters of the railroad line. Landsliding in this area also occurred during the 1964 earthquake (Potter Hill landslide), indicating that the bluffs are particularly susceptible to slope failures in this area. Figure 5-28 presents an image of the head scarp of the landslide.

5.4.1.2. Bluff failure Port of Alaska, Anchorage

A small slope failure occurred above the Port of Alaska in a public park (Lat/Long: 61.2303°, -149.8849°). Here a crack along the top of the bluff extended for ~50 m set back ~1-3 m from the edge of the bluff (Figure 5-29). The crack was generally arcuate and up to ~20 cm wide, 50 cm deep, and had limited vertical separation. There was sufficient motion in some locations to rotate a few signs and trees. On the day of the visit there was considerable snow which may have covered more extensive cracking. This slide poses a hazard to storage tanks located along the base of the bluff on the port property, and should be monitored.

5.4.1.3. Minnesota Boulevard embankment failure, Anchorage

A large embankment failure occurred along the northwest side of the north bound highway off ramp at Minnesota Boulevard and International Airport Road (Figure 5-30, Lat/Long: 61.171279°, -149.915547°). The failure was related to lateral spreading or slumping failure of the off-ramp fill resulting in cracking and settlement of the road making it impassable. The Alaska Department of Transportation & Public Facilities (AKDOT&PF) had the road repaired and restored to service by December 4, thus the GEER team was not able to directly observe the damage. Due to the cold weather and snow, the repairs are temporary until more permanent fixes can be accomplished in warmer weather. Based on inspection of photographs, the failure was associated with back tilting and down dropping of the roadway of at least 8 feet and was approximately a hundred feet long. Additional cracking of the roadway on the highway side of the off ramp was several feet wide and deep over a similar length.

5.4.2. Eagle River Area

5.4.2.1. Rivers Edge condominiums, Eagle River

Landsliding along the eastern side of River Heights Loop road in the Rivers Edge condominiums residential area in Eagle River resulted in the yellow-tagging of numerous homes and elevated concern regarding the potential for additional landsliding (Figure 5-31). The GEER Phase I team observed several landslide scarps along the steep slope extending above the eastern margin of the neighborhood. A small slump block (Lat/Long: 61.312346°, -149.571359°) approximately 80 feet long released from the basal part of the slope and was associated with a 5-6 foot high headscarp. This toe of this slide displaced a small shed from its foundation and buckled the fence. The scarp associated with this slide projects obliquely up the slope and is in line with major cracks in the flat graded property above the crest of the slope (Lat/Long: 61.312065°, -149.570379°). Cracks in the upper surface were observed to be about 3 inches wide and up to 4 feet deep and extend for over 325 feet subparallel to and 60 feet east of the crest of the slope. The cracks intersect a warehouse building where 3 inches of separation were noted between the building and the soil. At the southern edge of the graded property the crack was associated with 9 inches of vertical separation. The cracking of the surficial materials along the crest of the slope raised concerns regarding the potential for additional landsliding hazards for the residences below. Potential additional sliding is currently being evaluated by the local geotechnical engineering community.

5.4.2.2. Ptarmigan Drive neighborhood, Eagle River

Wall cracking was observed at several residences in the Ptarmigan Drive neighborhood in Eagle River likely related to strong ground shaking. Rock walls surrounding properties were noticeably shaken, with loose rocks dislodged from several walls. At one residence (Lat/Long: 61.30494°, -149.49582°), extensive cracking and failure of the brick facade was observed (Figure 5-32). At this house, a large back patio was associated with fence buckling, subtle backtilting of the yard surface, and cracking of the patio. The cracks projected to the margin of the house where a small side room was displaced from the house. A steep slope extends to the west of the slope, suggesting that the failure was related to landsliding along the steep valley margin.

5.4.2.3 Old Glenn Highway, MSE Wall Movement

Members of the GEER team visited the site of noted MSE wall movement along the Old Glenn Highway in Eagle River, Alaska, on 11 December 2018. The site was part of a recent (within the last 10 years) improvement running approximately six miles from Lower Fire Lake to Ski Hill Road, with construction to provide for safer shoulders and improved drainage. Various cuts and fills required the construction of gabion and mechanically-stabilized earth walls along the roadway. One MSE wall exhibited apparent seismically-induced sliding movements as document by the GEER Team.

Based on the geotechnical report supporting the design of the improvement (Golder 2009), this vegetative-faced MSE wall was of approximately 335 m length, and ranged in height from 1.2 to 4 m tall. The MSE wall was placed by cutting into the crest of the slope supporting the Old Glenn Highway and which ranged in height from about 8.8 to 13.4 m. The natural soil slope consisted of medium dense to dense, silty, sandy gravel (GP-GM) with pockets of silty gravel and occasional cobbles, and ranged from 2H:1V to 1.5H:1V (Figures 5-33 and 5-34). Groundwater was not encountered in the borings advanced to support the design of the roadway improvements. Design documents refer to the level of shaking expected for the 475-year design earthquake, with bedrock PGA equal to 0.36g and anticipated horizontal movements of 50 to 100 mm selected as the basis for seismic design. Although final as-built construction drawings were not available to the GEER team members, recommendations called for the use of welded wire mesh reinforcement on 0.6 m vertical spacing and length of reinforcement equal to 1.67 x wall height, with minimum and maximum lengths of 2.4 to 4.8 m, respectively, for an assumed wall face batter of 80 degrees from the horizontal.

Post-earthquake observations by the GEER team revealed an approximately 35 m long crack running more or less parallel with the roadway alignment, set back from the guardrail approximately 3 to 4 m (Figures 5-34 through 5-36). The guardrail offset distance correlates with the length of the tensile reinforcement separating the reinforced soil mass from the retained soil mass expected from the geotechnical report. Measurements of the crack depth by members of the Alaska DOT indicate the maximum depth of cracking to be approximately 3 m (Hemstreet 2018), and therefore did not appear to correspond to the reinforced soil mass owing to lack of obstructions (e.g., the welded wire mesh) when sounding the depth. The width of the longitudinal crack ranged from 19 to 75 mm, with the smallest crack width corresponding to the elevation low of 105.5 m (346 ft) and the largest crack width at the elevation high of 108.2 m (355 ft). In general, the predominant crack width noted was about 38 mm wide. Little settlement of the reinforced zone of the MSE wall was noted, with a maximum settlement of 25 mm accompanying the zone corresponding to the maximum crack width (Figure 5-37). Two full-width (with respect to the roadway width) cracks running transverse to the roadway were noted: one at the initiation of the longitudinal crack at the elevation low, and one approximately 7 m beyond the termination of the longitudinal crack at the elevation high. One of the transverse cracks occurred at the location of an existing crack that had developed due to thermal contraction and had been repaired prior to the earthquake; thus, this crack simply appeared to reopen following repair and it is uncertain as to whether the noted damage was seismically-induced. The other transverse crack appeared fresh and was unaccompanied by signs of repair.

In general, the outward lateral movement unaccompanied by significant settlement points to a seismically-induced sliding mechanism under the lateral ground shaking associated with the 30 November 2018 earthquake, whereby the reinforced soil mass advanced laterally away from the retained soil mass.

5.4.3. Wasilla Area

5.4.3.1. Vine Road, Wasilla

The failure of the road surface and embankment fill along Vine Road (Lat/Long: 61.56863°, -149.60215°) south of Wasilla received considerable media attention and numerous dramatic photographs were circulated on social media (Figure 5-38). The failure was confined to where it crosses a small peat bog and had been completely repaired by the time the GEER Phase I team evaluated the site, however deformation of the ground surface was clearly evident to the west and east of the road. Team members in the field prior to the arrival of the main team visited this site on December 2 and found that the failed segment is 304 ft long with a maximum lateral movement of the centerline of 12 ½ ft to the west and a maximum settlement of up to 6 ft. Boring logs provided by Mat-Su Borough engineers indicate that the substrate consists of gravelly silt deposits and a 6 foot thick layer of silty peat. Field observations indicate that the road fill is composed of rounded gravels and cobbles with a silt matrix. The failure appears to be related to strong ground shaking of the road bed resulting in settlement into the soft saturated peat substrate, mechanical cracking of the road fill, and lateral motion of fill materials. The lateral motion caused bulldozing and buckling of the fibrous sphagnum peat characterized by arcuate 3-foot-high push-up mounds that extend about 60-70 feet away from each side of the road.

5.4.3.2. Rail embankments and support roads for the Port Mackenzie Rail Expansion Project

The support roads, embankments, and railways related to the under-construction Port Mackenzie Rail Expansion project were inspected with Mat-Su Borough engineers. On the day the GEER team visited these sites there was significant snowfall and it was difficult to observe individual features. Furthermore, the majority of the road damage had already been repaired. Borough engineers provided GEER with pre-snow photographs. Along the rail alignment, only two locations experienced earthquake effects including one location where the embankment fill settled a few inches (Lat/Long: 61.43756°, -150.08219°) and another where minor settlement occurred along the support gabions at a bridge crossing (Lat/Long: 61.46432°, -150.10007°). A failure along the Lou Young road (Lat/Long: 61.28176°, -149.93002°) occurred along a cut and fill slope (Figures 5-39A and 5-39B). This failure was arcuate in shape and approximately 30 feet long. Major cracking and settlement of the roadway at mile marker 15.5 (Lat/Long: 61.31582°, -150.02627°) was associated with cracks up to 2 feet wide and 4 feet deep and was apparently related to shaking and squeezing of the soft peat substrate (Figures 5-39C and 5-39D). Approximately, 10 additional locations of minor road cracking were also observed. Minor settlement associated with an approximately 100-foot-long crack was observed in the fill platform (Lat/Long: 61.26818°, -149.91803°) at the main port along its northeastern margin. Large light poles were tilted adjacent to this crack.

5.5. Liquefaction

5.5.1. Liquefaction Observations

Within populated areas of Anchorage, surface evidence of liquefaction was difficult to discern. Our team began site visits on Monday December 10, ten days after the November 30 event. Several inches of precipitation (rain, ice, snow) had covered the ground since the earthquake, obscuring much of the potential surface evidence such as sand boils, ejecta, cracking, or settlement. Limited to no ejecta was observed by the GEER team. Settlement and cracking were observed and may be indicators of possible liquefaction. The GEER Phase I team focused reconnaissance in the areas noted by local engineers and geologists to have liquefaction damage observations - primarily the Sand Lake and Eagle River areas of Anchorage. Observations for each area are described below.

USGS conducted fly-overs of the less populated areas surrounding Anchorage and reported liquefaction observations including sand boils and cracking. The majority of these features were located in intertidal areas and were eroded and largely removed by tidal processes by the time the GEER reconnaissance commenced.

5.5.2. Rivers Edge condominiums, Eagle River

Several single-family residential homes in the Rivers View condominiums were red-tagged as being unsafe for occupancy, with two red-tags noting observations of liquefaction. At one red-tagged home (unoccupied), ejecta was observed at one location along the foundation perimeter (Figure 5-40). At this home, the red-tag notes that the north foundation wall buckled/collapsed due to soil liquefaction. At a second red-tagged home (occupied), the ground surface was not visible due to snow cover but the red-tag notes that the north foundation wall has been “compromised/broken by extreme ground pressure and soil liquefaction.” The resident allowed a GEER team member into the backyard to observe the ground failure and damage at the back of the house. Some evidence of subsidence and cracking was visible beneath the snow and the wooden deck structure was damaged significantly (Figure 5-40). Two homes were yellow-tagged, with the tags noting “ground fissures present” and “possible shifting of foundation.” The garage floor slabs at these homes had appeared to settle (<1-2”), separating from the garage door at the edges and with one garage door frame showing minor buckling of the sash. Soil that was possibly ejecta was observed at the ground surface under the entry walkway at one yellow-tagged home.

Although red- and yellow-tagged, several homes in the Rivers View condominiums were still occupied by residents when the GEER Phase I team was onsite.

5.5.3. Ptarmigan Drive, Eagle River

Severe cracking and lateral movement indicating slope instability were observed behind two properties on Ptarmigan Drive at the top of a slope. Settlement (up to 5 inches) was observed in the walkway at one home (Figure 5-41), with horizontal movement at another location in the walkway of about 1 inch. Ground failure and possible ejecta were observed under the deck (Figure

5-41). It was unclear if liquefaction had occurred or if movements were solely due to the position of the properties at the top of the slope.

5.5.4. Sand Lake – Jewel Lake - Campbell Lake, Anchorage

Settlements on the order of 12 inches were reported for residential properties in Sand Lake, Jewel Lake, and Campbell Lake areas. Many of the damaged homes in Sand Lake suffered settlement and minor tilting but remained occupied by residents at the time of GEER's visit. GEER team members were allowed onto one residential property in the Jewel Lake area, between Dimond High School and Campbell Lake. The resident shoveled snow away from the foundation to show GEER members the settlement that had occurred (~3 inches, with crack depths of 2-6 inches; Figure 5-42). GEER members were allowed to access the crawl space under the house to observe the ground failure and possible ejecta under the house (Figure 5-43) that had occurred near the outside settlement that was observed. Settlement and damage to the back porch were observed, as was cracking in the concrete backyard walkway. The house remained inhabited.

Significant settlement of single-family homes and duplexes was observed directly north of Campbell Lake. One home, on Arlene Drive (Lat/Long: 61.13337°, -149.93126°) experienced settlement that was associated with backtilting of the home towards the road and the generation of ground cracking roughly following the original foundation excavation. In the front of the house, the driveway was down-dropped (down-to-the-south) about 1 foot and was associated with a crack up to 6 inches wide and 2-3 feet deep (Figure 5-43A). Cracks around the sides of the house were up to 3 inches wide and 8 inches deep. Both sides of the house exhibited evidence of vented sand, likely sourced from the sand backfill materials used during foundation construction. Cracking and surface bulging were also observed in the backyard and along the margin of the lake.

Nearly all of the duplexes on Ticia Circle experienced some degree of settlement and were yellow tagged by the Municipality of Anchorage. Wall separation and settlement was inspected at one duplex unit (Lat/Long: 61.13794°, -149.9380°). Several street light poles were tilted. Several duplexes appear to have settled downward approximately 1-2 feet. The settlement was confined to the margins of the duplex foundations and caused deformation of stairways and formation of ground cracks that projected towards the driveways (Figure 5-43B).

5.5.5. C Street & Dowling Road Intersection, Anchorage

The GEER team received reports of settlements of 300 to 450 mm at the intersection of C Street & Dowling Road. At the time of GEER's visit, no settlement was visible below the snow or at traffic sign and signal pole foundations for the majority of the intersection and approximately 50 m down each of the intersecting roads. A concrete footing for an electrical junction box located at the northwest corner of the intersection experienced settlement of 50 mm at the northwest corner and 25 mm at the northeast corner (Figure 5-44), tilting preferentially towards the adjacent ground behind the sidewalk that sloped down to a small open culvert and marshy area. The open pipe culvert did not appear to be damaged. From the intersection sidewalks, a large crack running north from the south approach and arcing west through the center of the intersection could be observed; however, measurements of differential settlement or crack width could not be made due to the active traffic within this intersection.

5.5.6 Additional Observations

GEER team members continued to receive reports of liquefaction at residential structures following completion of the Phase 1 field reconnaissance. There appears to have been hesitation by homeowners and property owners to report liquefaction observations and related damage due to the possibility of the home or building being red-tagged, potentially impacting the current occupants and potential future valuation of the property. The 30 November earthquake occurred during the November-December US holiday season, heightening the potential disruption to family and community activities for residents whose homes had been red-tagged.

At one site, the GEER team received photos of sand boils and ejecta from the resident who documented the damage immediately following the earthquake (Figure 5-45). The resident had also taken bagged samples of the ejecta, which were shared with the GEER team. Particle size analysis was performed at the University of Alaska Anchorage soils laboratory. Based on the particle size distribution shown in Figure 5-46, the ejecta was classified as a well-graded silty fine sand (25% fines content).

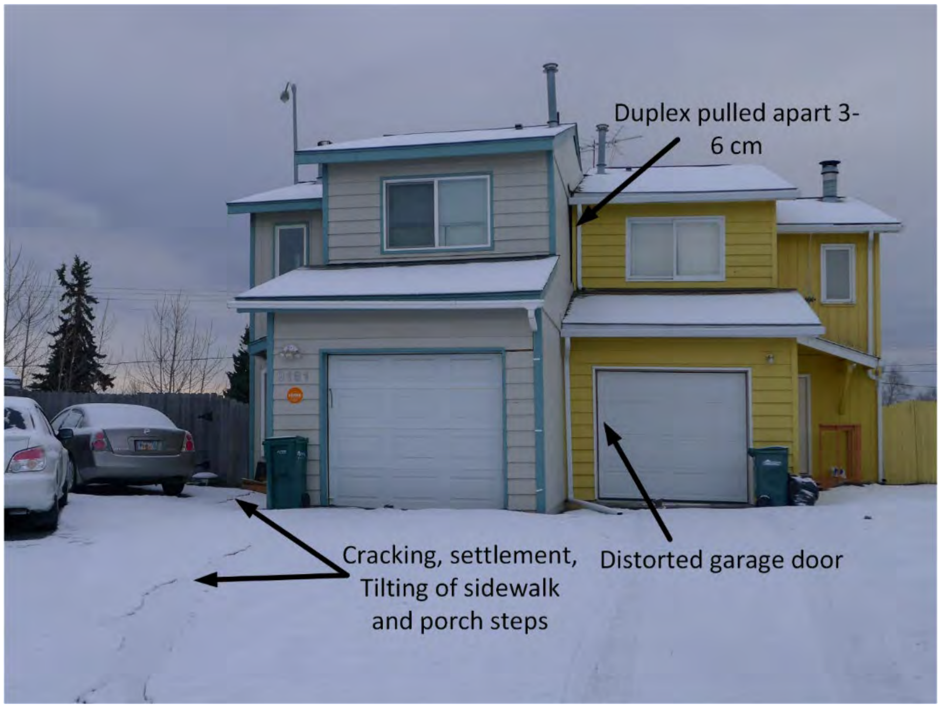

Figure 5-1. Example of the type of localized liquefaction-induced damage observed at many residences in Anchorage. In this example, slight settlement of the home is noted by cracks around the perimeter of fill materials (Lat/Long: 61.134291°, -149.919308°).

Figure 5-2. 4000 Ambassador Drive - brick deck structure exhibiting settlement and lateral movement (Lat/Long: 61.1826°, -149.8061°).

Figure 5-3. Photo of observed settlement at the south wing of the Alaska Department of Fish and Game Building (Lat/Long: 61.1592°, -149.8879°).

Figure 5-4. Settlement of condominium units along Jamestown Drive, Anchorage (Lat/Long: 61.12951°, -149.84587°). (A) Settlement cracks along the front driveways (black arrows). (B) Repair crews removing backfill materials.

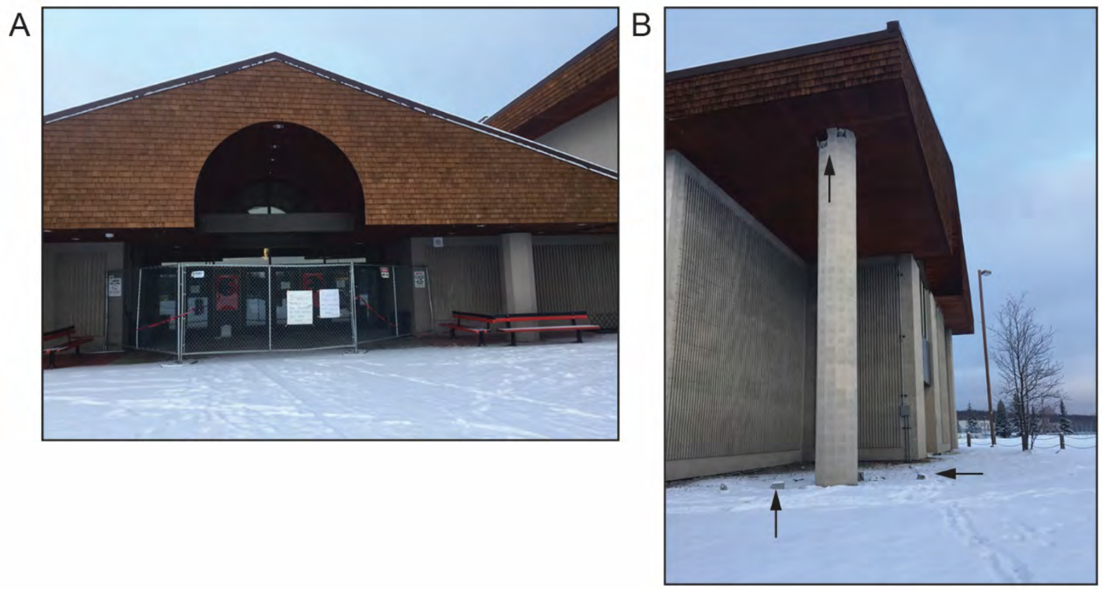

Figure 5-5. Red-tagged Houston Middle School in Houston (Lat/Long: 61.58634°, -149.77191°). (A) Fenced off entrance to the school. (B) Support column along southwest side of school showing displaced facade bricks (black arrows).

Figure 5-6. Building damage in downtown Eagle River. (A) bowing of the cinder block walls of the Eagle River pawn shop (Lat/Long: 61.33401°, -149.56367°), (B) partial collapse of the ceiling in the Eagle River pawn shop (Lat/Long: 61.33401°, -149.56367°), (C) sheared and cracked columns in the Garcias Cantina building (Lat/Long: 61.32774°, -149.57280°), and (D) water damage and ceiling tile failure in the Garcias Cantina building (Lat/Long: 61.32774°, -149.57280°).

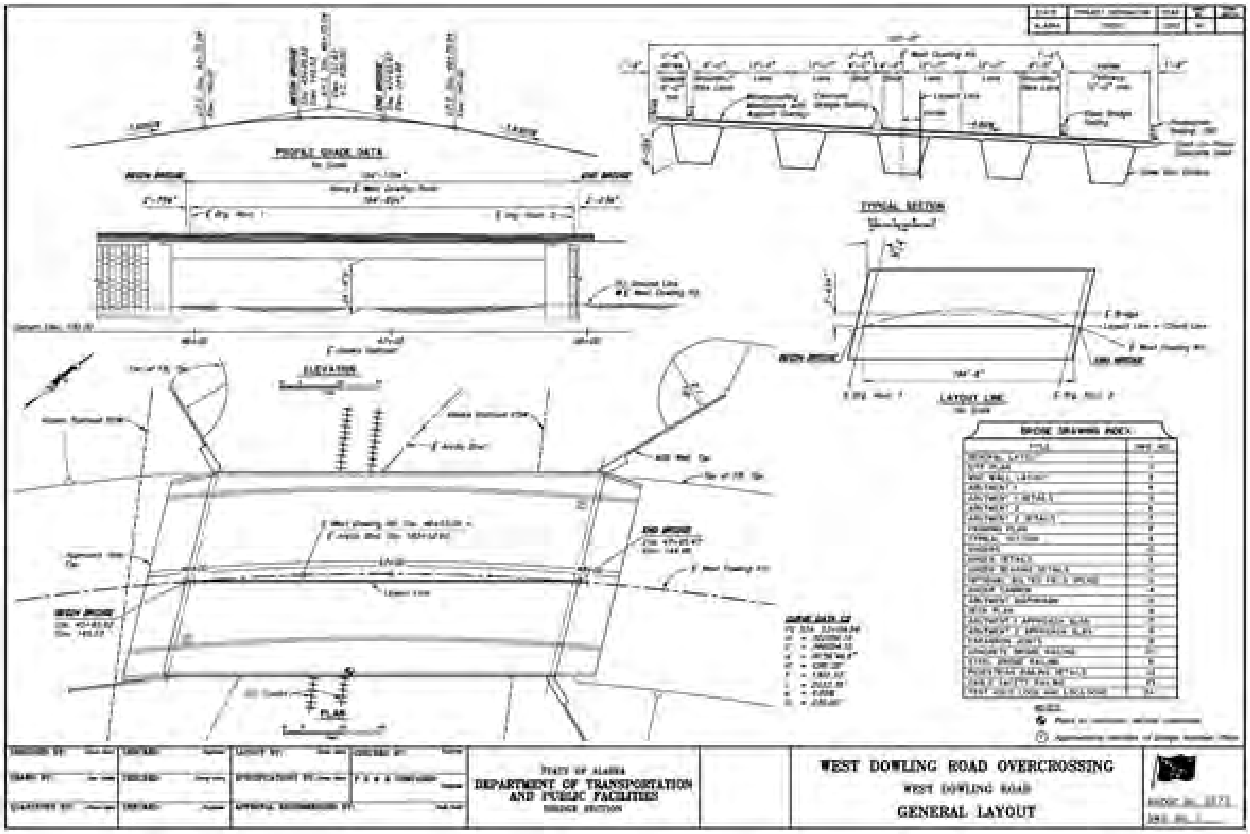

Figure 5-7. West Dowling Road Bridge – Plan and elevation of the West Dowling Road bridge crossing the Alaska Railroad tracks (courtesy of Dave Hemstreet, AKDOT).

Figure 5-8. West Dowling Road Bridge (Lat/Long: 61.1655°, -149.8977°) – photograph of bridge taken on 4 December 2018 (courtesy of Dave Hemstreet, AKDOT).

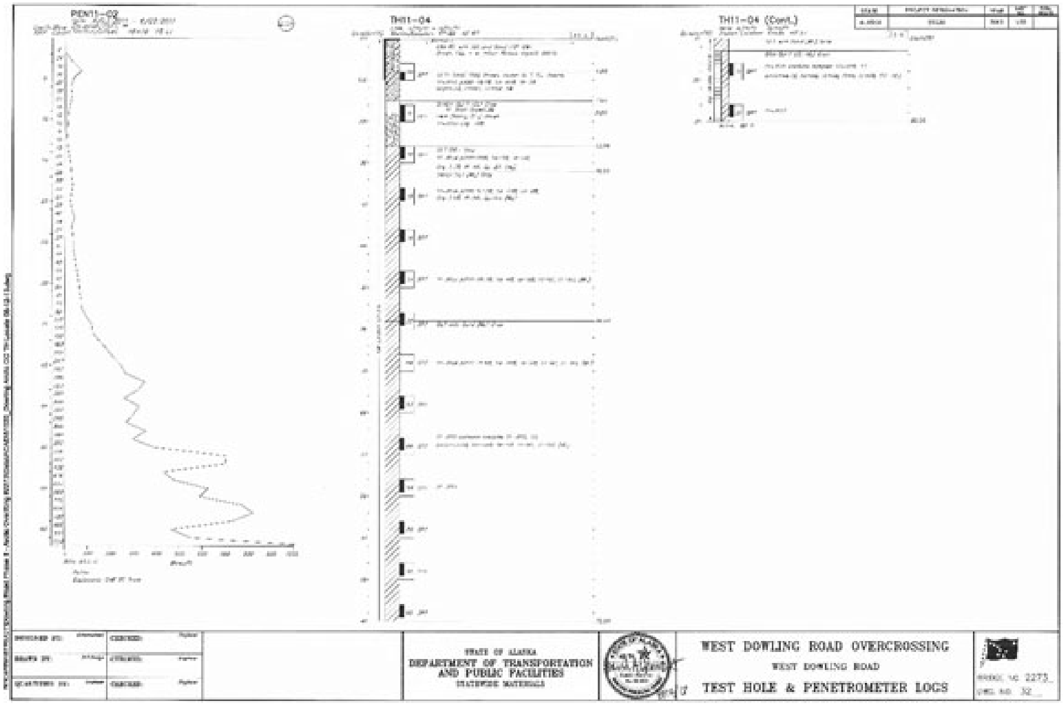

Figure 5-9. West Dowling Road Bridge – Sample borehole log and penetrometer results (courtesy of Dave Hemstreet, AKDOT).

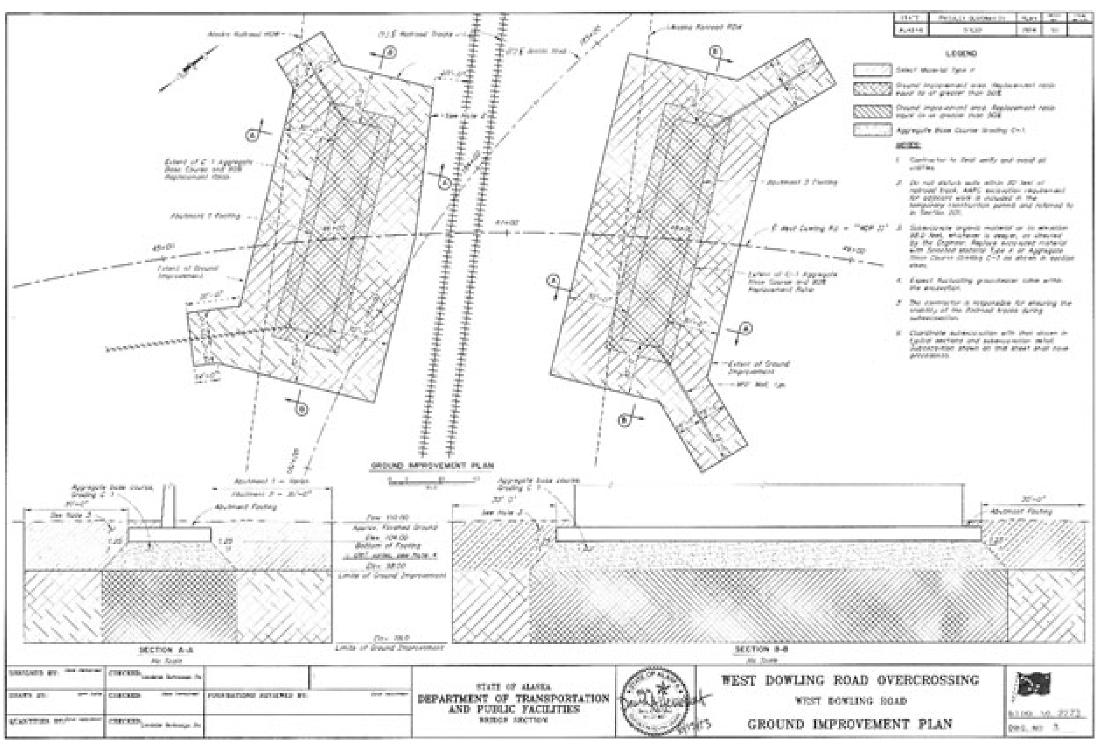

Figure 5-10. West Dowling Road Bridge – Plan and elevation view of DSM ground improvement used below the shallow foundations at the West Dowling Road Bridge.

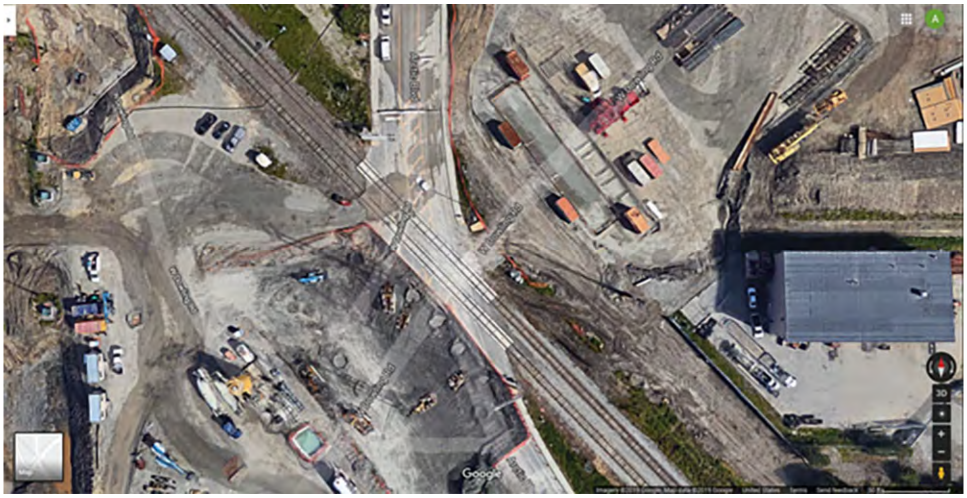

Figure 5-11. West Dowling Road Bridge – Google maps aerial photograph showing construction of the DSM columns for the West abutment under way, and the large shallow foundation formed and poured for the East Abutment.

Figure 5-12. West Dowling Road Bridge – View of out-of-plane deformation of light I-Sections supporting guardrails along the bridge deck.

Figure 5-13. West Dowling Road Bridge – View of (left) shear-cracking at the northeast transition from bridge span to approach fill, indicating possible evidence of pounding, and (right) permanent transverse movements at same location (courtesy of Dave Hemstreet, AKDOT).

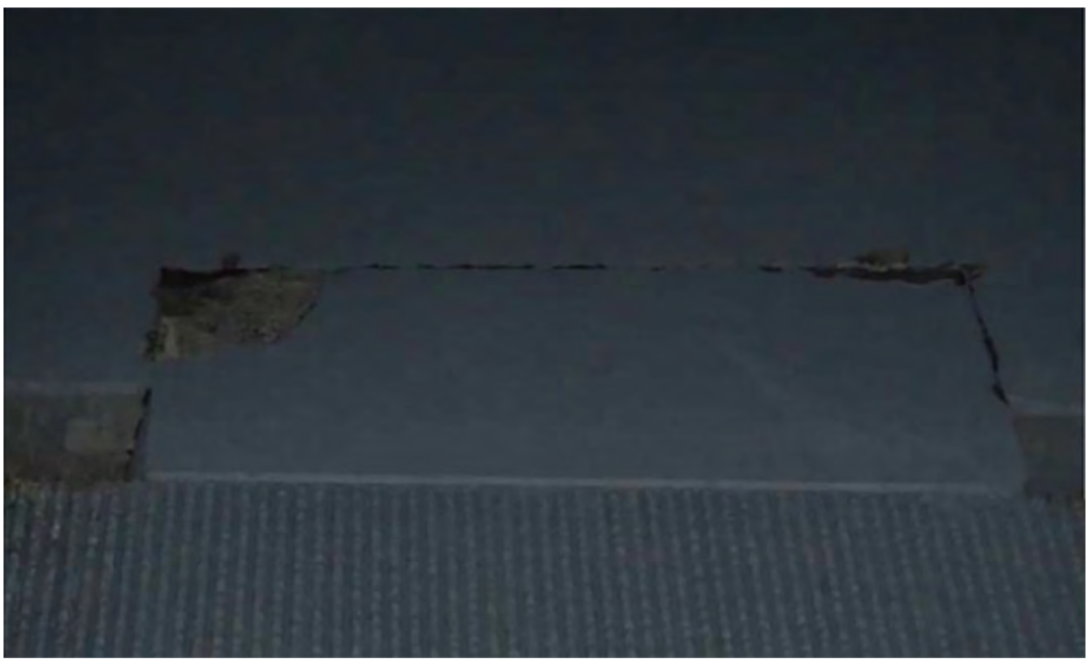

Figure 5-14. West Dowling Road Bridge – Spalling of concrete along shear key at abutments (courtesy of Dave Hemstreet, AKDOT).

Figure 5-15. West Dowling Road Bridge – overview and close-ups of wall panel movements (Lat/Long: 61.1651, -149.8991).

Figure 5-16. West Dowling Road Bridge – unloading of bearing pad (left) and tilt of panel towards culvert opening (right).

Figure 5-17. West Dowling Road Bridge – slope movement along East approach fill

Figure 5-18. Settlements and lateral deformations in the spill slope at the south abutment of the northbound Glenn Highway Bridge over Eagle River (Lat/Long: 61.3117°, -149.5760°)

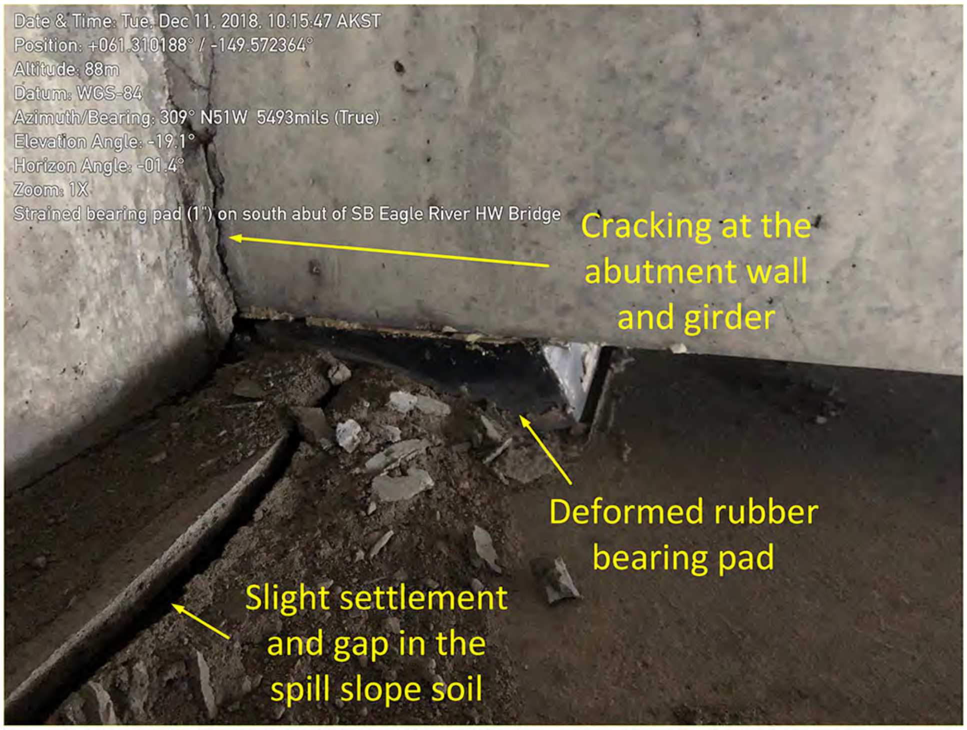

Figure 5-19. Observed girders and abutment seat at the southern abutment of the southbound Glenn Highway Bridge over Eagle River (Lat/Long: 61.1310°, -149.5724°).

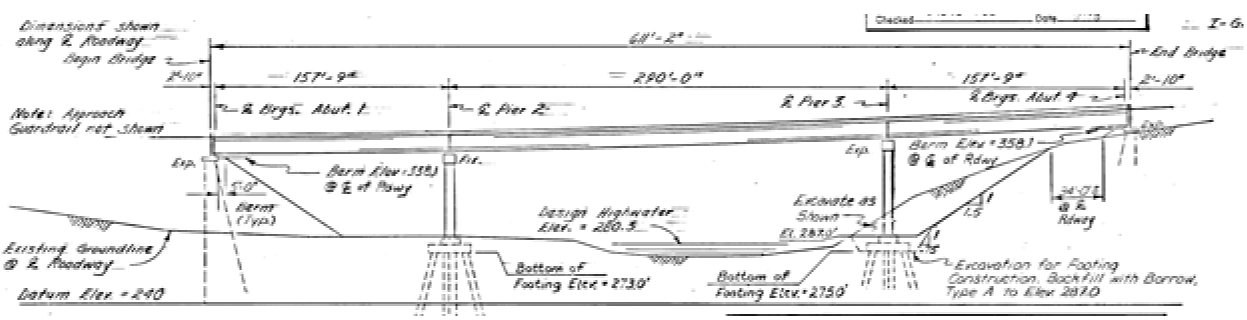

Figure 5-20. Elevation view of the Brigg's Bridge looking West (from AKDOT as-built drawings).

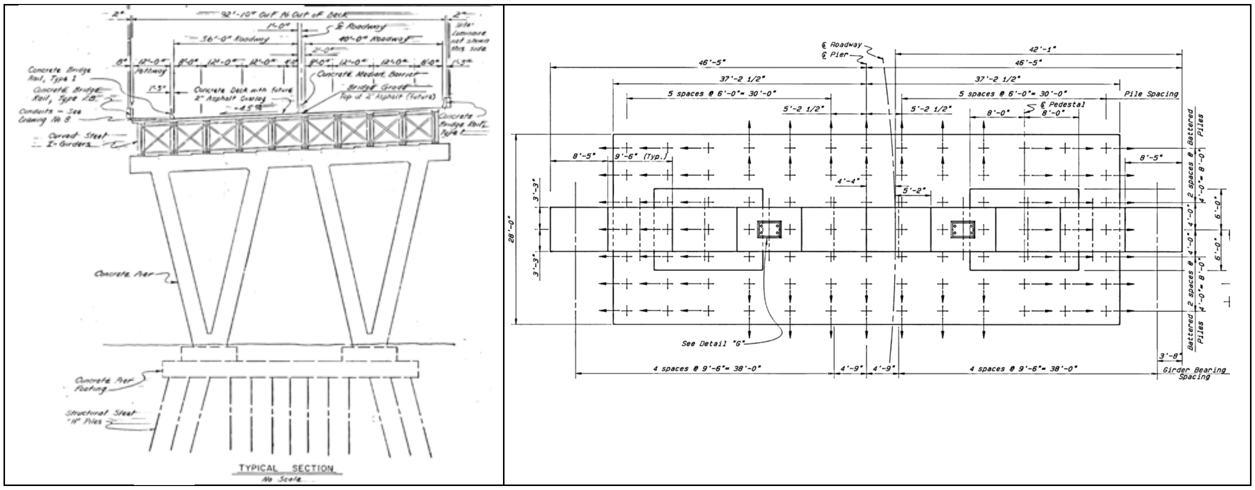

Figure 5-21. Schematics indicating typical section of bridge piers (left) and pile cap and pile arrangement (right) (from AKDOT as-built drawings).

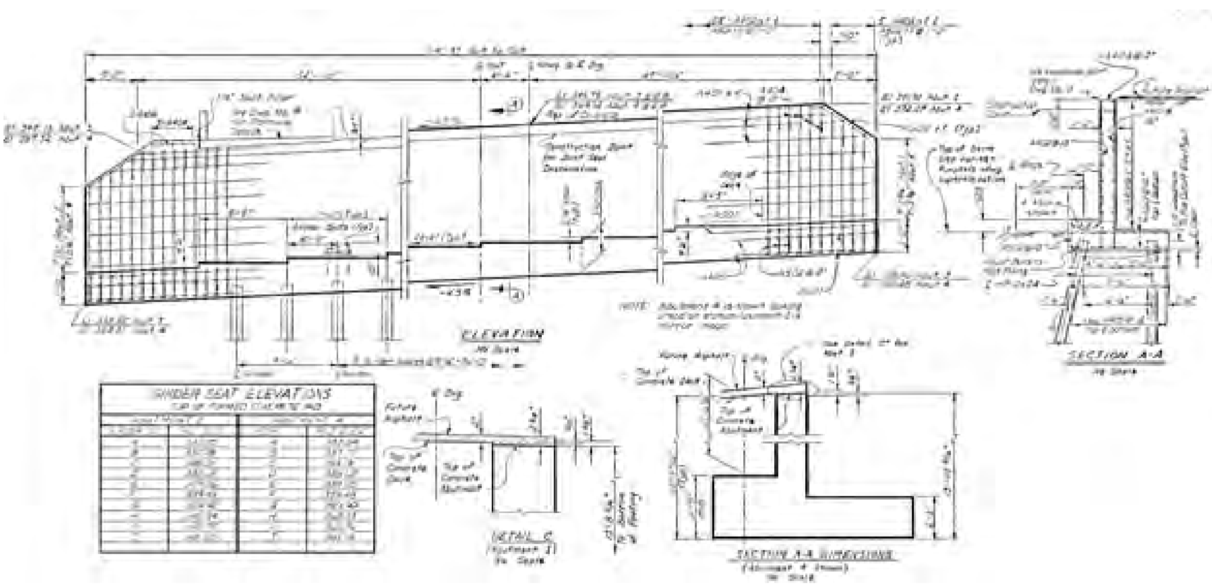

Figure 5-22. Typical elevation and sections for piled abutments at the Briggs Bridge (from AKDOT as-built drawings).

Figure 5-23. View of scarp along eastern edge of approach fill behind the north abutment.

Figure 5-24. View of eastern portion of the north abutment exhibiting vertical and lateral movements downslope.

Figure 5-25. View of western portion of the north abutment exhibiting vertical and lateral movements downslope.

Figure 5-26. View of western portion of the north abutment exhibiting vertical and lateral movements downslope.

Figure 5-27. Translation and settlement of abutments as indicated by lifted hex nuts attaching girders to bearing pads.

Figure 5-28. Head scarp of the Rabbit Creek Landslide Complex (Lat/Long: 61.0912°, -149.8470°).

Figure 5-29. Bluff landslide located above the Port of Alaska (Lat/Long: 61.2303°, -149.8849°).

Figure 5-30. Aerial image of the Minnesota Boulevard embankment failure (Lat/Long: 61.171279°, -149.915547°). Photo source: Ryan Marlow, Alaska Aerial Media.

Figure 5-31. Field photographs of the Rivers View condominiums landslide in Eagle River. Cracks at the crest of the slope extend for 325 feet from the north (A) to the south (B) part of a flat graded residential property (Lat/Long: 61.312065°, -149.570379°). The cracks are up to 3 inches wide and 4 feet deep. The cracks extend down the slope and intersect the headscarp of a small landslide (C) at the base of the slope (Lat/Long: 61.312346°, -149.571359°) that is associated with a 3 to 5 foot high headscarp. This slide impacted residences in the Rivers View condominiums.

A B

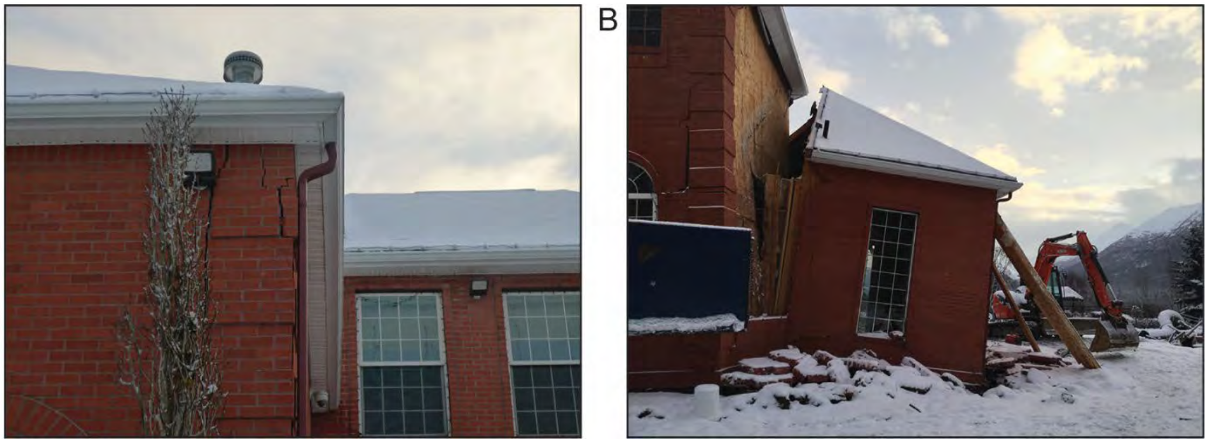

Figure 5-32. Damage to residence in the Ptarmagin Drive area of Eagle River (Lat/Long: 61.30494°, -149.49582°). Extensive facade cracking (A) and fill failure related tilting of a room associated with complete facade brick failure (B).

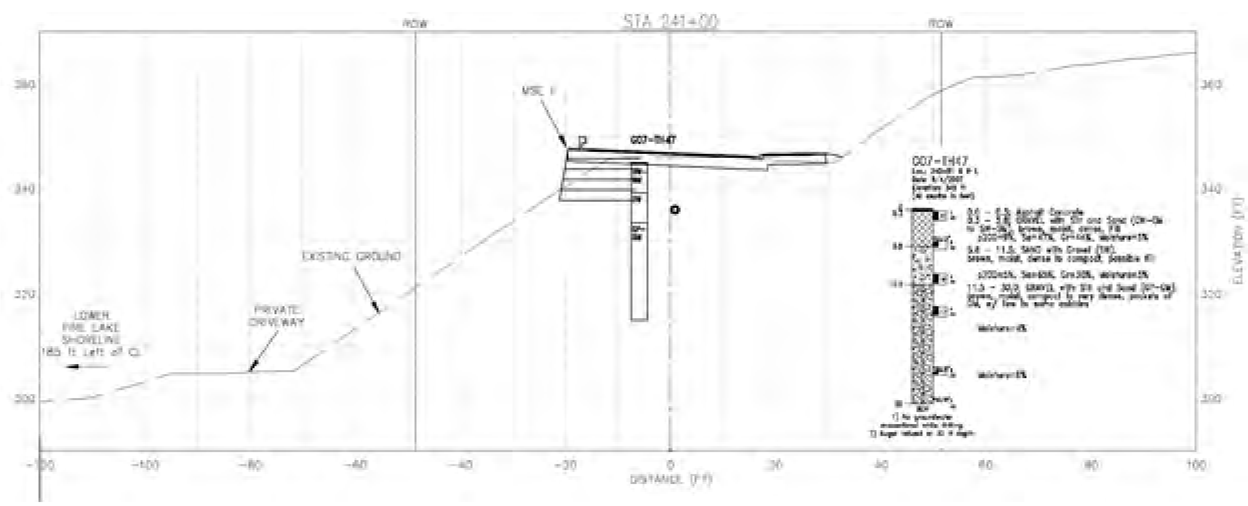

Figure 5-33. Generalized cross-section of MSE wall (proposed, not as-built) along Old Glenn Highway and subsurface conditions (after Golder 2009).

Figure 5-34. View of Old Glenn Highway from (Lat/Long: 61.352274°, 149.541972°) on 11 December 2018, looking southwest, indicating steep slope on the right with evidence of long-term slope movements (e.g., leaning trees) and longitudinal crack on the left.

Figure 5-35. View of Old Glenn Highway from (Lat/Long: 61.35229°, -149.54193°) on 5 December 2018, looking southwest, indicating longitudinal crack in the foreground (photo courtesy of Dave Hemstreet, AKDOT).

Figure 5-36. View of Old Glenn Highway from (Lat/Long: 61.352243°, 149.542052°) on 11 December 2018, looking south, indicating the longitudinal crack (corresponding to distance 32 m, see Figure 5-35) where settlement was noted.

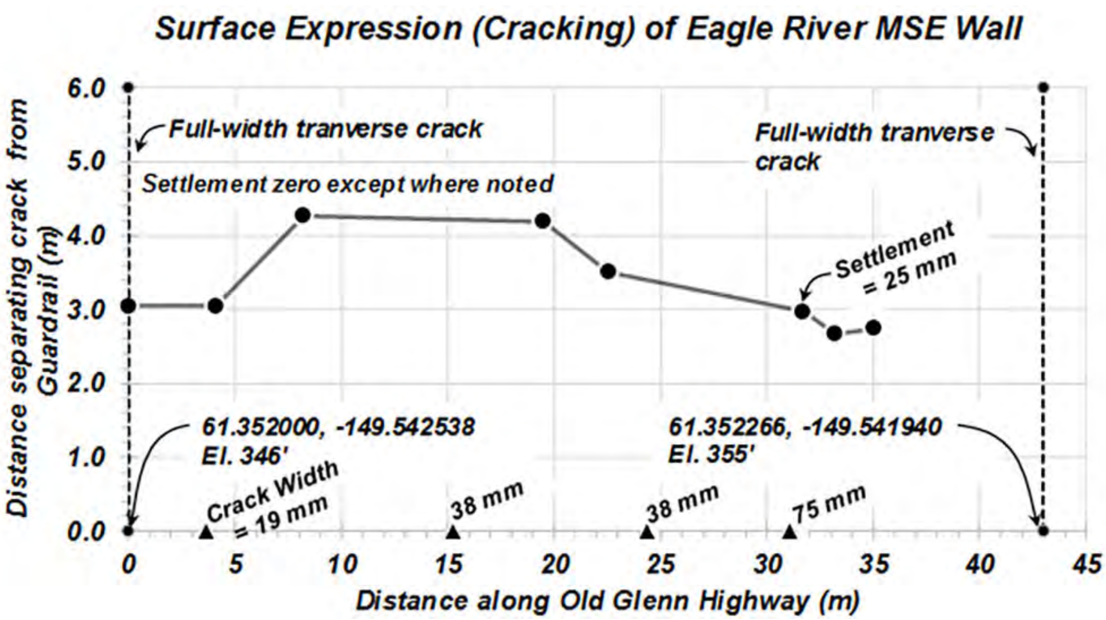

Figure 5-37. Spatial distribution of longitudinal and transverse cracking along MSE wall, along with measured lateral offsets and settlement.

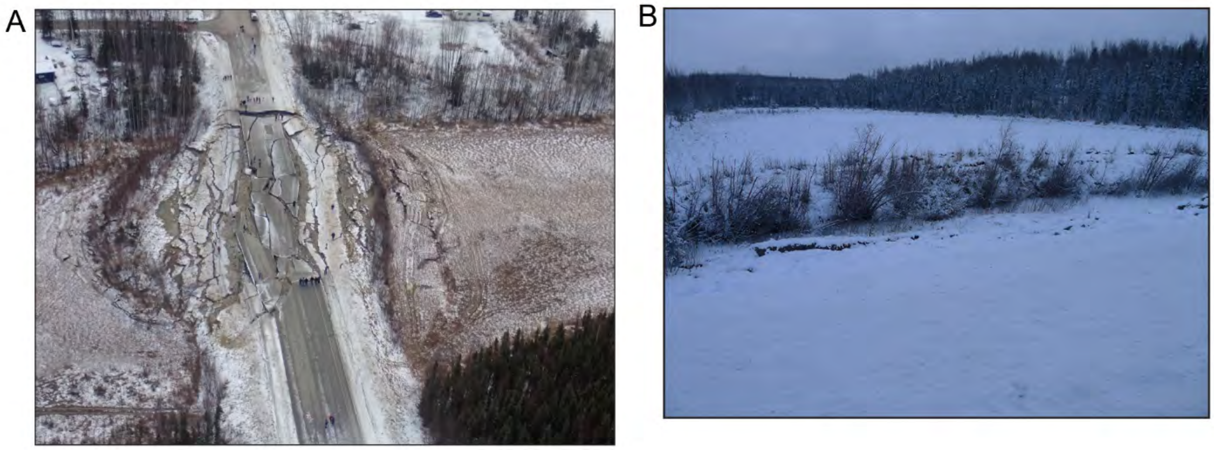

Figure 5-38. Damage to Vine Road (Lat/Long: 61.56863°, -149.60215°) south of Wasilla. (A) Aerial photograph of the road after the earthquake taken by Rob Witter (USGS) during helicopter reconnaissance. (B) ground photograph of pressure ridges (peat mounds) west of the road formed by lateral motion of the road fill. Note back-tilted trees.

Figure 5-39. Road failure along the Port Mackenzie industrial area access road (Lou Young Road, Lat/Long: 61.28176°, -149.93002°) before (A) and after (B) repair. Road failure at mile 15.5 of the Port Mackenzie Road (Lat/Long: 61.31582°, -150.02627°) before (C) and after (D) repair. Pre-snow photographs provided by Bob Walden of Mat-Su Borough.

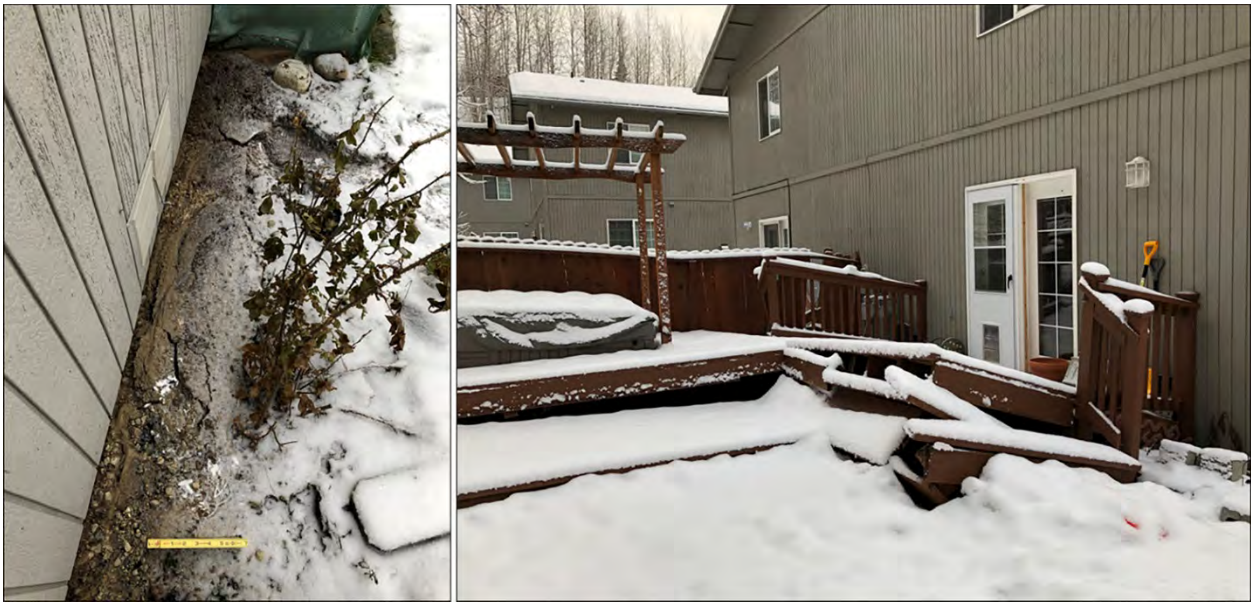

Figure 5-40. (Left) Ejecta observed at red-tagged home (Lat/Long: 61.3121°, -149.5714°), (Right) Backyard damage at another red-tagged home (Lat/Long: 61.3121°, -149.5721°).

Figure 5-41. Ptarmigan settlement (left) and ground failure (right) (Lat/Long: 61.3067°, -149.4968°).

Figure 5-42. Jewel Lake residential damage: (a) settlement along foundation perimeter, (b) ground failure and possible ejecta in crawl space under the home, (c) settlement relative to back porch. (Lat/Long: 61.1380°, -149.9380°).

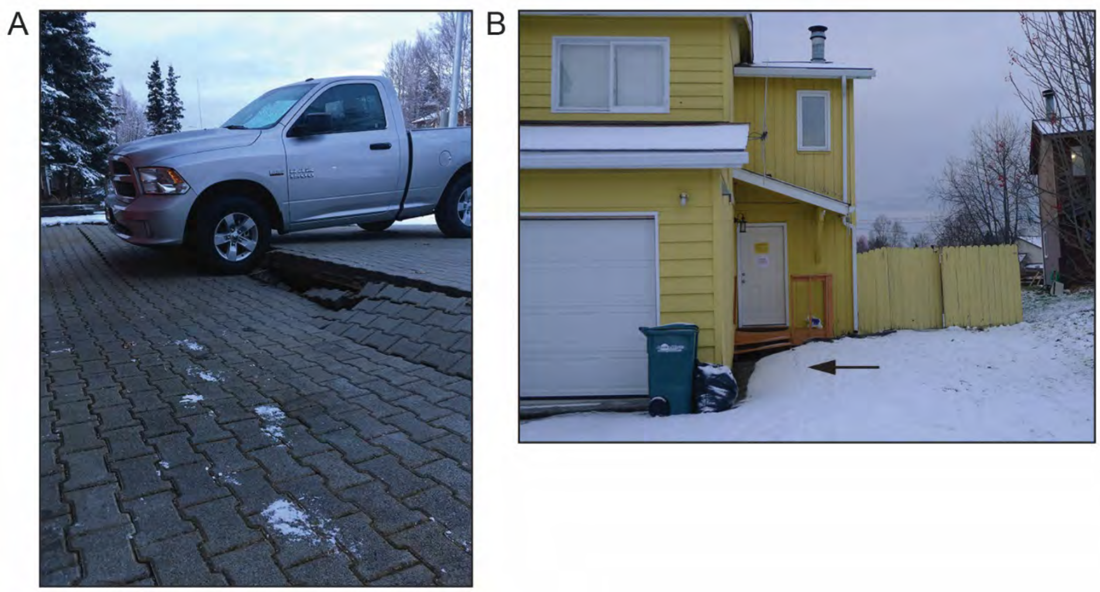

Figure 5-43. Typical foundation settlement damage in the Campbell Lake area of south Anchorage. (A) Drive way settlement (Lat/Long: 61.13337, -149.93126). (B) Duplex settlement along arrow (Lat/Long: 61.13794°, -149.9380°). Settlement was about 1 foot at each site.

Figure 5-44. C Street & Dowling Road Intersection - settlement at electrical junction box (Lat/Long: 61.1670°, -149.8870°).

Figure 5-45. Photos of sand boils and ejecta at a residential property, received after Phase 1 field reconnaissance completed (Lat/Long: 61.1481°, -149.9033°).

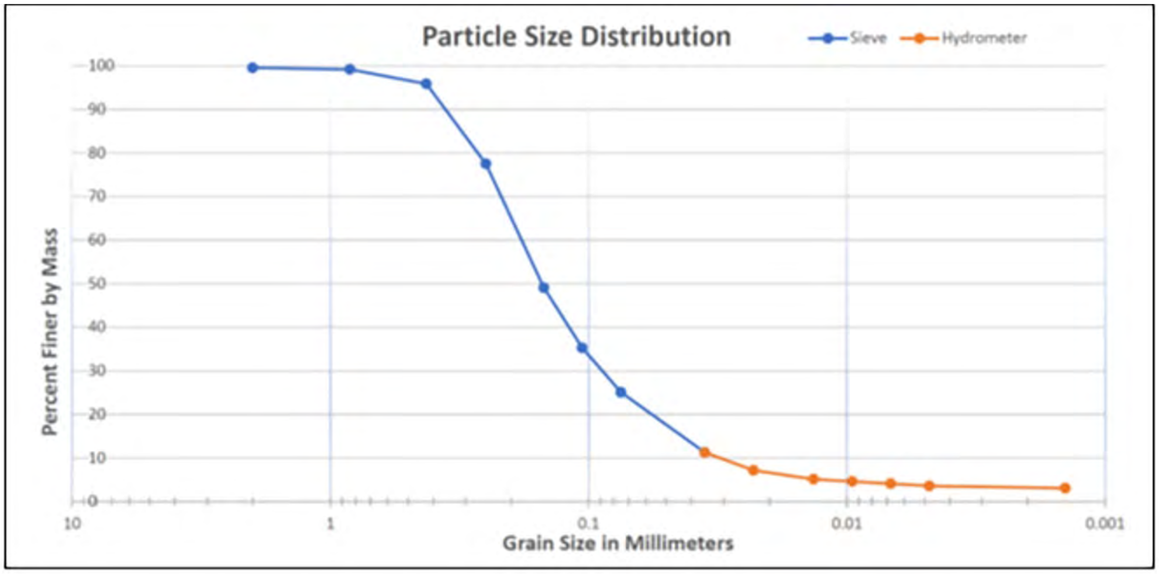

Percentages						
Total Fines		Total Sand			Total Gravel	
25.1		74.9			0.1	
Clay	Silt	Fine Sand	Medium Sand	Coarse Sand	Fine Gravel	Coarse Gravel
3.1	22.0	70.8	3.7	0.4	0.1	0.0

Figure 5-46. Particle size distribution for ejecta from residential property shown in Figure 5-45.

6.0 Port of Alaska

Given the location of the State of Alaska more than 90% of inbound freight arrives by marine vessels. The Port of Alaska (PoA, previously known as the Port of Anchorage) is the State of Alaska's primary inbound cargo handling facility and is responsible for transferring 45% of all goods entering the state (approximately 3.5M tons/year). Further, approximately 85% of Alaskan residents and businesses consume goods handled by the PoA on a weekly basis, with half of the freight delivered to final destinations outside of the Municipality of Anchorage (MOA).

Situated approximately 2 km north of Downtown Anchorage (lat/long: 61.2393°, -149.8883°), the PoA opened in 1961 and now consists of three terminals, a fuel tank farm, and a cement handling facility. Figure 6-1 presents a plan of the Port of Alaska and some of its features. Despite the MOA's long history as the State's air hub and population center, prior to the 1964 Good Friday Earthquake, the Port of Seward served as the State's cargo and freight hub. Owing to the destruction of Seward due to the M9.2 subduction zone earthquake and more critically the tsunami that followed, the PoA became the critical cargo handling facility in the state. Studies by the Port of Alaska and its consultants have shown that while at risk of earthquake damage, its location along the Knik Arm of the Cook Inlet greatly minimizes risks associated with catastrophic tsunamis often accompanying subduction zone earthquakes. This is a critical aspect for the State of Alaska, as the port serves significant roles in commerce, national defense, and disaster recovery. Members of our Phase I team visited the PoA on December 5th through 7th and on December 12th; the following summary is derived from interviews with Port personnel, our site visit, photos provided by Port personnel, and the substantial, direct involvement by members of the team on current projects for the PoA.

6.1 Geologic Setting and Subsurface Conditions

Subsurface soils encountered at the PoA generally consist of six units; coarse-grained fill materials (Unit I); over tidal silt deposits (Unit II); over glaciofluvial deposits (Unit III); over Bootlegger Cove Formation (BCF) Clay (Unit IV); over older glaciofluvial deposits (Unit V). Underlying the older glaciofluvial deposits is another layer of the BCF which is underlain by a Glacial Drift Layer (Unit VI). The depth of bedrock is interpreted to be the depth corresponding to a shear-wave velocity of 2,500 feet per second and is at approximately elevation -450 feet based on microtremor array measurements at the south end of the Port.

Anthropogenic fill associated with the development of the existing Port facilities consists of loose to medium-dense mixtures of sand, gravel, and silt. The fill near the water front facilities was likely placed hydraulically. The tidal deposits consisting of estuarine silt is composed of liquefaction-susceptible, loose to medium dense, low plastic silt (PI = 0 to 10) with little to trace fine sand. Cyclic Direct Simple Shear (DSS) laboratory testing of the loose and medium dense tidal deposits has indicated that liquefaction triggering, defined as the development of 90% excess pore pressure, is possible under design cyclic loading representative of the Operating Level Earthquake (OLE), Contingency Level Earthquake (CLE), and Maximum Credible Earthquake (MCE), and CLE and MCE, respectively, in recent engineering studies (COWI 2018). The Bootlegger Cove Clay Formations consists of stiff to very stiff clay and, depending on the facies, can be susceptible to cyclic softening. The glaciofluvial soils primarily consist of dense to very dense sand and gravel with interbedded hard clay layers. The glacial drift deposit underlying the lower BCF consists of dense to very dense sand and gravel. The glacial drift deposit overlies the pre-Quaternary deposits or metamorphic bedrock.

The subsurface conditions at Terminals 1, 2, and 3 are similar and consist of a loose granular fill with is underlain by loose tidal silt followed by dense glaciofluvial sand and gravel which is underlain by stiff Bootlegger Cove Clay. Generalized subsurface conditions for Terminals 2 and 3 are presented on Figure 6-2 and 6-3.

Transit Yard A is located east of Terminal 1 (see Figure 6-4) and the administration building. The subsurface conditions at Transit Yard A consist of loose granular fill underlain by loose tidal silt underlain by stiff Bootlegger Cove Clay. Figure 6-5 and Figure 2-6 present boring TB-1 and grain size analyses for the loose granular fill and tidal silt, respectively.

The subsurface conditions at the northern expansion include engineered fill associated with the construction of the open cell sheet pile bulkheads. The construction of the open cell bulkhead utilized a gravel dike consisting of cobble to boulder sized material. Compacted gravel and sand was placed behind the bulkhead sheet piles and inland behind the rock fill dike. Underlying the rock dike and engineered fill is a layer of tidal silt underlain by stiff Bootlegger Cove Clay followed by dense glacialfluvial sand and gravel. Figure 6-7 presents generalized subsurface conditions at the northern expansion bulkhead wall.

At the new PCT site near the cement dome, the subsurface conditions consist of loose sand fill underlain by loose to medium dense tidal silt. Below the tidal silt is a layer of medium dense to dense glacialfluvial sand and gravel which is underlain by stiff Bootlegger Cove Clay followed by dense to very dense older glacialfluvial sand and gravel and another layer of Bootlegger Cove Clay. Underlying the lower Bootlegger Cove Clay is very dense glacial drift deposits which is followed by bedrock, both of which are interpreted from shear wave velocity measurements. Figure 6-8 presents a subsurface profile taken thorough the center of the proposed PCT trestle. Figure 6-9 presents a deep shear wave velocity profile from a microtremor array providing one of the few depth to bedrock estimates at the Port.

6.2 Ground Motions

Several ground motions near the port were reviewed in order to provide a range of possible site responses. The closest available stations at the time of this report are Government Hills Elementary, the Port Access Bridge, Central, and the Hilton Hotel which are presented on Figure 6-10. Acceleration response spectra for these motions are presented on Figure 6-11. In general, all of the stations with the exception of the Port Access Bridge produce similar response spectra with the PGA ranging from 0.20 g to 0.30 g. The sole records available from the Port Access Bridge station were observed from a triaxial seismometer located some 200 ft away from the bridge and represented relatively free-field conditions. This triaxial seismometer recorded a PGA of about 0.40 g and exhibited strong motions with a large spectral spike of 2 g between periods of 0.2 and 0.3 seconds. Differences in the motion at this site, as compared to those observed from nearby locations, should be investigated further. In general, the ground motions presented in Figure 6-4 offers potential ranges in site response at the Port.

6.3 Observations of Seismic Performance

Damage to the structures and ground deformation to the PoA associated with the November 30th earthquake was observed within its terminals, administration building, slopes (coastal bluffs) along the eastern margin of the property, and along the waterfront.

6.3.1 Terminals and Administration Building and Transit Yard A

The administration building suffered permanent relative movements, damage to the elevator, and dislocation of non-structural components. Figure 6-12 presents relative movements within the building at the location of expansion joints, ranging in magnitude from one-quarter to one-half inch. Figure 6-13 indicates the relative severity of inertial loading experienced by office staff, with overturned filing cabinets and tables, among other office items.

Observable damage to the terminals (i.e., pile-supported wharfs running parallel to the shoreline) was largely limited to spalling along the expansion joints separating Terminal 1 and Terminal 2 indicating the development of out-of-phase dynamic response resulting in pounding during the earthquake (Figure 6-14). The piles supporting the wharfs and trestles (approximately 1,420 piles) are predominantly 610 mm (24”) pipe piles with 11 mm (7/16”) original wall thickness, with 760 mm diameter pipe piles used for support of dolphin berthing structures and other pile types serving as protective fenders along the outer row of dock bents.

A significant number of the piles have experienced corrosion to levels consistent with a “Loss of Service” rating. Degradation of the piles has resulted in the PoA’s 10-year goal of replacing each terminal. For example, studies conducted by the Port have shown piles commonly exhibit loss of half of their original wall thickness, and in some cases up to three-quarters of their thickness. The Port initiated a pile jacketing program in 2004 to reinforce piles with severe loss of wall thickness and maintain wharf operability. Approximately 40 percent of the piles supporting Terminals 1 through 3 had been jacketed by December 2016. Owing to the staged jacketing program, those jackets installed towards the beginning of the program have exhibited wear and are approaching the end of their service life.

The degradation of the steel piles has affected port operations; for example, in recent years, a fender decoupled from the wharf due to the loss of structural integrity and came to rest along the mudline, presenting challenges to visiting ships and yearly dredging operations. As a result, the Port had chained the remaining fenders to the dock, and this likely contributed to the zero-loss of fenders during the earthquake (Figure 6-15). An immediate, although partial, water-born inspection did not reveal above-water damage to piles or pile-dock connections following the earthquake (Figure 6-16). The pile jacketing program to shore up the corroded piles appears to have largely prevented damage during the earthquake, along with estimated low levels of inertial and kinematic loading as inferred by the relatively small slope movements east of the terminals.

The three gantry cranes were not in use during the earthquake and were tied to the crane rails following typical good port practices (Figure 6-17), which may have contributed to reduced damage levels to the wharfs. No damage to the cranes were noted by Port personnel.

Within the main port property, the greatest extent of ground movement appeared to occur due to lateral spreading in features that largely were expressed parallel to open faces running along the north-south Port alignment at Transit Yard A located across from the Administration Building. Port personnel reported crack widths ranging from 10 to 30 cm and vertical offsets of block failures of up to 1 m in height. A near-continuous crack was observed to run along three-quarters of the 670 m long, rip-rap covered, partially-submerged slopes which separate the Port uplands from the three terminal docks. Although the setback of the crack from the crest of the rip-rap lined sloped varied, it was frequently observed at a setback of about 3.6 m. Evidence of liquefaction was observed in the form of a sand boil located at the toe of the rock-lined slope providing some evidence that the loss of bearing support may be responsible for some of the settlement of the slope face. Photographs taken the day after the earthquake showing the 1 m vertical offset, sand boil, and tension crack behind the slope are presented in Figure 6-18 and Figure 6-19. At the time of our Phase I team visit, crack widths of 15 to 50 mm were noted, however Port personnel and photographs provided to the team taken on the day of the earthquake suggest that the crack widths were originally larger. Locally along this area, slumping of failed soil blocks within the partially-submerged slopes occurred, and these blocks had exhibited vertical offsets of up to 1 m in height. These ground failures had been temporarily repaired by the Port with more permanent repairs planned for the spring. Photos taken on December 5th after the temporary repair was made are presented in Figure 6-20 and Figure 6-21.

6.3.2 PCT Ground Improvement and Cement Dome

No damage was observed along the circular, perimeter grade beam-supported cement storage dome structure located south of the port terminals and immediately east of the waterfront (see Figure 6-22 and Figure 6-23. The cement storage dome was placed on ground improved with a 3 m tall surcharge, is of 40,000 tons dry cement capacity, and was 80% full during the earthquake. The lack of damage is likely due to an insufficient number of cycles to trigger liquefaction in the loose to medium dense tidal silt layer which is encountered approximately 4.5 m below the ground surface. Other contributing factors to the latter observation may have been consolidation of the tidal silt due to the construction surcharge and the new deep soil mixing (DSM) ground improvement zone placed between the waterfront and the cement storage dome during the summer of 2018 in anticipation of construction of the new petroleum and cement terminal planned to resume in 2019. The DSM program consisted of interlocking shear panels (i.e., DSM cells) that toed into the glaciofluvial deposits underlying the medium dense silt layer, which serve to protect the trestle piles planned for installation in 2019. Photos showing the ground improvement construction and the shoreline at the time of the post seismic survey are presented in Figure 6-24. During construction of the DSM a gravel platform was placed to allow offshore access for the construction equipment. The thickness of the gravel platform ranged from approximately 6 m (offshore) to 1 m (onshore). Figure 6-25 presents the configuration of the DSM grid and PCT trestle configuration.

During the December 5th visit both lateral and vertical displacements ranging from 5 to 30 cm were observed on the shoreline slopes within the tidal flats adjacent to the DSM zone. Within the DSM zone, however, there were no signs of vertical or lateral displacement. The preservation of the tension cracks and scarps several days after the earthquake is attributed to the ground being frozen. However, due to tide action, by the time of the December 12th visit evidence of the lateral spread was no longer visible by our team.

Prior to the November 30th earthquake, the shoreline in the vicinity of the new PCT sloped at approximately 1V:5H and did not exhibit vertical scarps or tension cracks. A side-by-side comparison of the shoreline at the PCT during coring of the DSM taken on October 2nd, 2018 and a post-seismic view of the same slope on December 5th, 2018 (Figure 6-26) shows a pronounced settlement scarp which measured from 150 mm to 300 mm (Figure 6-27). In addition to settlement, tension cracks ranging from 50 mm to 75 mm inches wide were observed both north and south of the DSM ground treatment (Figure 6-28 and Figure 6-29).

6.3.3 Bluffs

Several vegetated and bare bluffs running north-south and lying immediately to the east of the Port property experienced shallow, surficial failures (Figure 6-30 and Figure 6-31). It appears that significant movements (Figure 6-31 [right]) were restricted to shallow failures in colluvium that commonly mantles the coastal bluffs in the Anchorage region. A large crack running the length of the crest of a bluff was investigated by other members of our Phase I team after the initial Port visit and is described in the Slopes and Embankments Section. Several pinnacled bluffs (triangular bluffs produced by closely-spaced drainage features) along the east margin of the northern expansion area experienced surficial and planar slope failure consistent with “infinite slope” failure mechanisms that appeared to originate from the top of the slope and slough along previously exposed native, non-colluvial soils (Figure 6-31[left]).

6.3.4 Northern Expansion

The northern expansion area of the PoA represents port development that had initiated in 2009 but was terminated following the observation of loss of fill behind sheet pile bulkhead structures. The site presently consists of rip-rap lined and partially submerged slopes and vertical grade separations behind open sheet pile cells designed to act as a membrane structure. No significant differential movements or connection interlock failures were observed within the sheet pile structure, although 5 mm wide crack was observed at the northern most open cell bulkhead just behind the return wall (Figure 6-32). Lateral spreading-type ground failure involving multiple blocks of soil were observed by Port personnel in the northern expansion area in close proximity to the rip-rap lined slope immediately following the earthquake. Cracks of up to 300 mm in width and up to and possibly exceeding 3 m depth were observed. Photos taken by the Port personnel show widespread water on the ground surface but unaccompanied by ejecta. On December 6th and 12th, these cracks were still visible to members of the reconnaissance team. Photos taken by Port personnel and the Phase I team are presented Figure 6-32 through Figure 6-39.

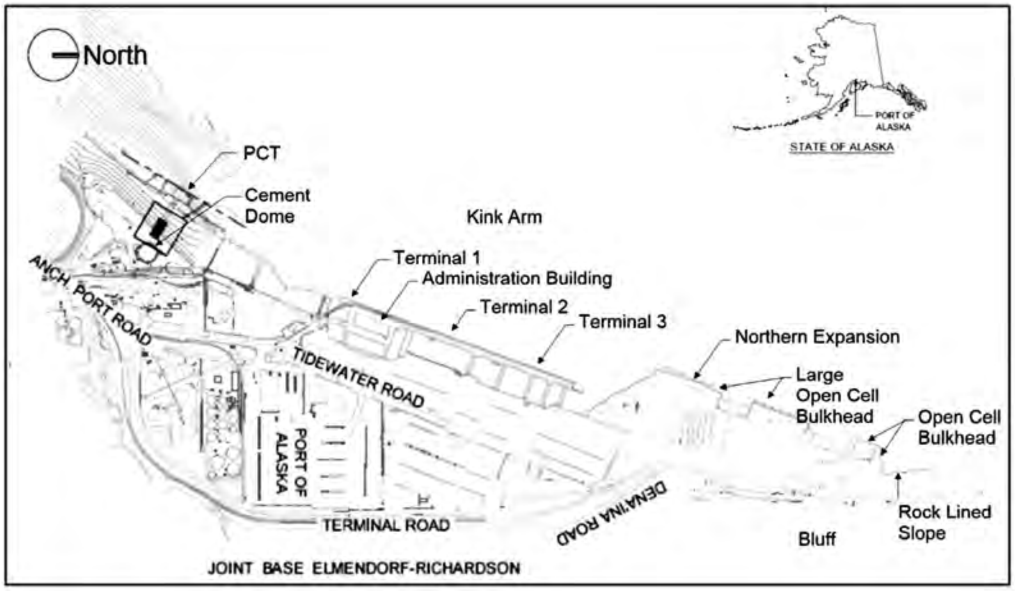

Figure 6-1. Port of Alaska – Site Plan

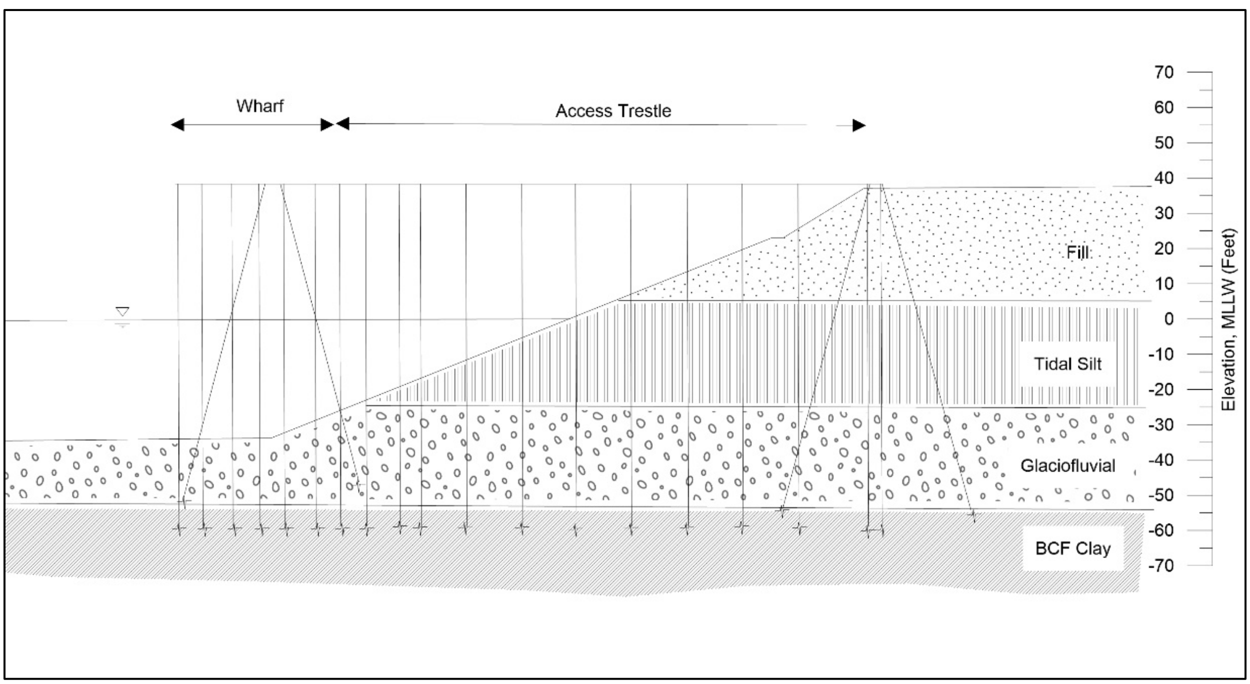

Figure 6-2. Port of Alaska – Generalized Subsurface Conditions at Terminal 2

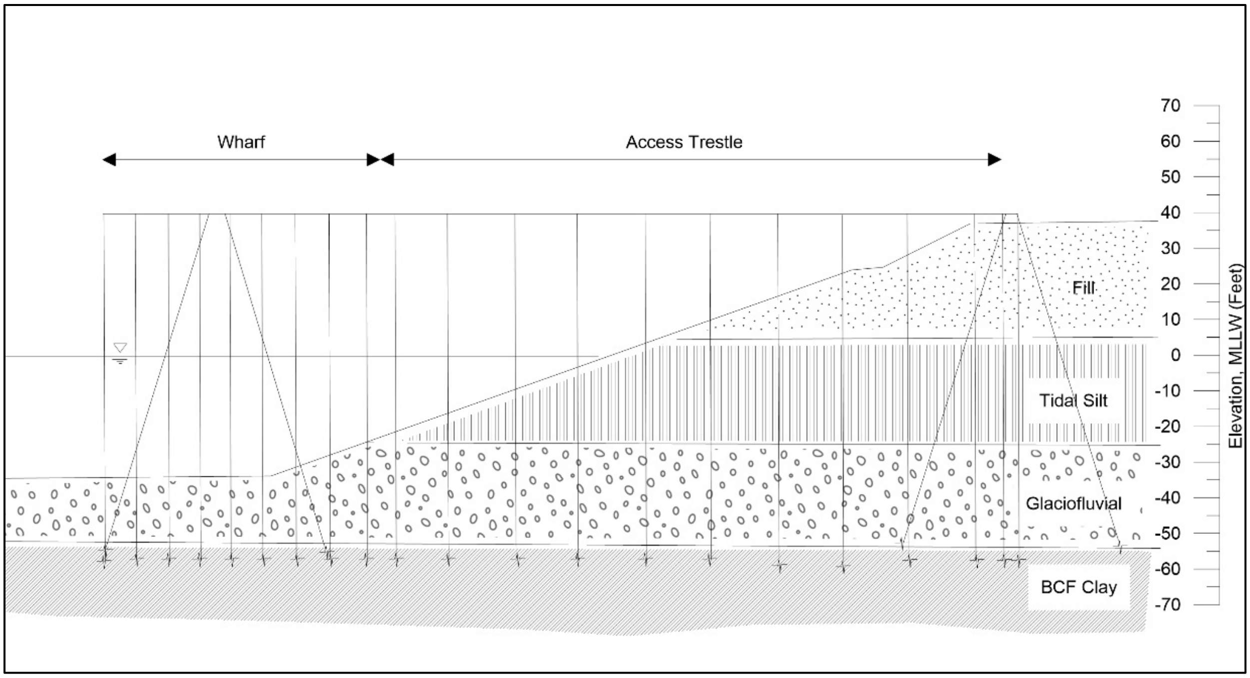

Figure 6-3. Port of Alaska – Generalized Subsurface Conditions at Terminal 3

Figure 6-4. Port of Alaska – Aerial view of port facilities east of Terminal 1 indicating location of boring TB-1 (after Shannon & Wilson 2016)

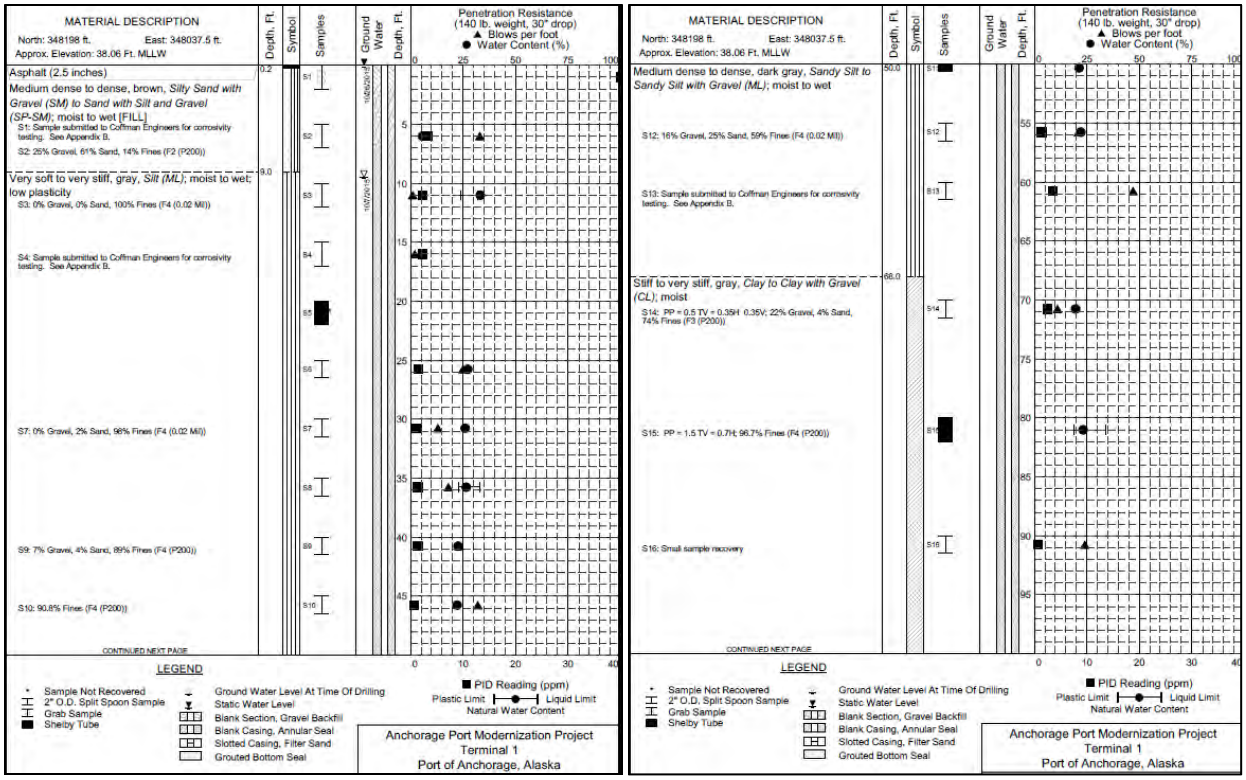

Figure 6-5. Port of Alaska – Boring TB-1 (Shannon & Wilson 2016)

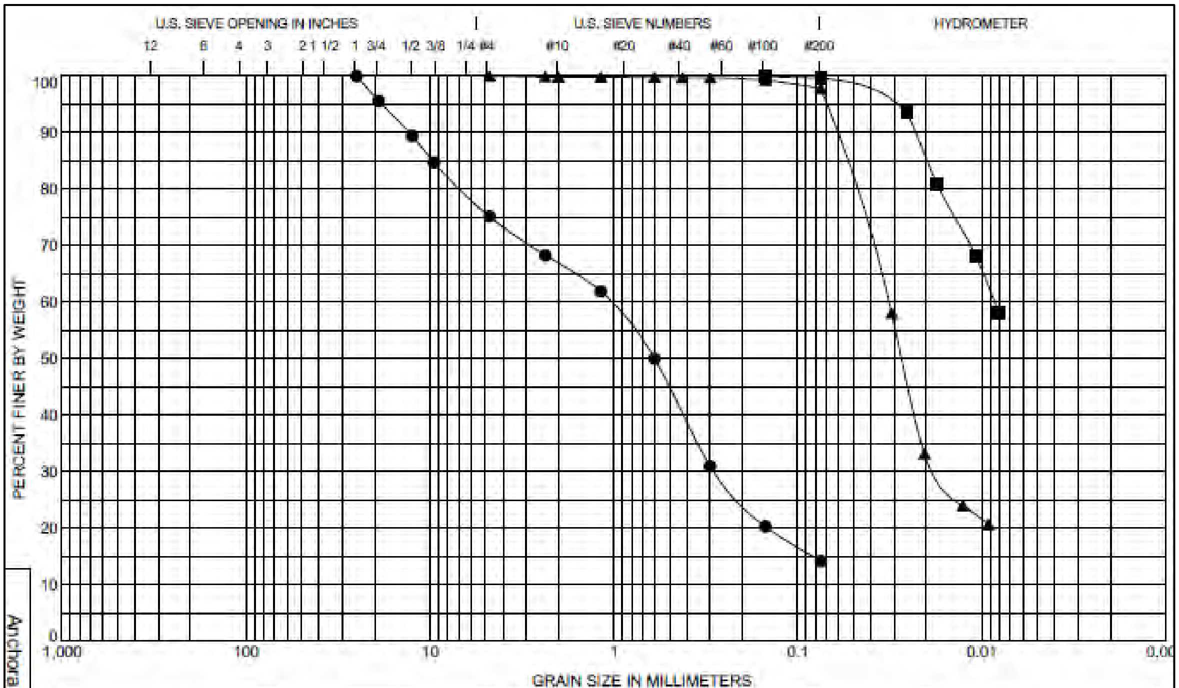

COBBLES	GRAVEL		SAND			SILT OR CLAY
	coarse	fine	coarse	medium	fine	

Sample		Depth, Ft	Classification	LL	PL	PI	Cc	Cu
●	TB-1 S2	5.0 - 6.5	Silty Sand with Gravel (SM)					
■	TB-1 S3	10.0 - 12.0	Silt (ML)	32	24	8		
▲	TB-1 S7	30.0 - 31.5	Silt (ML)					

Sample		Depth, Ft	D100	D60	D30	D10	%Gravel	%Sand	%Silt	%Clay
●	TB-1 S2	5.0 - 6.5	25	1.06	0.28		25	61	14	
■	TB-1 S3	10.0 - 12.0	0.15	0.01			0	0	100	
▲	TB-1 S7	30.0 - 31.5	4.75	0.03	0.02		0	2	98	

Figure 2-6. Port of Alaska – Grain Size and Index Test Results for TB-1 (Shannon & Wilson 2016)

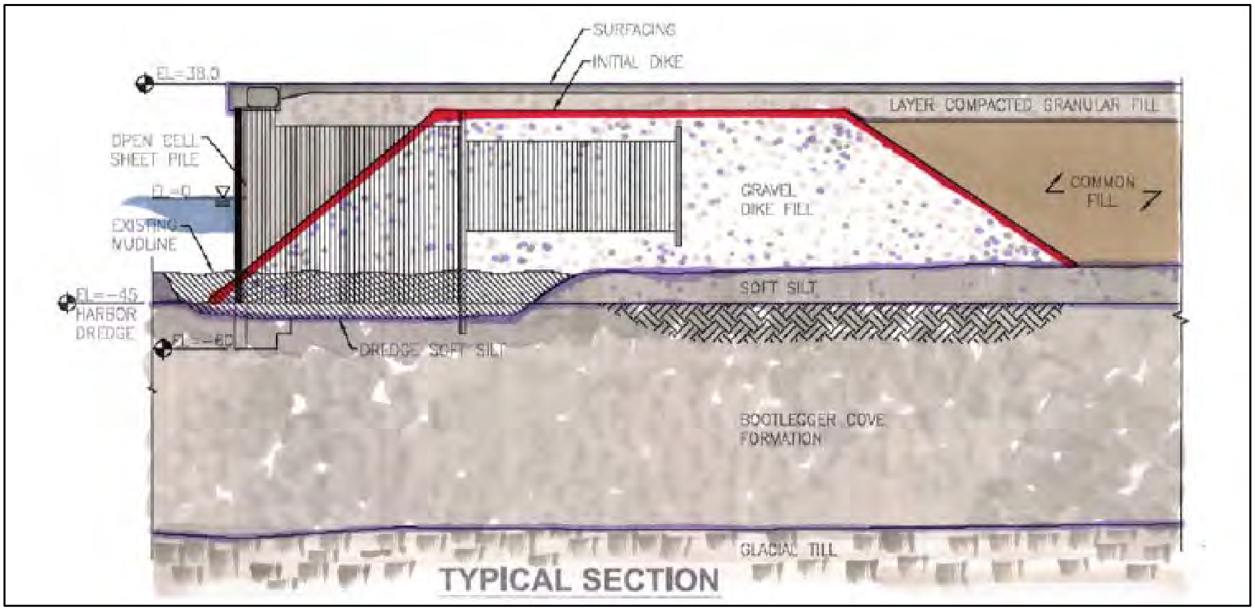

Figure 6-7. Port of Alaska – North Extension Generalized Subsurface Conditions (after PND 2009)

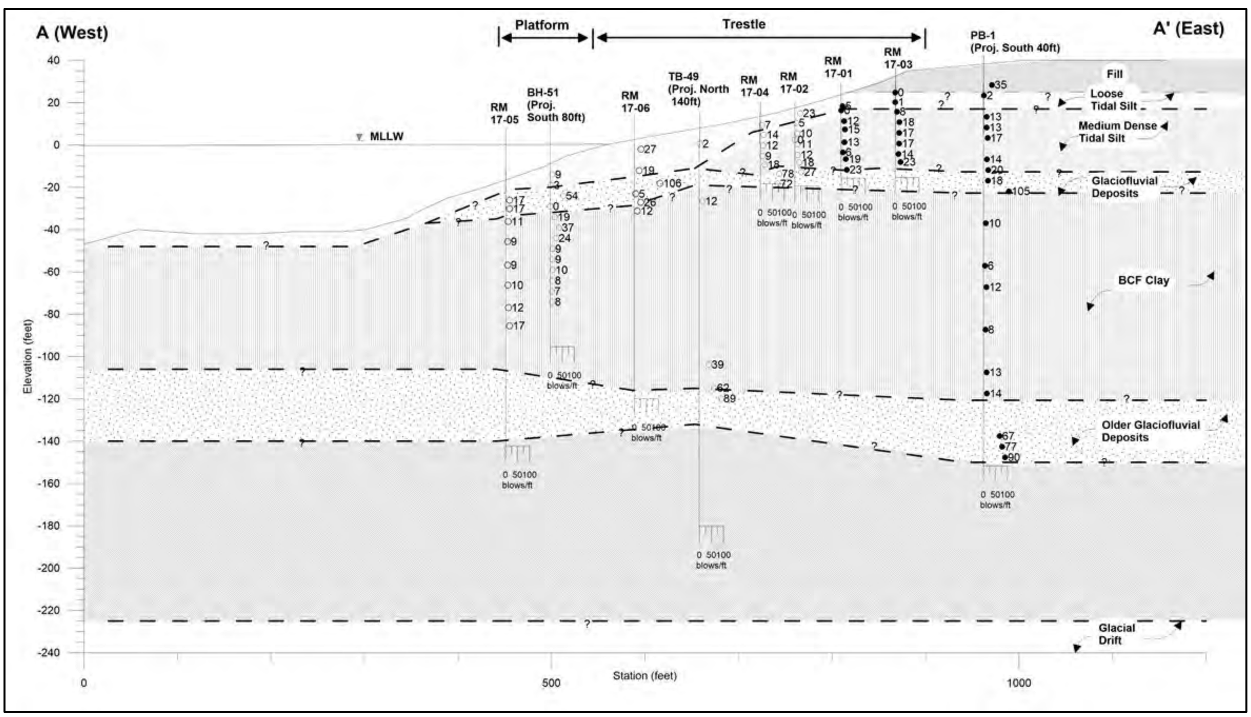

Figure 6-8. Port of Alaska – PCT Generalized Subsurface Conditions (COWI 2018)

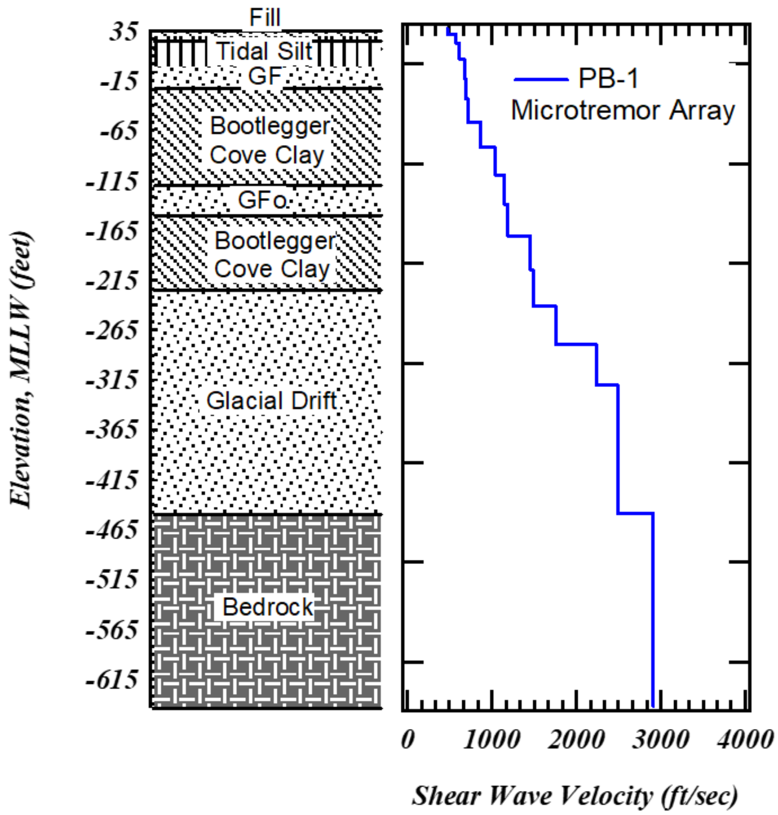

Figure 6-9. Port of Alaska – Microtremor Array at PCT Site (Christie et. al. 2019)

Figure 6-10. Port of Alaska – Monitoring Station Plan

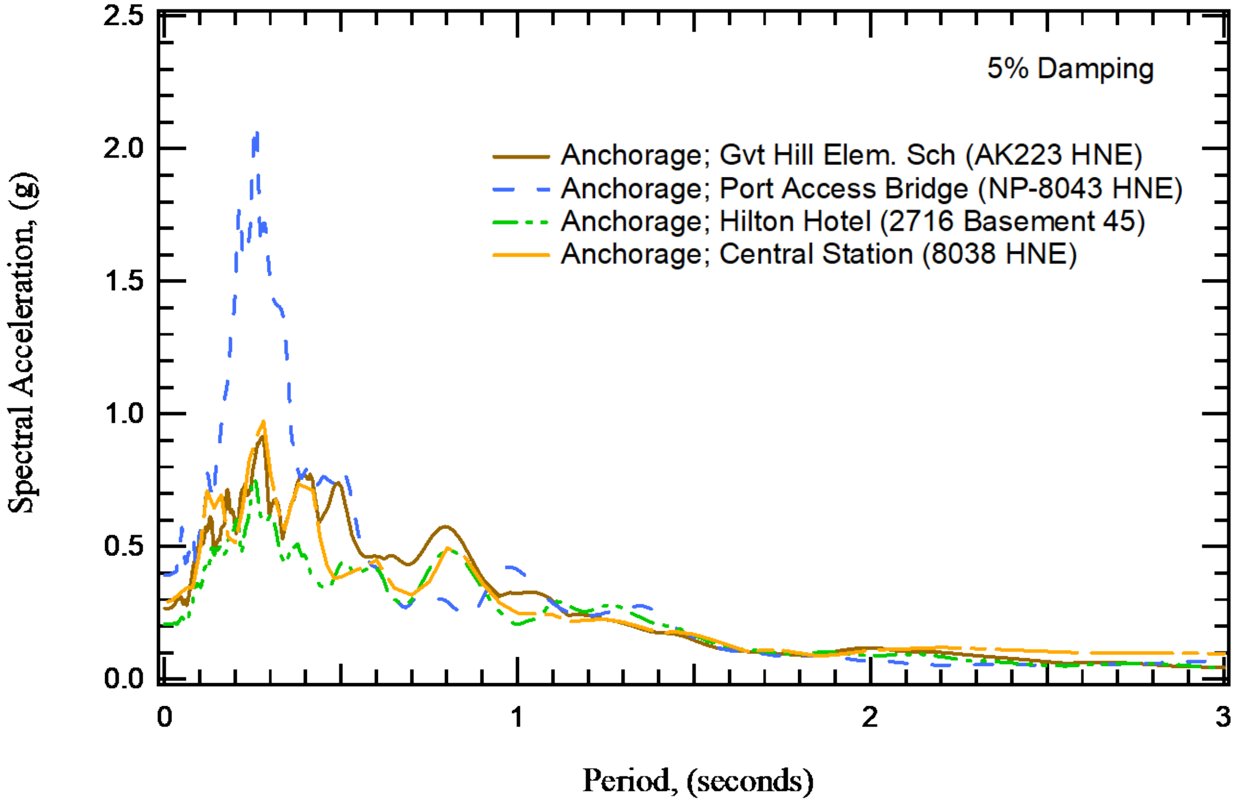

Figure 6-11. Port of Alaska – Nearby Monitoring Station Response Spectra

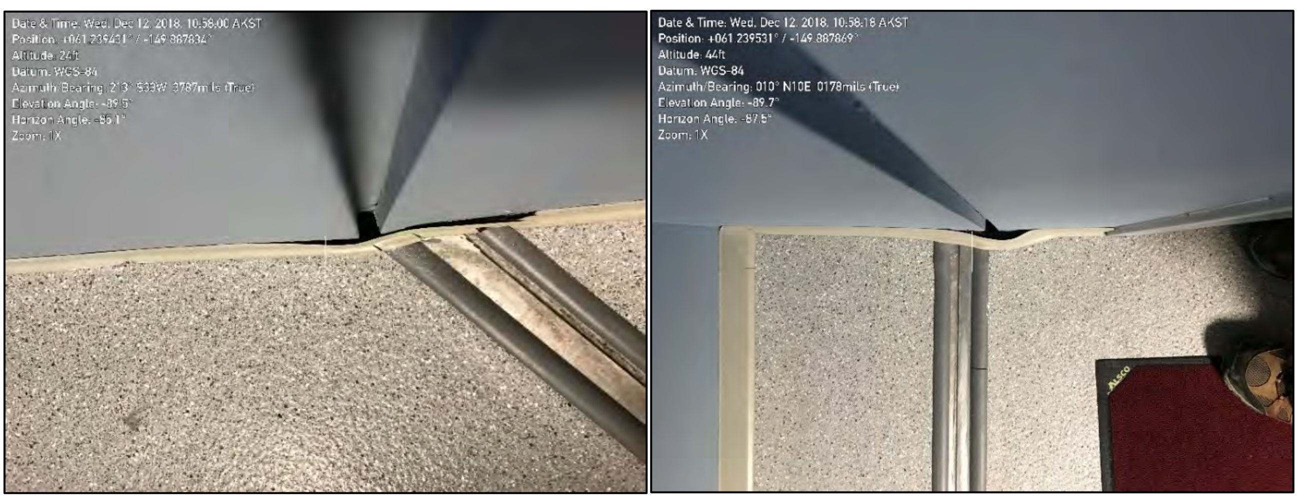

Figure 6-12. Port of Alaska – View of permanent movement of approximately one-quarter inch (left) and one-half inch (right) on the second floor of the Administration Building

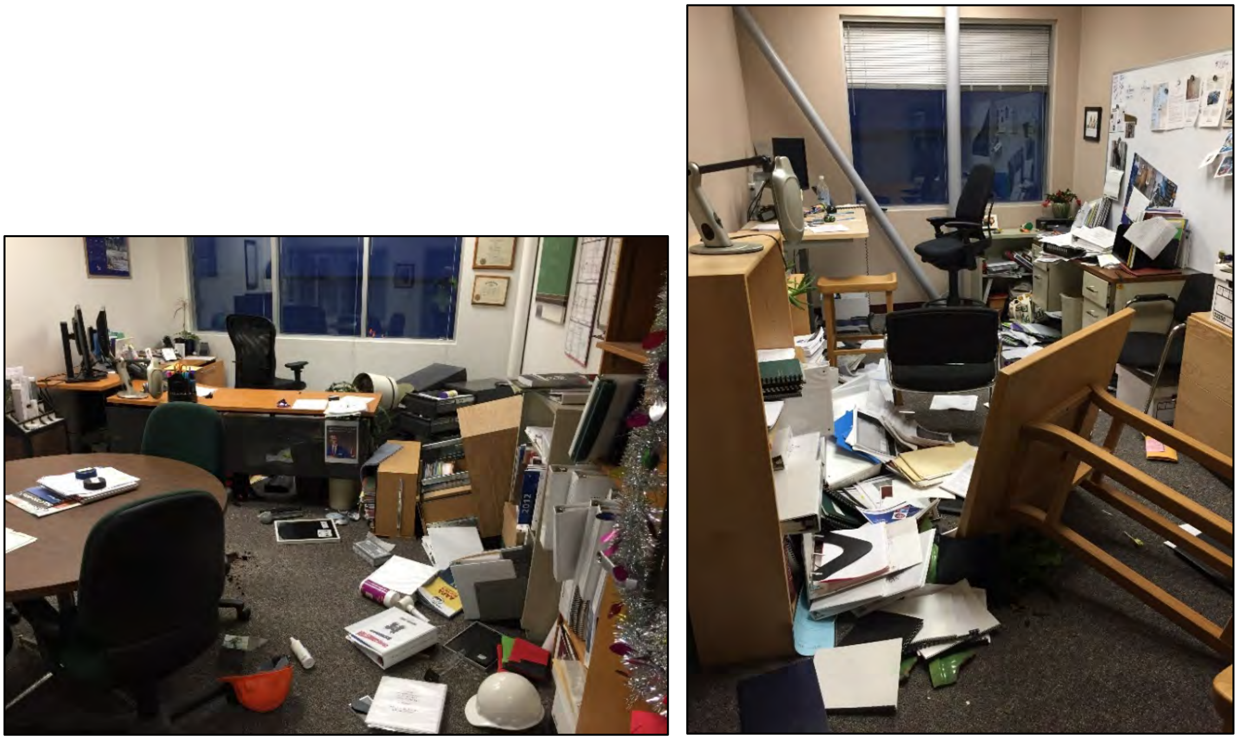

Figure 6-13. Port of Alaska – Post-earthquake view of offices at the Administration Building on 30 November 2018 (photographs courtesy of Jim Jager, PoA)

Figure 6-14. Port of Alaska – Evidence of pounding at the transition from Terminals 1 and 2, with spalling at the top and sides of the concrete apron (right) on 30 November 2018 (photographs courtesy of Jim Jager, PoA)

Figure 6-15. Port of Alaska – View of pile-to-apron connections and chained fenders on 30 November 2018 (photographs courtesy of Jim Jager, PoA)

Figure 6-16. Port of Alaska – View of piles below wharf, pile-to-apron connections, and chained fender on 30 November 2018 (photographs courtesy of Jim Jager, PoA)

Figure 6-17. Port of Alaska – View of gantry cranes along Terminal 1, chained to crane rails while not in use

Figure 6-18. Port of Alaska – Transit Yard A: Across from Administration Building on 31 November 2018 (Viewing South). (Photographs courtesy of John Daley, R&M Consulting)

Figure 6-19. Port of Alaska – Transit Yard A: Tension cracks across from Administration Building on 31 November 2018 (Viewing South). (Photographs courtesy of John Daley, R&M Consulting)

Figure 6-20. Port of Alaska – Transit Yard A: Across from Administration Building (Viewing South)

Figure 6-21. Port of Alaska – Transit Yard A: Across from Administration Building (Viewing South)

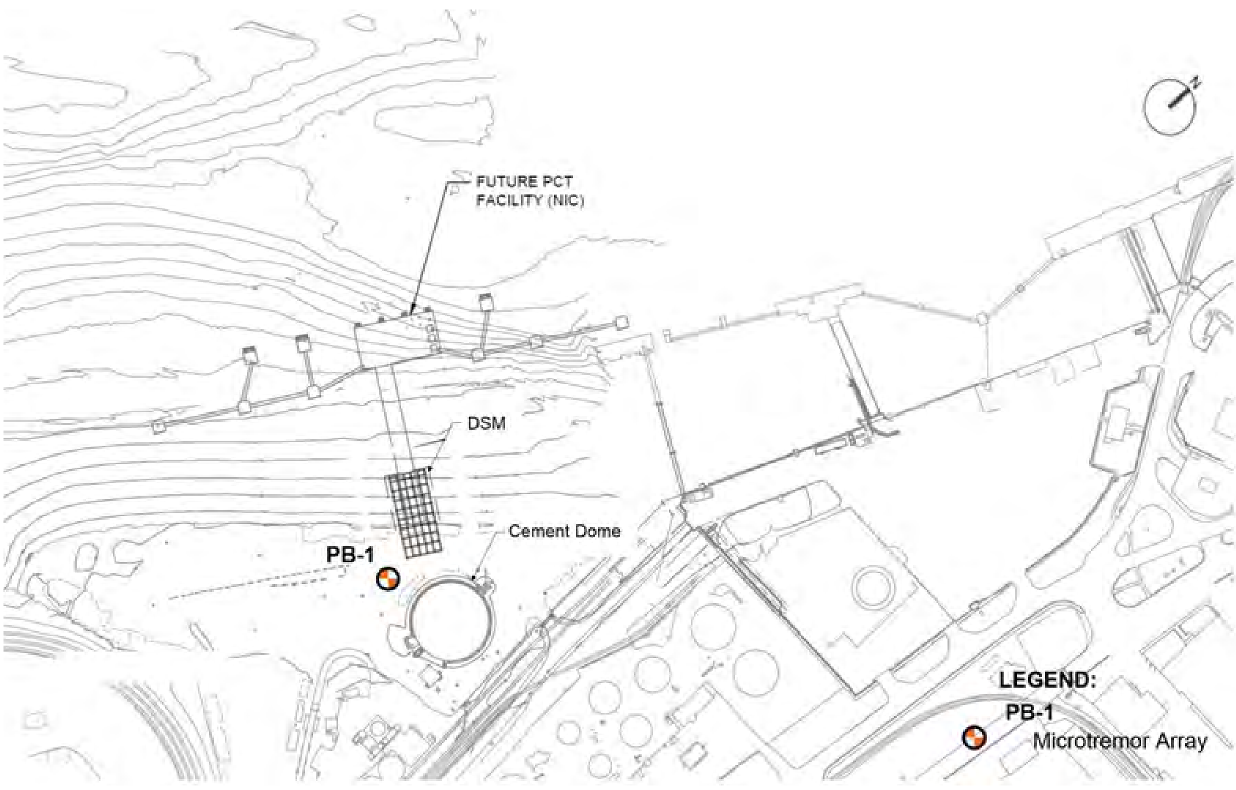

Figure 6-22. Port of Alaska – PCT Site Plan (Christie et. al., 2019)

Figure 6-23. Port of Alaska –View of cement storage dome and earthquake-induced movements along shore on 30 November 2018 (Photographs courtesy of Jim Jager, PoA)

Figure 6-24. Port of Alaska – Pre- and post-earthquake view of shoreline at the PCT

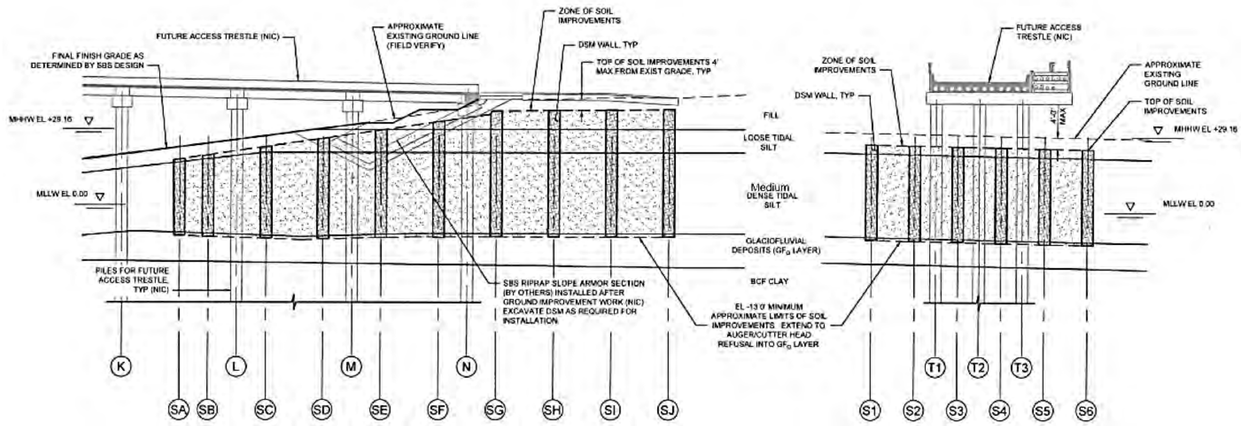

Figure 6-25. Port of Alaska – DSM Layout (Christie et. al. 2019)

Figure 6-26. Port of Alaska – Pre- and post-earthquake view of shoreline at the PCT (Viewing South of DSM)

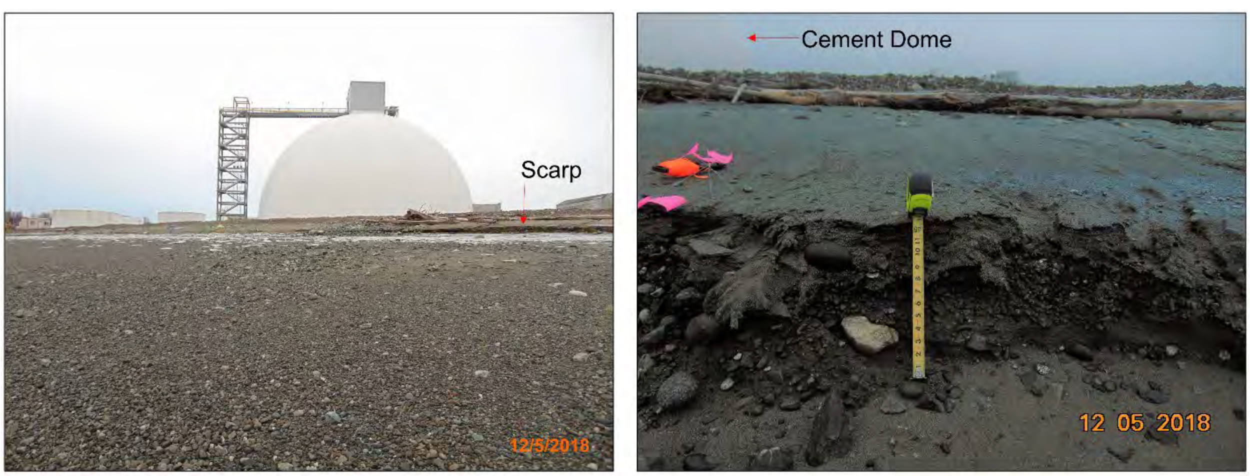

Figure 6-27. Port of Alaska – PCT Shoreline Scarp (Viewing Landward)

Figure 6-28. Port of Alaska – Tension Cracks on PCT Shoreline South of Cement Dome

Figure 6-29. Port of Alaska – PCT Shoreline Tension Cracks (Viewing North of DSM)

Figure 6-30. Port of Alaska –View of surficial bluff failure on 30 November 2018 (Photographs courtesy of Jim Jager, PoA)

Figure 6-31. Port of Alaska – Fig. G. View of surficial bluff failure (left) and shallow slope movements (right) on 30 November 2018 (Photographs courtesy of Jim Jager, PoA)

Figure 6-32. Port of Alaska – East to West Tension Crack behind North Open Cell Bulkhead Return Wall

Figure 6-33. Port of Alaska – North Expansion Tension Cracks (Viewing South) on 30 November 2018 (Photographs courtesy of Jim Jager, PoA)

Figure 6-34. Port of Alaska – North Expansion Tension Cracks (Viewing South)

Figure 6-35. Port of Alaska – Northern Expansion Tension Cracks (Viewing North)

Figure 6-36. Port of Alaska – Northern Rock Slope Tension Cracks

Figure 6-37. Port of Alaska – Northern Rock Slope Tension Crack (Viewing Northeast) (photographs courtesy of Jim Jager, PoA)

Figure 6-38. Port of Alaska – Northern Rock Slope Tension Cracks (Viewing South)

Figure 6-39. Port of Alaska – segments of lateral crack system

7.0 Next Steps

As described in Section 4.9, further subsurface characterization is warranted at recording stations and throughout the Anchorage basin, including geotechnical investigations such as cone penetration tests (CPTs) or borings with sampling. These investigations would complement the geophysical testing performed during the Phase II GEER efforts and provide the opportunity for geotechnical characterization (e.g., penetration resistance, particle size distributions, Atterberg limits). Subsequent research funding will be pursued by the authors of this report to perform additional geotechnical and geophysical investigation at identified sites of interest.

8.0 References

Abrahmson, N., Kueh, N., Gulerce, Z., Gregor, N., Bozorgnia , Y., Parker, G., Stewart, J.P., Chiou B., Idriss, I.M., Campbell, K., Youngs, R., 2018, Update of the BCHydro Subduction Ground-Motion Model Using the NGA-Subduction Dataset, PEER Report, Berkeley, California.

Alaska Earthquake Center, https://strongmotioncenter.org/cgi-bin/CESMD/iqr_dist_DM2.pl?iqrid=us1000hyfh (last accessed 05/28/2019 1:00 pm EST).

Atkinson, G. M., and Boore, D. M., 2003, Empirical Ground-Motion Relations for Subduction-Zone Earthquakes and Their Application to Cascadia and Other Regions, *Bulletin of the Seismological Society of America* 93, 1703-1729.

Blewitt, G., Hammond, W.C., and Kreemer, C., 2018, Harnessing the GPS data explosion for interdisciplinary science, Eos, 99, https://doi.org/10.1029/2018EO104623.

Boore, D.M., 2004, Ground Motion in Anchorage, Alaska, from the 2002 Denali Fault Earthquake: Site Response and Displacement Pulses, *Bulletin of the Seismological Society of America*, Vol. 94, No. 6B, pp. S72–S84.

Carver, G., and Plafker, G., 2008, Paleoseismology and neotectonics of the Aleutian subduction zone-An overview. In: Freymueller, J.T., Haeussler, P.J., Wesson, R.L., and Ekstrom, G., eds., active Tectonics and Seismic Potential of Alaska: American Geophysical Union Geophysical Monograph Series, v. 179, p. 43-63.

CESMD Strong Motion Data-Set, https://strongmotioncenter.org/cgi-bin/CESMD/iqr_dist_DM2.pl?iqrid=us1000hyfh (last accessed 05/28/2019, 3:30 pm EST).

Christie S., Zhang, Y., Dickenson, S., and Pintner, B., 2019, "Seismic Analysis and Ground Improvement Design for the PCT Marine Terminal at the Port of Alaska." American Society of Civil Engineers, Ports 2019, Pittsburgh, Pennsylvania.

COWI, 2018, Port of Alaska Modernization Program Petroleum and Cement Terminal Geotechnical Engineering Report, prepared for the Port of Alaska, May 11, 2018.

Dutta, U., and Yang, Z, 2010, "Anchorage Strong Motion Network: Maintenance and Data Archival." Final Technical Report G09AC00102, National Earthquake Hazards Reduction Program, U.S. Geological Survey, Washington, D.C. 125 pp.

Dutta et al., 2007, *S*-Wave Velocity Structure of Sediments in Anchorage, Alaska, Estimated with Array Measurements of Microtremors. Bulletin of the Seismological Society of America, Vol. 97, No. 1B, pp. 234–255, doi: 10.1785/0120060001

Dutta, U., Biswas, N., Martirosyan, A., Papageorgiou, A., and Kinoshita, S., 2003, Estimation of earthquake source parameters and site response in Anchorage, Alaska, from strong-motion network data using generalized inversion method, *Phys. Earth Planet. Interiors* 137, 13–29.

Dutta, U., Martirosyan, A., Biswas, N., Papageorgiou, A., and Combellick, R., 2001, Estimation of *S*-Wave Site Response in Anchorage, Alaska, from Weak-Motion Data Using Generalized Inversion Method. Bulletin of the Seismological Society of America, 91, 2, pp. 335–346.

Dutta, U., Biswas, N., Martirosyan, A., Nath, S., Dravinski, M., Papageorgiou, A., and Combellick, R., 2000, Delineation of spatial variation of shear-wave velocity with high frequency Rayleigh wave, Geophys. J. Int. 143, 365–376.

Escamilla, J., 2018, *Personal Electronic Communication to David Hemstreet*.

Golder, 2009, "Final Report, Structural Foundation Engineering Report for Retaining Walls, Old Glenn Highway Fire Lake To Ski Road." ADOT&PF PROJECT 52515/STP-0558(2), Anchorage, Alaska. 60 pp.

Hansen, W.R., Eckel, E.B., Schaem, W.E., Lyle, R.E., George, W., and Chance G., 1966, The Alaska Earthquake March 27, 1964: Field investigations and reconstruction effort, U.S. Geological Survey Professional Paper 541.

Hartman, D. C., Pessel, G. H., and McGee, D. L., 1974, Stratigraphy of the Kenai group, Cook Inlet, Alaska Div. Geol. Geophys. Surv. Open-File Rept. 49. Available at www.dggs.dnr.state.ak.us/pubs/pubs?reqtype.

Hemstreet, 2018, *Personal Communication* (electronic mail).

Hirschmüller, H., 2008, Stereo Processing by Semi-Global Matching and Mutual Information, IEEE Transactions on Pattern Analysis and Machine Intelligence, 30, 328-341.

Hirschmüller, H., 2005, Accurate and Efficient Stereo Processing by Semi-Global Matching and Mutual Information, in Proceedings, IEEE Conference on Computer Vision and Pattern Recognition, June 2005, San Diego, CA, USA, 2, 807-814. Lowe, D. G., 2004.Distinctive image features from scale-invariant keypoints, International Journal of Computer Vision, 60, 91-110.

Jones, J., Kalkan, E., and Stephens, C., 2017, Processing and Review Interface for Strong Motion Data (PRISM)—Methodology and automated processing, Version 1.0.0, U.S. Geol. Surv. OpenFile Rept. 2017-1008, 80 pp., doi: 10.3133/ofr20171008.

Koehler, R.D., Farrell, R.E., Burns, P.A.C., and Combellick, R.A., 2012, Quaternary faults and folds in Alaska: A digital database: Alaska Division of Geological & Geophysical Surveys Miscellaneous Publication 141, 31 p., 1 sheet, scale 1:3,700,000.

Koehler, R.D., 2013, Quaternary Faults and Folds (QFF): Alaska Division of Geological & Geophysical Surveys Digital Data Series 3.

Kramer, S., Sideras, S.S., and Greefield, M.W., 2016, The Timing of Liquefaction and Its Utility in Liquefaction Hazard Evaluation. 6th International Conference on Earthquake Geotechnical Engineering, 1-4 November 2015, Christchurch, New Zealand.

Lowe, D.G., 2004, Distinctive image features from scale-invariant keypoints, International Journal of Computer Vision, 60, 91-110.

Marr, D. and Nishihara, H. K., 1978, Representation and recognition of the spatial organization of three-dimensional shapes, in Proceedings, Royal Soc. London B: Biolog. Sciences, 200, 269-294.

Martirosyan, A., Dutta, U., Biswas, N., Papageorgiou, A., and Combellick, R., 2002, Determination of site response in Anchorage, Alaska, on the basis of spectral ratio methods, *Earthq. Spectra* 18, 85–104.

Martirosyan, A., and Biswas, N., 2002, Site response at a rock site in Anchorage, Alaska from borehole strong-motion records (abstract), *Seism. Res. Lett.* 73, 267.

Miller, R.D. and Dobrovolny, E., 1959, Surficial geology of Anchorage and vicinity Alaska, U.S. Geological Survey Bulletin 1093, 129 p.

Nath, S. K., Chatterjee, D., Biswas, N. N., Dravinski, M., Cole, D. A., Papageorgiou, A., Rodriguez, J. A., and Poran, C. J., 1997, Correlation study of shear-wave velocity in near-surface geological formations in Anchorage, Alaska, *Earthquake Spectra* 13, 55–75.

Nath, S. K., N. N. Biswas, M. Dravinski, and A. S. Papageorgiou, 2002, Determination of *S*-wave site response in Anchorage, Alaska, in the 1–9 Hz frequency band, *Pure Appl. Geophys.* 159, 2673–2698.

Plafker, 1969, Tectonics of the March 27, 1964 earthquake, U.S. Geological Survey Professional Paper 543-I.

PND, 2009, "Port of Anchorage Expansion Design Study Report", PND Project 061028, dated April 2009.

Reger, R.D., and Updike, R.G., 1993, Upper Cook Inlet Region and the Matanuska Valley. In: Pewe, T.L., and Reger, R.D., eds., 1993, Alaska: Guidebook to Permafrost and Quaternary Geology Along the Richardson and Glenn Highways Between Fairbanks and Anchorage, Alaska, Alaska Division of Geological & Geophysical Surveys, p. 185-259.

Reger, R.D., Combellick, R.A., and Brigham-Grette, J., 1995, Late-Wisconsin events in the Upper Cook Inlet region southcentral Alaska. In: Combellick, R.A., and Tannian,R., eds., Short notes on

Alaska Geology 1995, alaska Division of Geological & Geophysical Surveys Professional Report 117D, p. 33-45.

Shannon & Wilson, 2016, “Geotechnical Data Report Anchorage Port Modernization Project Terminal 1 Port of Anchorage, Alaska.” report number 32-1-02480-001, February, 2016.

Snavely, N., Seitz, S. M., and Szeliski, R., 2008, Modeling the world from internet photo collections, Inter. J. Comp. Vision, 80, 189-210.

Somerville, P.G., Smith, N.F., Graves, R.W., Abrahamson, N.A, 1997, Modification of empirical strong ground motion attenuation relations to include the amplitude and duration effects of rupture directivity. Seismol Res Lett 68(1):199–222.

Thompson, E.M., Allstadt, K.E., Grant, A., Jibson, R.W., Bender, A.M., Witter, R.C., Hearne, M., Wald, D.J., and McBride, S.K., 2019, USGS Near-real-time ground failure product for the 2018 Anchorage earthquake, Seismological Research Letters, v. 90, no. 2B, p. 1005.

Trifunac, M.D., and Brady, A.G., 1975, Study on duration of strong earthquake ground motion. Bull. Seismol. Soc. Am., 65(3):581–626.

Updike, R.G., 1984, the Turnagain Heights landslide: an assessment using the electric-cone-penetration test, Alaska Division of Geological & Geophysical Surveys Report of Investigation 84-13, 48 p.

West et al., in prep, Initial observations from the 30 November 2018 Mw7.1 Anchorage Earthquake

West, M.E., Haeussler, P.J., Ruppert, N.A., Freymueller, J.T., and the Alaska Seismic Hazards Safety Commission, 2014, Why the 1964 Great Alaska Earthquake matters 50 years later, Seismological Research Letters, v. 85, no. 2, p. 1-7.

Wilson, F.H., Hults, C.P., Schmoll, H.R., Haeussler, P.J., Schmidt, J.M., Yehle, L.A., and Labay, K.A., comps., 2012, Geologic map of the Cook Inlet region, Alaska, including parts of the Talkeetna, Taldeetna Mountains, Tyonek, Anchorage, Lake Clark, Kenai, Seward, Iliamna, Seldovia, Mount Katmai, and Afognak quadrangles: U.S. Geological Survey Scientific Investigations Map 3153, 76 p., 2 sheets, scale 1:250,000.

Yamasaki, K., Hemstreet, D., Gerondale, A., Shao, L., 2015, “Wet soil mixing for Supporting Bridge Abutment Spread Footings.” Proc., Annual Meeting of the Deep Foundations Institute, Oakland, CA, 10 pp.

Youngs, R. R., S.-J. Chiou, W. G. Silva, and J. R. Humphrey (1997). Strong Ground Motion Attenuation Relationships for Subduction Zone Earthquakes, *Seismological Research Letters* 68, 58-73.

Appendices

Appendix A.

Table A1. Recording stations from the Center for Engineering Strong Motion Data (CESMD) with available records from the mainshock.

Network	Station Number	Station Name	Latitude (N)	Longitude (W)	R_{epic} km	Visited by GEER	NEHRP Site Class	V_{s30} (m/s)
UAGI	K223	AK:Anchorage;Gvt Hill Elem Sch	61.234	149.868	13.4	Y	-	-
NSMP	2716	AK:Anchorage;Hilton Hotel	61.219	149.892	13.7	Y	-	-
NSMP	8043	AK:Anchorage;Port Access Br	61.222	149.885	14.4	N	-	-
NSMP	8038	AK:Anchorage;FS 01 (Central)	61.218	149.883	14.8	Y	D	-
NSMP	8040	Anchorage - R B Atwood Bldg	61.215	149.893	15.1	Y	D	-
NSMP	8045	AK Anchorage - VAMC	61.233	149.744	15.8	N	-	-
NSMP	8023	Anchorage - Football Stadium	61.205	149.876	16.3	N	C/D	-
NSMP	8041	AK:Anchorage;Turnagain ELMN	61.194	149.947	16.9	N	-	-
NSMP	8016	AK:Anchorage;BP Bld	61.192	149.864	16.9	Y	C/D	-
NSMP	8042	AK:Anchorage;Frontier Bld	61.188	149.884	17.2	N	-	-
NSMP	8011	Anch - Russian Jack Spr St Pk	61.209	149.786	17.8	N	C	-
NSMP	8007	AK:Anchorage;Intl Arpt	61.182	149.997	17.8	N	C	-
UAGI	K203	AK:Anchorage;St Christo Epi Ch	61.22	149.745	18	N	C	474
NSMP	8036	AK:Anchorage;DOI OAS	61.178	149.966	18.7	Y	C	-
UAGI	K208	AK:Anchorage;Spenard Rec Ctr	61.176	149.922	19	N	D	274
UAGI	K204	AK:Anchorage;Signature Flt Sup	61.176	150.012	19.2	N	D	309*
NSMP	8047	AK:Anchorage;USGS ESC	61.189	149.802	19.4	Y	-	-
NSMP	8028	AK:Anchorage;Coll Gate Elem	61.193	149.782	19.5	N	C	-
NSMP	8029	AK:Anchorage;Tudor Elem Sch	61.174	149.85	20	N	C	-
NSMP	8030	Anchorage - Police HQ	61.179	149.806	20.2	Y	C	-
NSMP	8027	AK:Anchorage;St Fish&Game	61.161	149.889	20.9	Y	C/D	-
UAGI	K209	AK:Anchorage;Scenic Prk Bib Ch	61.185	149.747	21.1	N	C	582
NSMP	8037	Anchorage - NOAA Weather Fac	61.156	149.985	21.2	Y	D	-
UAGI	K221	AK:Anchorage;St James Ortho Ch	61.152	149.951	21.6	N	D	-
NSMP	8025	Anchorage - BS Lutheran Ch	61.147	149.894	21.6	N	C/D	-
UAGI	K220	AK: Anchorage;Kincaid Park	61.154	150.055	22.1	N	D	-
UAGI	K211	AK:Anchorage;HQ Fire Dept #12	61.149	149.858	22.5	N	C	394*
UAGI	K212	AK:Anchorage;BLM	61.156	149.793	22.9	N	C	514
UAGI	K217	AK:Anchorage;Chugiak FS	61.396	149.516	24.1	N	-	-
UAGI	K210	AK:Anchorage;Mears Jr HS	61.129	149.931	24.2	N	D	269
NSMP	8021	AK:Anchorage;Klatt Elem Sch	61.113	149.91	26.1	Y	D	-
UAGI	K213	AK:Anchorage;ASD Operation Ctr	61.113	149.859	26.5	N	C/D	354
UAGI	K222	AK:Anchorage;Chapel by the Sea	61.088	149.837	29.5	N	C	-
UAGI	RC01	Rabbit Creek AK USA	61.089	149.739	30.9	N	-	-
UAGI	K215	AK:Anchorage;Rabbit Creek FS10	61.086	149.752	30.9	N	C	412
UAGI	SSN	Susitna AK USA	61.464	150.747	44.1	N	-	-
UAGI	K218	AK:Anchorage;PTWC	61.593	149.133	51.5	N	-	-
UAGI	KNK	Knik Glacier AK USA	61.413	148.459	80.1	N	-	-
UAGI	CAPN	Captain Cook Nikiski, AK, USA	60.768	151.154	91.1	N	-	-
UAGI	SAW	Sawmill AK USA	61.807	148.332	100	N	-	-
UAGI	PWL	Port Wells, AK	60.858	148.333	102.7	N	-	-
UAGI	SKN	Skwentna AK USA	61.98	151.532	109	N	-	-
UAGI	SWD	Seward, AK, USA	60.104	149.453	140.8	N	-	-
UAGI	GLI	Glacier Island AK USA	60.879	147.096	162.1	N	-	-
UAGI	WAT7	Susitna Watana 7 AK USA	62.833	148.848	175.1	N	-	-
UAGI	WAT1	Susitna Watana 1 AK USA	62.83	148.551	180.4	N	-	-
UAGI	DAM1	Bradley Dam 1 AK USA	59.755	150.851	183.6	N	-	-

Table A2. Recording stations from the Center for Engineering Strong Motion Data (CESMD) with available records from the mainshock (cont.).

Network	Station Number	Station Name	Latitude (N)	Longitude (W)	R_{epic} km	Visited by GEER	NEHRP Site Class	V_{s30} (m/s)
UAGI	DAM2	Bradley Dam 2 AK USA	59.755	150.856	183.6	N	-	-
UAGI	BRLK	Bradley Lake, AK, USA	59.751	150.906	184.9	N	-	-
UAGI	HOM	Homer Trailer, AK	59.657	151.651	209.5	N	-	-
UAGI	CNP	China Poot, AK, USA	59.525	151.237	214.4	N	-	-
UAGI	HIN	Hinchinbrook, AK, USA	60.396	146.503	214.6	N	-	-
UAGI	DIV	Divide Microwave AK USA	61.129	145.775	225	N	-	-
NSMP	2738	AK:Cantwell;ADOT Maint Sta	63.389	148.885	233.7	N	-	-
UAGI	DHY	Denali Highway AK USA	63.075	147.376	234.2	N	-	-
UAGI	RND	Reindeer AK USA	63.406	148.86	235.8	N	-	-
UAGI	EYAK	Cordova Ski Area AK USA	60.549	145.75	243.8	N	-	-
UAGI	KTH	Kantishna Hills AK USA	63.553	150.923	250.3	N	-	-
UAGI	CAST	Castle Rocks AK USA	63.419	152.084	255.2	N	-	-
UAGI	CDVT	Cordova Airport AK USA	60.494	145.47	260.3	N	-	-
UAGI	MCK	McKinley Park AK USA	63.732	148.937	270.3	N	-	-
UAGI	BMR	Bremner River AK USA	60.968	144.605	290.1	N	-	-
UAGI	PAX	Paxson AK USA	62.97	145.47	294.7	N	-	-
UAGI	RAG	Ragged Mountain AK USA	60.386	144.677	305	N	-	-
UAGI	BPAW	Bear Paw Mountain AK USA	64.1	150.987	310.6	N	-	-
UAGI	GLB	Gilahina Butte AK USA	61.442	143.812	327.2	N	-	-
UAGI	HMT	Hamilton AK USA	60.335	144.262	328.3	N	-	-
UAGI	VRDI	Verde Repeater AK USA	61.228	143.455	347.5	N	-	-
UAGI	RIDG	Independent Ridge AK USA	63.74	144.846	373.4	N	-	-
UAGI	CRQ	Cirque AK USA	60.752	143.093	375.2	N	-	-
UAGI	DOT	Dot Lake AK USA	63.648	144.07	396	N	-	-
UAGI	WAX	Waxell Ridge AK USA	60.448	142.853	396.9	N	-	-
UAGI	FA12	Watershed School Fairbanks AK USA	64.827	147.868	401	N	-	-
UAGI	FA01	AK:Fairbanks;Chena-GS Fire Station	64.835	147.937	401	N	-	-
UAGI	FA02	Ester Fire Station AK USA	64.846	148.009	401.2	N	-	-
UAGI	FA10	Bus Barn Fairbanks AK USA	64.819	147.778	401.3	N	-	-
UAGI	FA09	DNR Fairbanks AK USA	64.838	147.817	402.8	N	-	-
UAGI	FA07	AK:Fairbanks;Arctic Lights Elem. School	64.827	147.695	403.4	N	-	-
UAGI	FA05	AK:Fairbanks;Denali Elem. School	64.839	147.752	403.9	N	-	-
UAGI	FA11	AK:Fbnks;Cold Climate Housing Res. Cntr	64.854	147.838	404.3	N	-	-
UAGI	FA06	AK:Fairbanks;Nordale Elem. School	64.846	147.696	405.4	N	-	-
GSN	COLA	College Outpost Alaska USA	64.874	147.862	406.1	N	-	-
NSMP	2767	AK:Fairbanks;Moose Creek Dam	64.793	147.181	407.9	N	-	-
UAGI	TAPE	Goshawk Ln Fairbanks AK	64.893	147.789	409.1	N	-	-
UAGI	MLY	Manley Hot Springs AK USA	65.03	150.744	411.5	N	-	-
UAGI	SCRK	Sand Creek AK USA	63.976	143.991	422.2	N	-	-
UAGI	CYK	Cape Yakataga AK USA	60.082	142.487	429.8	N	-	-
UAGI	CTG	Chitna Glacier AK USA	60.965	141.34	464.1	N	-	-

CESMD announcement for data related to the Mw7.1 Anchorage Earthquake of November 30, 2018 (last updated 3/5/2019)

The CESMD is pleased to announce the availability of the 11/30 M7 Anchorage earthquake dataset. As of 3/5/2019, processed data from over 80 sites have been made available.

Before using this data for analysis and interpretation, there are several critical features to be aware of:

-- Some of the early data posted at CESMD had incorrect metadata. These were corrected in mid December - and then an error in a test system resulted in the reposting of the erroneous data in late February. In order to ensure that you are working with the most recent data, we urge users to re-download the entire dataset:
NP.2738: corrected 12/20/2018; incorrect metadata posted 2/24/19-3/5/19
NP.8047: corrected 12/21/2018; incorrect metadata posted 2/24/19-3/5/19

--A number of the AEC stations are sampled at 50 sps. Prior to the USGS processing, data are resampled to 200 sps as described in Jones et al., 2017. The resulting processed data files have data at 200 sps but have been filtered above 20 Hz. These filter corners are documented in the V2 file headers. The V1 data (unprocessed) for these stations is available at CESMD and remains at the original 50 sps. Users should refer to the list below to make sure that they understand which data are limited to below 20 Hz. All other stations processed data for this event have been filtered above 40Hz.

A temporary staffing shortage at the USGS NSMP data center resulted in a significant delay in getting this data processed and made available to the public. The CESMD thanks the community for their patience while this dataset was being processed.

Jones, J., E. Kalkan, and C. Stephens (2017). Processing and Review Interface for Strong Motion Data (PRISM)—Methodology and automated processing, Version 1.0.0, U.S. Geol. Surv. Open-File Rept. 2017-1008, 80 pp., doi: 10.3133/ofr20171008.

Stations with original data recorded at 50 sps:
AK.BMR
AK.BPAW
AK.BRLK
AK.CAPN
AK.CAST
AK.CNP
AK.CRQ
AK.CTG

AK.CYK
AK.DHY
AK.DIV
AK.DOT
AK.EYAK
AK.GLB
AK.HMT
AK.HOM
AK.KNK
AK.KTH
AK.MCK
AK.MLY
AK.PAX
AK.PPLA
AK.RAG
AK.RC01
AK.RIDG
AK.RND
AK.SAW
AK.SCRK
AK.SKN
AK.SSN
AK.SWD
AK.VRDI
AK.WAT7
AK.WAX

Appendix B.

Phase II investigation of the M7.1 Anchorage Alaska earthquake

GEER Phase II investigations were completed in Spring of 2019 after snowmelt between April 27 and May 1, 2019. The multidisciplinary team consisted of experts in earthquake geology, remote sensing, and ground motions and was led by Rich Koehler (University of Nevada, Reno). The team was comprised of six members including Bryce Berrett (Brigham Young University), Nicole Hastings (Brigham Young University), Chen ZhiQiang (University of Missouri-Kansas City), Shawn Herrington (University of Missouri-Kansas City), Xiang Wang (University of California, San Diego), Fikret Atalay (Georgia Tech University), and Zhaohui Yang (University of Alaska, Anchorage). Assistance in data processing and archiving was conducted by Eric Lo, Tara Hutchinson, and Falko Kuester at the University of California, San Diego. Logistical support and guidance during the Phase II investigation was provided by Kevin Franke (Brigham Young University) and David Frost (Georgia Tech University).

The purpose of the Phase II investigation was to further document and archive perishable data related to ground deformation and landslides in the vicinity of damaged infrastructure using ground and unmanned aerial photography, hyperspectral imagery, and ground based lidar. The lack of snow on the surface resulted in the recognition of cracks and other damage that were more extensive than originally observed during the December 2018 Phase I reconnaissance when snowstorms impacted observational effectiveness. Repeat UAV surveys were acquired at multiple sites to evaluate the effectiveness of various drone models and processing methods. Additionally, the Phase II team conducted shallow geophysical investigations including active and passive MASW surveys at sites co-located with strong ground motion instrumentation. Further analyses of the data collected by the Phase II team is in progress and is anticipated to be incorporated into future publications.

This appendix provides a summary and archive of data collected during the Phase II investigation and contains links to the raw data that are available to the public. Data has been archived via NHERI DesignSafe at: https://www.designsafe-ci.org/data/browser/public/designsafe.storage.published//PRJ-2336/Phase2.

Ground based photography

Ground based photography was acquired during the Phase II investigation at multiple sites that were initially evaluated during GEER's Phase I investigation (Figures B1-B8). The purpose of revisiting these sites was to document cracks, settlement, liquefaction, and other ground deformation that may have been obscured by snow during the December 2018 reconnaissance. Photographs were also acquired at three additional sites including foundation settlement at 2100 Minerva Road (Figure B9), a potentially earthquake triggered bank failure along Eagle River near the southern abutment of Briggs Bridge in the town of Eagle River (Figure B10), and liquefaction and ground settlement on Aircraft Drive near the Ted Stevens International airport (Figure B11). Although the ground-based photographs are not co-located with photographs taken during the Phase I investigation, general references to figures in the report are provided where available for general comparison purposes (winter vs. spring).

Figure B1. (A) Headscarp of the Rabbit Creek landslide showing slide blocks and backtilted trees. (B) Slide blocks near the toe of the Rabbit Creek landslide possibly related to lateral spreading. Movement of these blocks may have caused the larger failure at the headscarp. (C) Liquefied sand (dark gray material adjacent to yellow field book) on the surface of slide blocks near the toe of the slide. General location of the Rabbit Creek landslide (Lat/Long: 61.0912°, -149.8470°). See figure 5-28 in the body of the report.

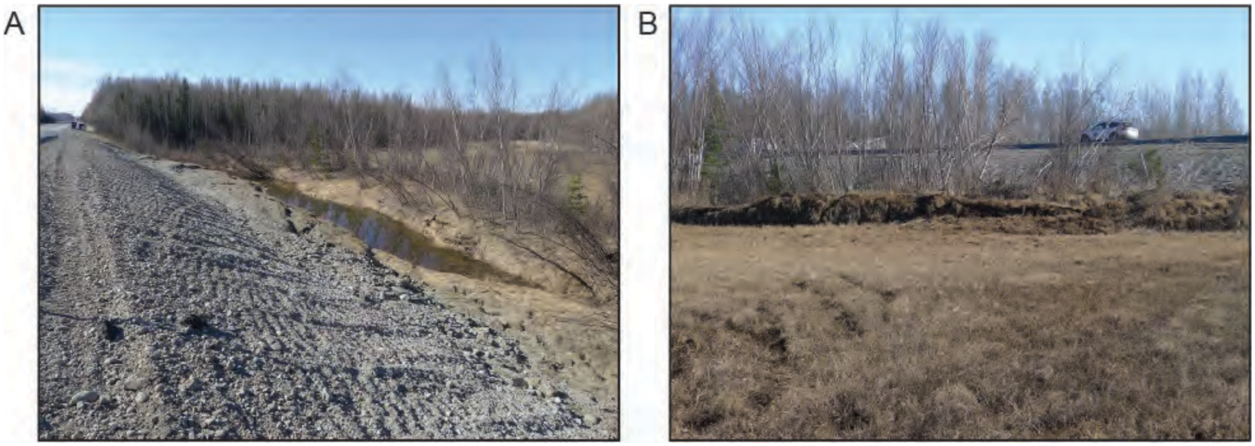

Figure B2. (A) View southwest of the road repair along the western side of the Vine Road failure showing lateral spread mounds adjacent to the roadway. (B) View east towards vine road showing soil mounds. (Lat/Long: 61.56863, -149.60215). See figure 5-38 in the body of the report.

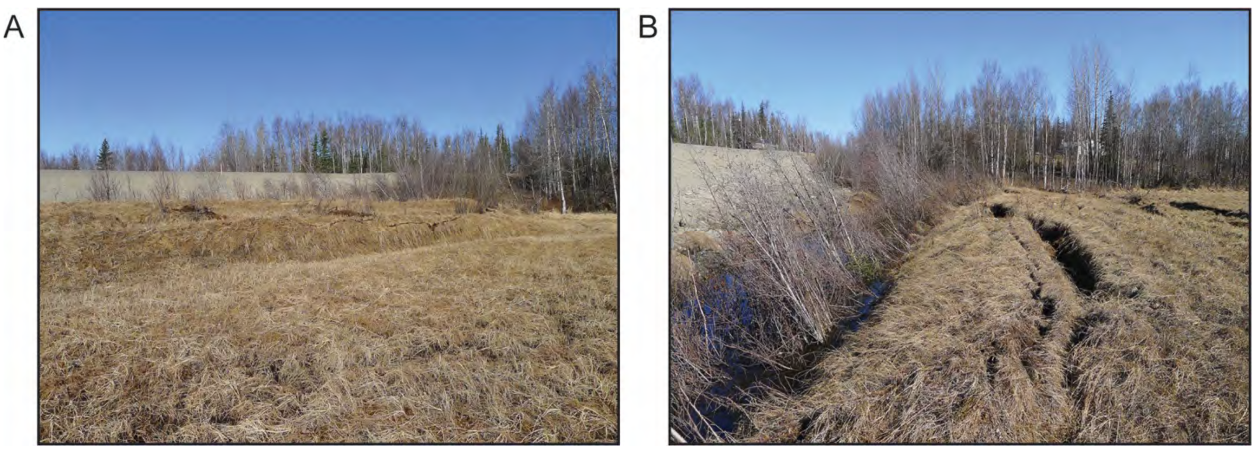

Figure B3. View west (A) and view north (B) of laterally spread soil mounds along the eastern side of the Vine Road failure. (Lat/Long: 61.568414, -149.601286). See figure 5-38 in the body of the report.

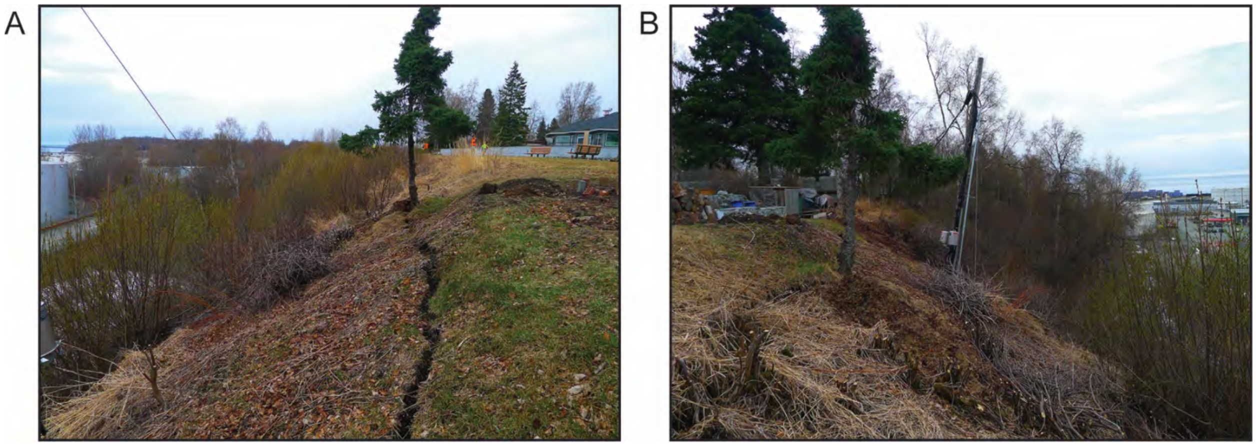

Figure B4. Photographs of a landslide along the steep bluff bordering the southeastern side of the Port of Alaska (Lat/Long: 61.2303°, -149.8849°). Movement of the slide did not affect storage tanks and other infrastructure along the base of the slide. (A) crack along the headscarp. (B) Tilted power pole on the slide surface. See figure 5-29 in the body of the report.

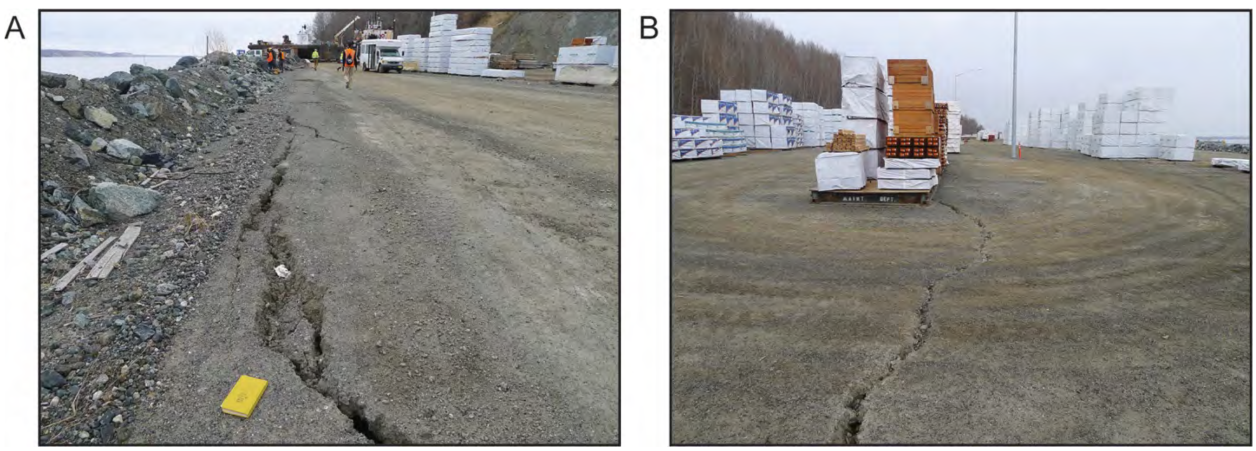

Figure B5. Tension cracks in fill at the North Expansion area of the Port of Alaska (Lat/Long: 61.253183, -149.880492). The cracks were observed during the Phase I investigation, however, no additional movement was observed in spring 2019. See figures 6-33 to 6-39 in the main body of the report.

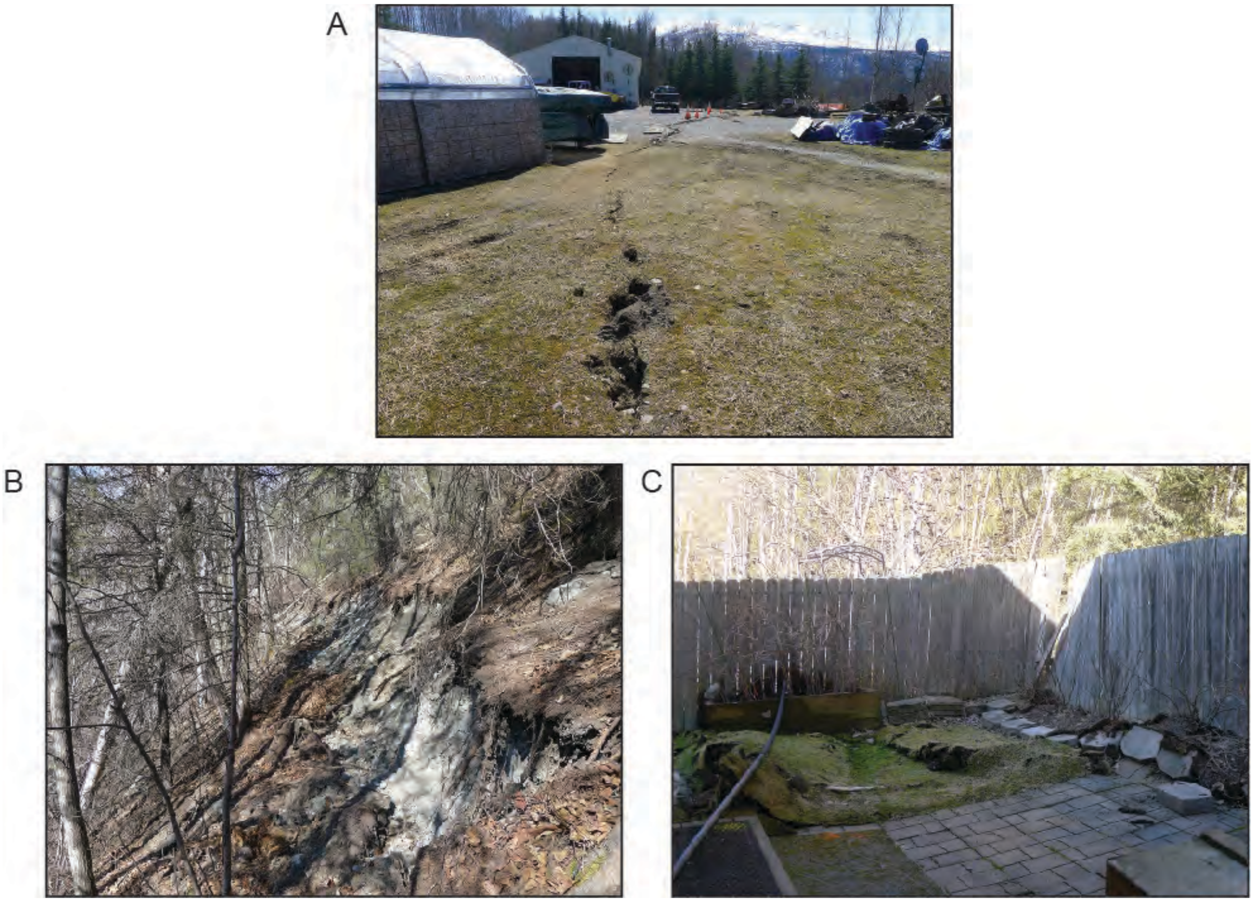

Figure B6. Photographs of the landslide above the Rivers Edge condominiums in Eagle River Lat/Long: 61.312065°, -149.570379°). Landslide features were observed during the Phase I investigation, however, no additional movement was observed in spring 2019. (A) Extensional cracks along the graded fill surface along the crest of the slope. (B) Landslide scarp along the base of the slope. (C) Buckled ground in the backyard of a Rivers Edge condominiums residence. See figure 5-31 in the body of the report.

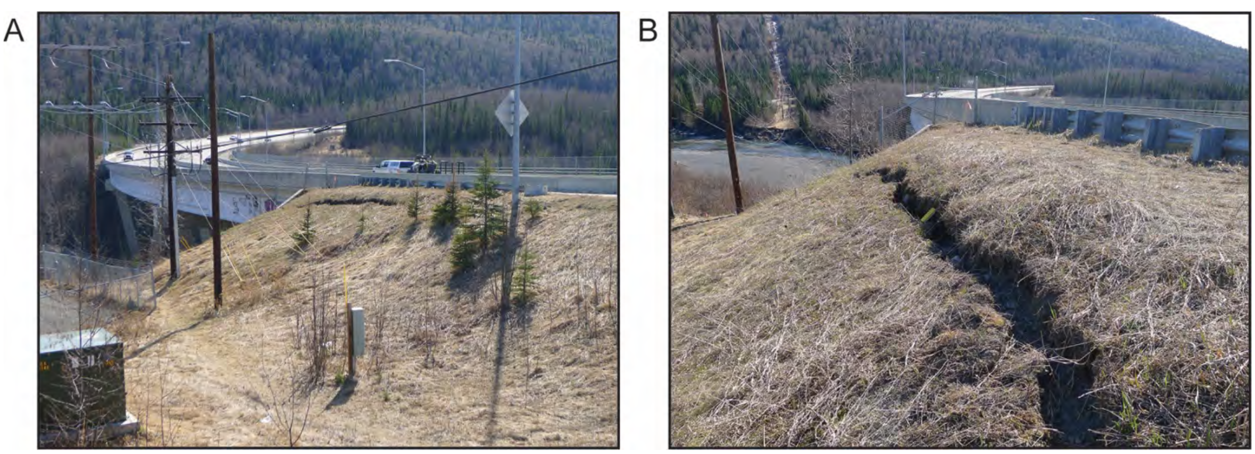

Figure B7. Settlement of fill along the north abutment of the Briggs Bridge in Eagle River (Lat/Long: 61.298906, -149.539131). Settlement cracks were observed during the Phase I investigation, however, no additional movement was observed in spring 2019. See figures 5-23 and 5-24 in the main body of the report.

A

B

Figure B8. Photographs of ground cracks and settlement in the south abutment of the northbound Glen Highway bridge in Eagle River (Lat/Long: 61.310222°, -149.577127°). Cracks in the abutment fill were observed during the Phase I investigation, however, no additional movement was observed in spring 2019. See Figure 5-18 in the main body of the report.

A

B

C

Figure B9. Photographs around the perimeter of the 2100 Minerva Road eastern apartment building showing ground settlement cracks (Lat/Long: 61.134367, -149.919633). The identical western apartment building was relatively undamaged.

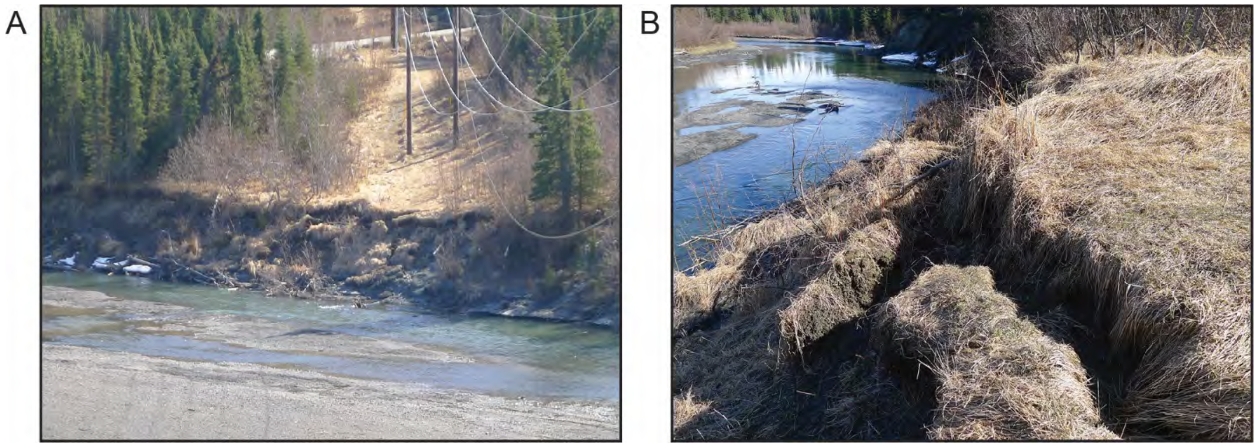

Figure B10. Photographs of a bank slump along Eagle River ~60 m east of the south abutment of Briggs Bridge (Lat/Long: 61.297339, -149.539022). Slump may have been caused by strong ground shaking during the November 30, 2018 earthquake but did not affect the adjacent power poles.

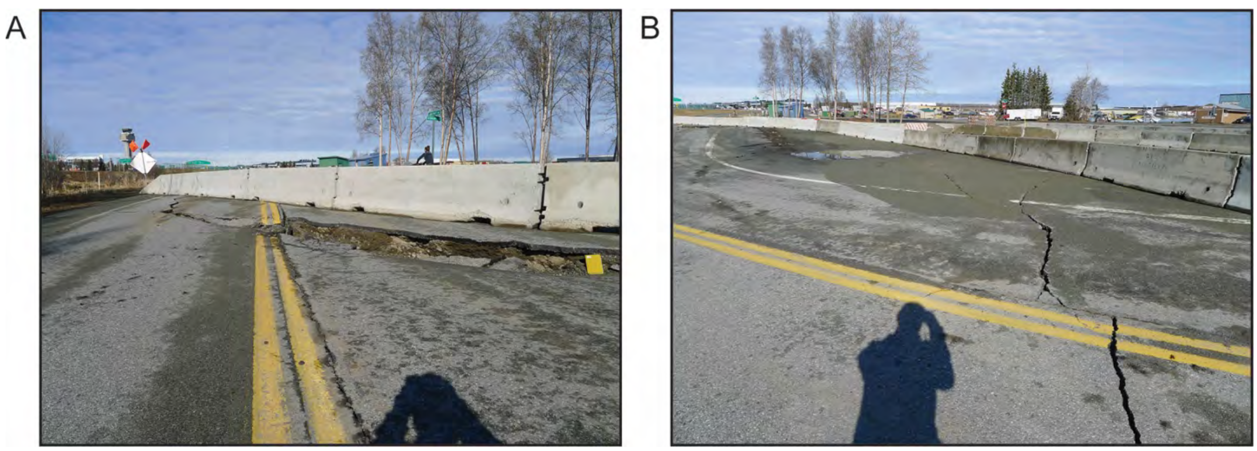

Figure B11. Photographs of ground settlement (A) and liquefaction (B) on Aircraft Drive near the Ted Stevens International airport adjacent to Rusts Flying Service (Lat/Long: 61.178331, -149.97205). Road repairs were still in progress during the GEER Phase II investigation.

Unmanned Aerial photography (Brigham Young University team)

The BYU team acquired aerial photography using a DJI Inspire 2, DJI Spark, and DJI Phantom 4 Pro drones at 5 sites (Table B1). Supplemental ground photographs were collected at each site using a D750 DSLR Nikon camera. The BYU team also acquired differential GPS ground control points to support the terrestrial lidar point cloud acquisitions and photomosaic models at the Eagle River highway bridge, Vine Road, and Rabbit Creek landslide. Additionally, the BYU team conducted site visits to strong ground motion station locations to acquire permission for the Phase II team to conduct the Multi-Spectral Analysis of Surface Waves (MASW) surveys.

Table B1. Sites surveyed by the BYU team

Site	Location
Rabbit Creek landslide	Lat/Long: 61.089°, -149.739°
Rivers Edge condominiums landslide	Lat/Long: 61.312065°, -149.570379°
Eagle River slump (possibly earthquake triggered)	Lat/Long: 61.297339, -149.539022
Vine Road	Lat/Long: 61.56863°, -149.60215°
Old Glen Highway, MSE wall	Lat/Long: 61.352243°, 149.542052°
Residential Settlement Damage	Lat/Long: 61.134291°, -149.919308°

Orthorectified photo models were produced for all sites imaged by the BYU team and are available at: https://www.designsafe-ci.org/data/browser/public/designsafe.storage.published//PRJ-2336/Phase2/Photogrammetry/BYU.

Unmanned aerial photography, hyperspectral imagery and mobile technology data (University of Missouri-Kansas City team)

The University of Missouri-Kansas City team collected UAV and hyperspectral data at seven sites (Site # A-G, Table B2). The location of these sites is shown on the Google map in Figure B12 and can be viewed at:
https://drive.google.com/open?id=1MOug_Vi3hTyT74XQt2873Fv7VXipzV2I&usp=sharing

Both UAV (drones) and mobile technologies were used during the reconnaissance. The emphasis was to use the mobile GPS based app to record the footprints of the sites and to image visible features at key waypoints.

UAVs used by the UMKC team include (Figure B13):

(1) DJI Inspire 2 RGB optical imaging drone. This drone has a native DJI FC6510 camera gimbled by the Zenmuse X4s system.

(2) DJI Matric M600 DJI Matric M600. This large drone was equipped with a hyperspectral camera that can produce real-time hyperspectral images (data cubes).

A smart app 'GPS-tracks' was used at all sites to record waypoint coordinates and timing records.

Table B2. Site #'s, dates/times, locations, and attributes for sites recorded by the UMKC team.

Site#	Date	Site location	GPS coordinates	Attributes
A	04/25/2019 PM	2100 Minerva	61.134457, -149.919852	Apartment complex
C	04/25/2019 PM 04/26/2019 AM	1271 W 82nd Ave	61.148112, -149.903273	Single family house
D1	04/26/2019 PM	Eagle river bridge	61.310331, -149.577228 (a close address number is 10103 Vfw Rd, Eagle River, AK)	The Frontage road old bridge [1].
B	04/27/2019AM	2200 Minerva Way	61.134734, -149.920927	Apartment complex
E	04/27/2019PM	Rabbit Reek Bluff	61.089390, -149.842500 (closest address number is 14460 Old Seward Hwy)	Bluff
F	04/28/2019AM	Vine road, Wasilla	61.567585, -149.601888 (closest address number is 6100 Shalestone Loop, Wasilla, AK 99623)	Highway
G	04/28/2019PM	Rivers Edge Condominium	61.311934, -149.571920 (one close address number is 16625 River Heights Loop Eagle River, AK 99577)	Condominium Community
D2	04/28/2019PM	Glenn Highway Bridges	61.309970, -149.579660	All three bridges (north-/southbound and front road bridges)

Note:

Three bridges cross Eagle River. Two new bridges completed in 2015 are called Glenn highway south/north bound bridges; and the old frontage bridge was constructed in 1981.[1] It is also referred to the Glenn Highway over Eagle River northbound. An overview of the three bridges and details on the construction phases can be viewed at the following links:

http://bridgereports.com/1000241

https://www.adn.com/alaska-news/anchorage/2019/08/07/work-begins-on-second-phase-of-glenn-highway-bridge-project-in-eagle-river/#_

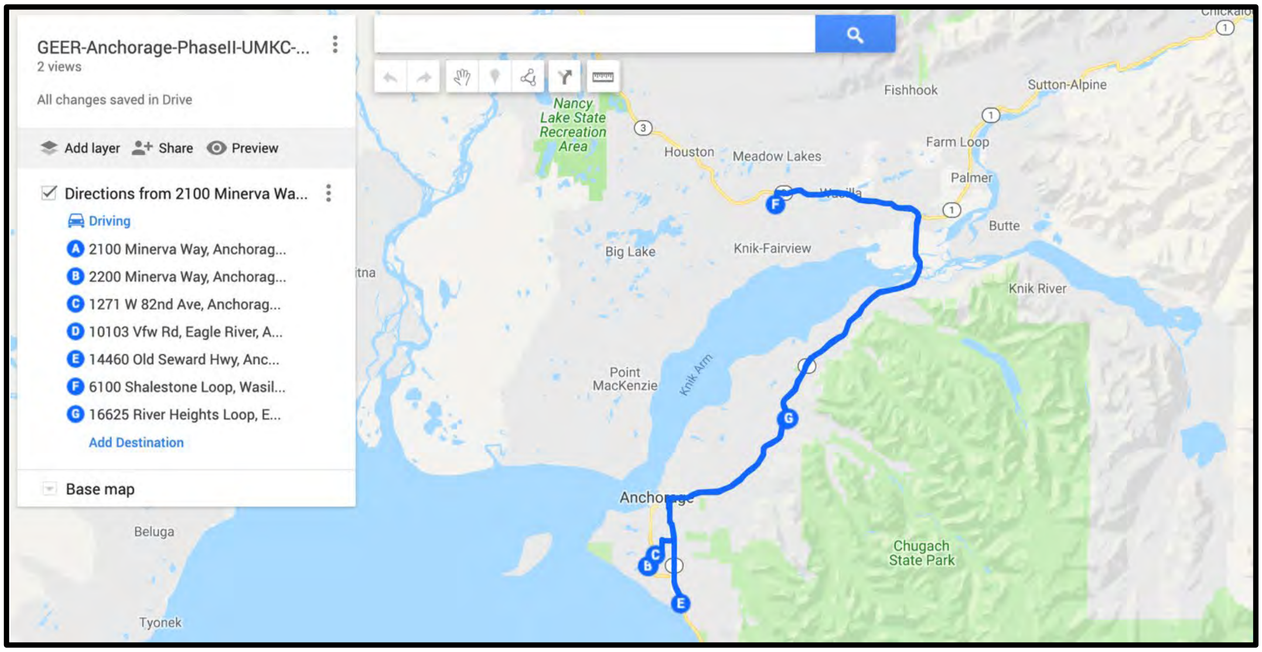

Figure B12. UMKC UAV team survey locations.

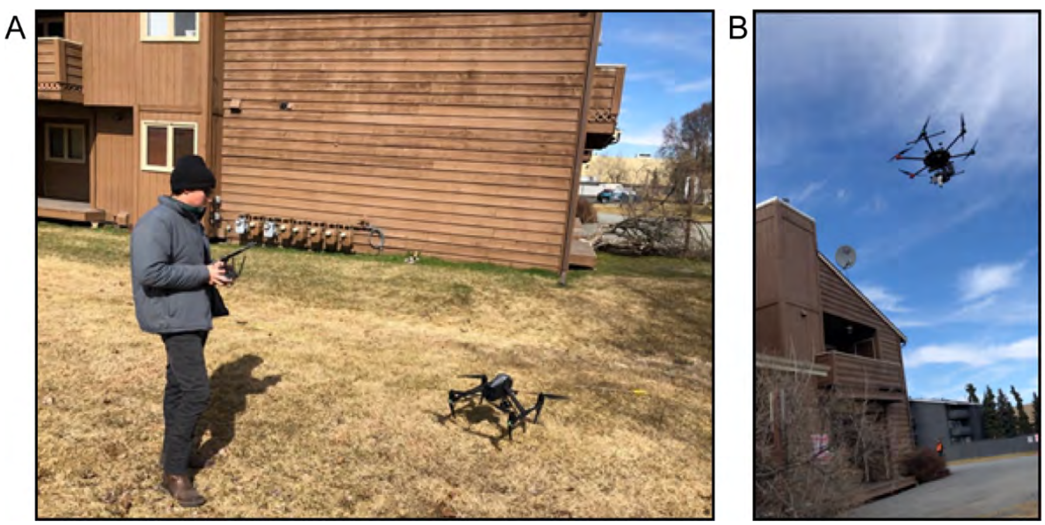

Figure B13. UAVs (drones) used in the reconnaissance in the field: (a) the DJI Inspire 2 and (b) DJI Matrice M600 (both operated by Mr. Shawn Herrington, who is a graduate student at UMKC and a licensed UAV pilot).

UMKC data collection

Data collected in the field includes three main components (Table B3):

(1) UAV images

a. Hyperspectral images
b. Georeferenced RGB images
c. Format: JPG; special hyperspectral cube format

(2) GPS tracks

a. GPS tracks were recorded, and ground photos were recorded at key locations.
b. Format: exported as Google Earth

(3) Ground photos with / without reference boards

a. At each site if smart phone taken, when available or needed, a reference board was used.
b. Format: JPG

Table B3. summarizes the types of UAV imagery and other data acquired by the UMKC team at each site.

Site#	Site	UAV images (RGB)	UAV images (Hyperspectral)	Ground photos	GPS tracks
A	2100 Minerva	x	x	x	x
C	1271 W 82nd Ave	x	x	x	x
D1	Eagle river bridge	x		x	x
B	2200 Minerva Way		x	x	x
E	Rabbit Reek Bluff	x	x	x	x
F	Vine road, Wasilla	x	x	x	x
G	Rivers Edge Condominiums			x	x
D2	Glenn Highway Bridges	x		x	x

Besides the imagery data, ground soil samples were collected at Site D (1271 W 82nd Ave) and Site E (Rabbit Creek Bluff). These soil samples are intended to be used to study the effectiveness of hyperspectral imaging in soil type and moisture detection.

UMKC Photogrammetric processing

UAV based georeferenced images can be used to develop 3D mapping products for all the visited sites. In the following, we brief the technical specification and steps for UAV image processing. It is noted that the hyperspectral imagery data is a data set that needs special programs to visualize and to conduct any photogrammetric or vision-based extraction. To this end, only research-grade codes are available, including advanced 4D spatial-spectral learning methods we are currently developing. Only sample illustrations are illustrated in this section.

Geotagged real-color (RGB) images from the UAV were the prime dataset acquired for creating (GIS-ready) photogrammetric products. These products can include:

1. Processed orthomosaic remote-sensing images by a computational 'stitching' approach, such as the Structure-from-Motion (SfM) method, from multiple, usually a large number of, overlapped images.
2. Digital point-cloud (DPC) data and digital surface models (DSM) for the ground, including terrain, buildings, vegetation, and other landscape features.

To generate these, the geolocated dataset needs to be ingested into a photogrammetric software application. To this date, there are a number of commercial, freely-available, or open-source packages for this purpose. Pix4D Mapper Pro, created by a Switzerland company, is one of the widely used ones [2] due to its advanced functionality and user-friendliness. This software is used in this project.

By using Pix4D Desktop Mapper Pro, the following steps are followed:

- Check the photo dataset for its integrity and positional accuracy based on the geolocation coordinated in the metadata of each image.
- Establish a desired coordinate system and units of measurement. In this case, all data are in UTM14N Meters, with elevations referenced to Ellipsoidial WGS84.
- Establish options for the processing quality, processing speed, data outputs, and other related parameters.
- Generate data outputs such as 3D models, Digital surface models, and orthomosaics. Different imagery data formats can be exported, including GeoTiff and GoogleEarth compatible files. Intermediate product quality reports are generated by the program automatically.

The resulting point clouds can be rendered by standard software such as Pix4D Mapper Pro for an even more photorealistic model. Area, linear, and volumetric measurements can be taken from the DSM. It is noted that the UAV images were captured without using either ground control or high-precision RTK. Therefore, survey-grade georeferencing is not pursued. In addition, for preliminary products, the low-resolution option was chosen for the computing speed and the chance of modifying parameters before spending very long computational times (if a regular desktop computer is used). As such, the global accuracy is 1 to 5 meters when the low-resolution option is used. Table B4 lists the basic products for a typical Pix4D based photogrammetric processing. These data correspond to the names of the subfolders that contain the data and data products. All photogrammetric modeling results and products from the seven sites (Table B2) are available at DesignSafe-CI at: https://www.designsafe-ci.org/data/browser/public/designsafe.storage.published//PRJ-2336/Phase2/LiDARPointClouds/UCSD.

[2] https://www.pix4d.com/product/pix4dmapper-photogrammetry-software

Table B4. Properties of photogrammetric products from Pix4D Mapper.

Imaging Location: 2100 Minerva Way, Anchorage, AK 99515		
Data (subfolder names)	**Format**	**Product Name**
RawPhotos	.JPG	Unprocessed photos
Orthomosaic	.TIF, .TFW, .PRJ .KML	Orthomosaic Geotiffs and supporting files
DSM	.TIF, .TFW, .PRJ	Digital Surface Models and supporting files
Pix4D_QualityReport	.PDF	Process Report
Jefforsonmapping.log	.TXT	Processing log

UMKC Data examples

The following representative data examples illustrate the primary photogrammetric products generated by the UNKC team.

UMKC Site A – 2100 Minerva Way

A total of 547 high-resolution Inspire2 images were collected with GPS tags, as shown in Figure B14A. When we planned the flight, a simple fly protocol was used. For the sidewalls, three flights were used in which the camera was tilted at various angles (-45, 0, and 45 degrees). For the roofs, three flights were conducted with a nadir view but at different heights (Figure B14B). These images were processed using Pix4D; for rapid processing speed, the low-resolution option was used. Figure B14C shows the obtained Orthomosaic (3D) map showing the backside of the apartment building complex. In Figure B14D, the east side-wall is shown. The ground cracking was identifiable from this 3D map, including the seismic related ground cracking (maximum width 2 inches); and the pavement cracking (maximum width is about 0.5 inch). Another interesting product was the 3D DSM (digital surface model), which shows the relative terrain elevation. This 3D volume model, as shown in Figure B14E, can be used to detect volumetric loss (e.g., ground sinking or partial structural collapse) when needed.

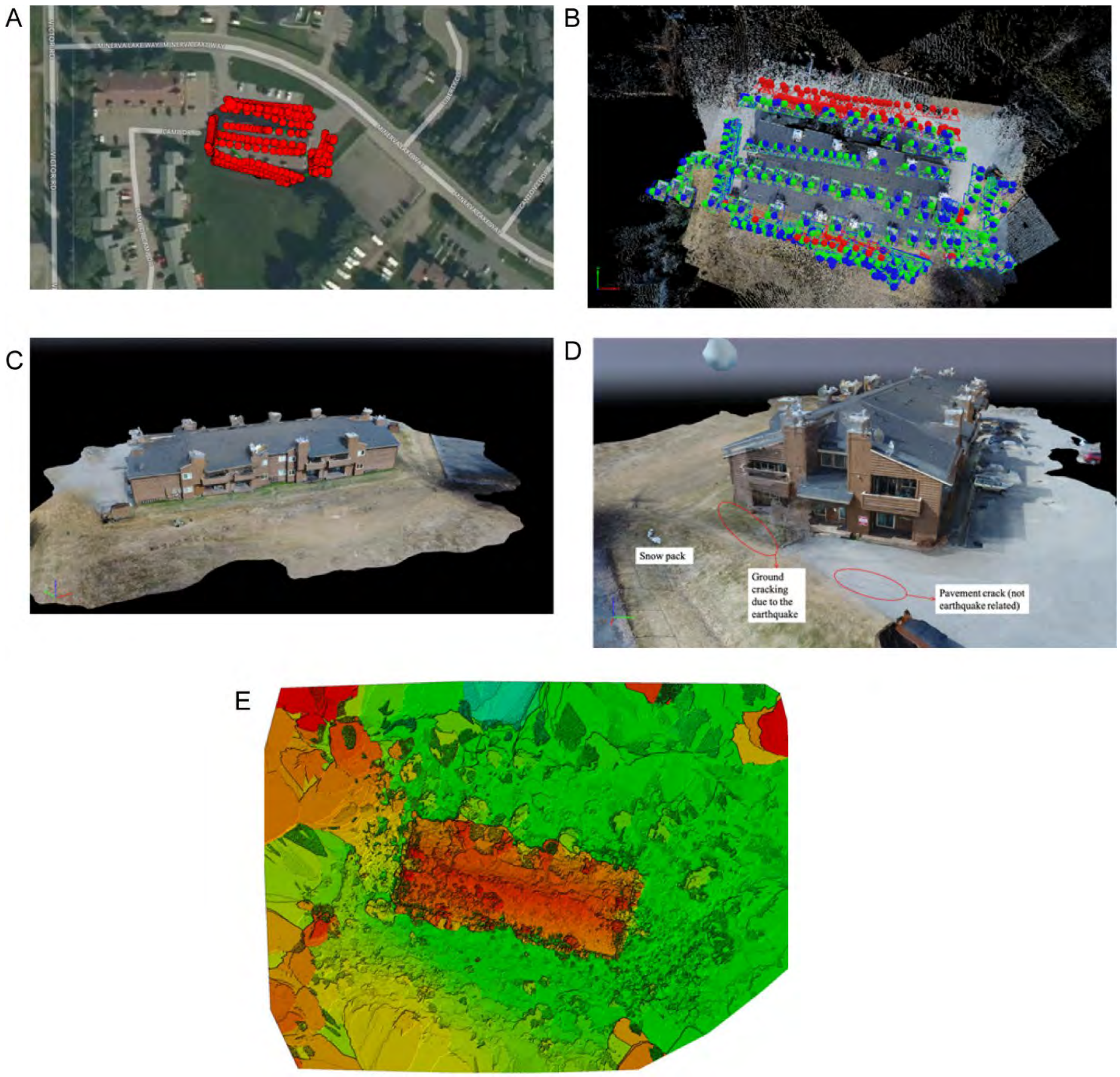

Figure B14. Inspire 2 flights and photogrammetric products from 2100 Minerva Way including (A) the fly paths; (B) the camera rays; (C) the 3D textured maps of the backside of the building; (D) the east side-wall of the building, and (E) 3D digital surface model.

UMKC Site C – 1271 W 82nd Ave.

The structure at this site is a single-family residential building. This building partially subsided due to foundation failure and/or liquefaction. When the UMKC team visited this site, a local contractor was working to lift the house at the foundation level using push piers (Figure B15A and B15B). Figure B16A shows the front view of the residential building from Google street view. DJI Inspire was used to fly around the house. When flying this single-family house, the goal was to create a 3D model (not a map) product for the structure, including the ditch and the positions of the piers. Due to the adjacent trees and other safety concerns, the focus was on the front and the front-top view of the building. Figures B16B and B16C show sample shots of the obtained 3D model allowing comparison with the Google street view and the reconstructed 3D scene.

Figure B15. Foundation lifting work at the residence. (A) push piers installed in place pending to lift the foundation, and (B) hydraulic driving.

Figure B16. (A) Google street view of the building before the earthquake, and Pix4D output 3D models, (B) the front side, and (C) the zoom-in of the south-west corner of the building.

UMKC Site D – Glenn Highway and Eagle River Bridges

At UMKC Site D, three bridges exist, including the Glenn Highway South and North-bound bridges and the old Eagle River Bridge. On 4/26/2019, the team visited the Eagle River bridge, and the temporary drone fly permit was not through based on the Airmap APP (which was lifted when the team revisited on April 28[3]). Therefore, only ground-based reconnaissance was conducted. A large number of ground photos were taken during this visit.

On 4/28, the UMKC drone flew over the three bridges mostly at an off-nadir view. 3D mapping products were created for the three bridges. Among the Eagle River bridge, the flight was mostly in parallel (north-south) to the bridge. Figure B17 provides a comparison of the Google Satellite view of the bridge and the 3D mapping of the bridge. Figure B18 similarly provides such comparison for the Glen highway north- and south-bound bridges. It is noted that the Google satellite image is dated to prior to the construction of the north-bound bridge. The flight was mostly operated within the corridor between the two bridges. Therefore, a high-density point cloud was achieved in this region.

A B

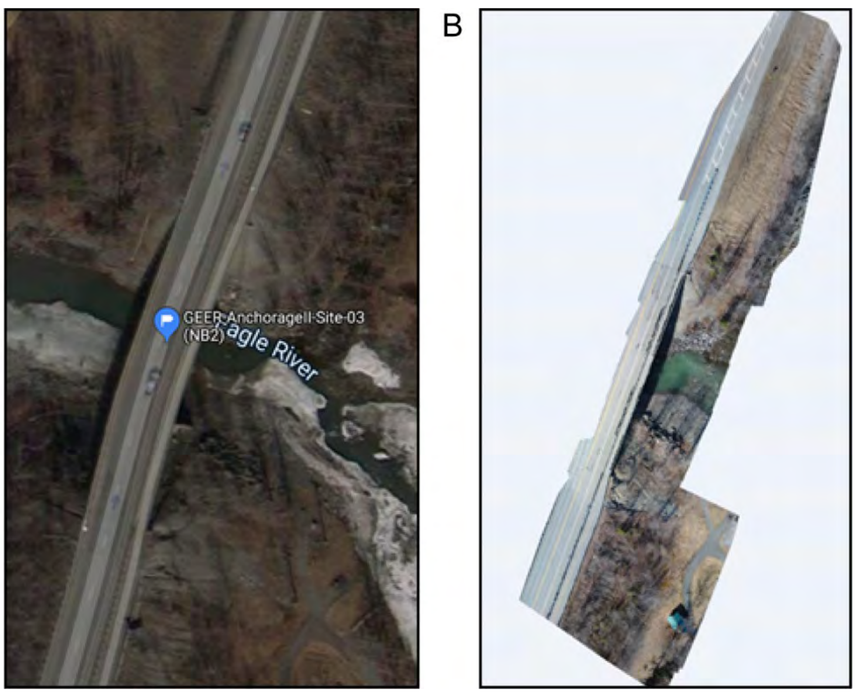

Figure B17. Eagle River bridge: (A) the satellite view (courtesy of Google Map), and (B) the reconstructed 3D map of the east side of the bridge.

[3] It was speculated that it was because the site was close to the perimeter of a Class D space; but in fact it was outside of the Class D space.

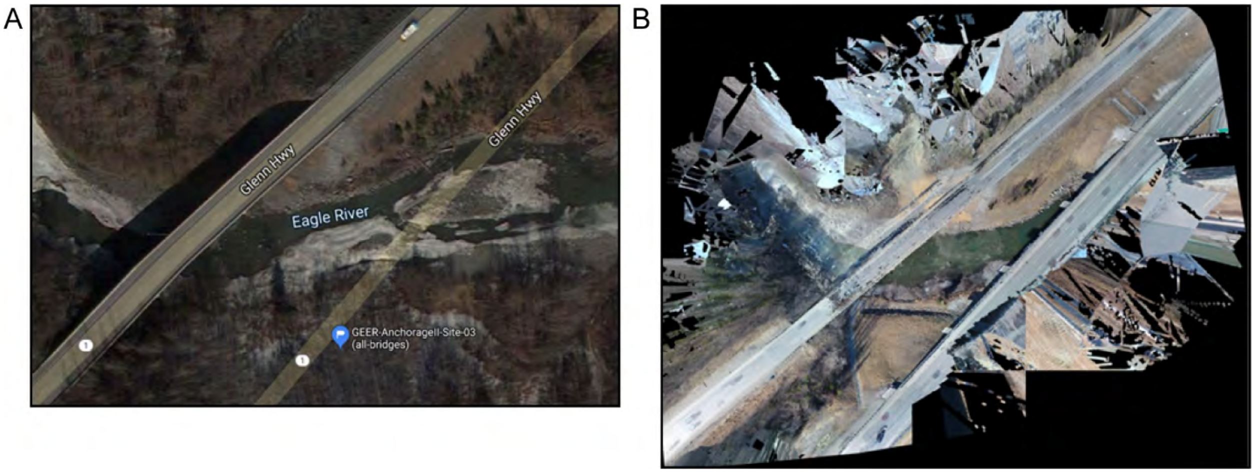

Figure B18. Glen highway bridges. (A) the satellite view (courtesy of Google map); and (B) the reconstructed 3D map.

UMKC Site E – Rabbit Reek Bluff

The Rabbit Reek Bluff was visited on 04/27/2019. Slope sliding was observed at this location. Field images in Figure B19 show that slope collapse, ground sink, and falling trees occurred during the earthquake. The UMKC team worked with others and flew along the bluff. A large number of images (1061 high-resolution 3000 x 4000 images) were collected and used in the reconstruction. The resulting Geotiff image is more than 800 MB. To view this Geotiff, an opensource GIS software (QGIS) was used to read the tile images, which can create a hierarchical structure for fast zoom-in and zoom-out (Figure B20).

Figure B19. Observed scenes at the Rabbit Creek Bluff showing collapsed slope, sunk holes (probably due to liquefaction), and falling trees.

Figure B20. Reconstructed scenes of the Rabbit Creek landslide at different zoom-in details including (A) the overall map (the background map is OpenStreetMap), (B) area near the top of the bluff, and (C) the edge of the woods along the bluff.

UMKC Site F - Vine road, Wasilla

The Vine road was visited on 4/28, considering that a segment of this road sunk after the earthquake. The UMKC team visited the site and identified that the road had been repaired. However, ground rupture and cracks were still spotted along the embankment of the highway (Figure B21), and along with the water puddles in the proximity of the road. With a focus on mapping the ground rupture along both sides of the road, two flight events were planned for the scenes separately along the two sides. Figure B22 shows the reconstruction of the west side and the east side of the road, respectively.

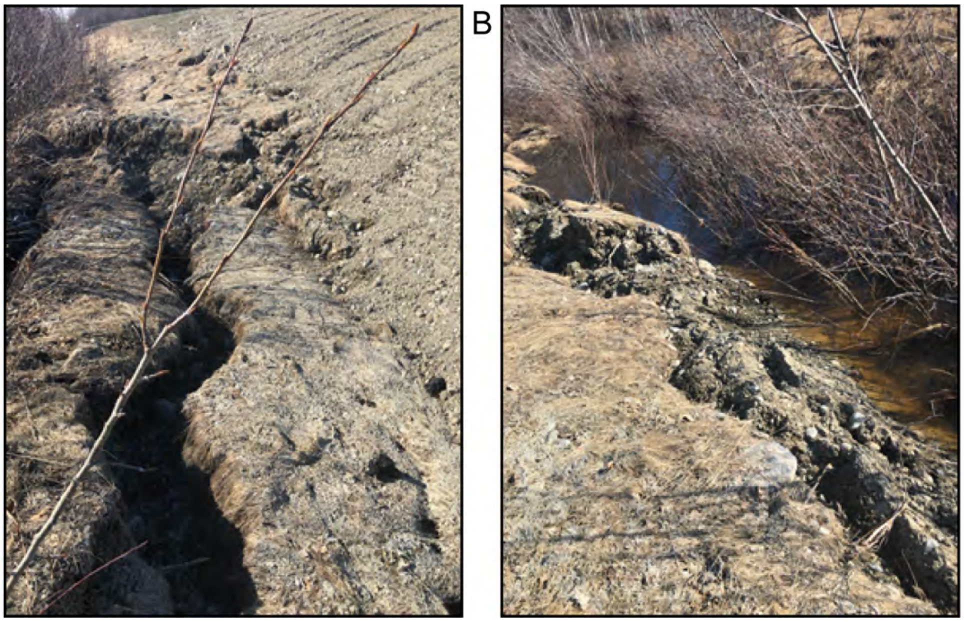

Figure B21. Embankment cracks along Vine road at both sides of the road. (A) cracks along the embankment; and (B) cracks along the water puddle that is near the road.

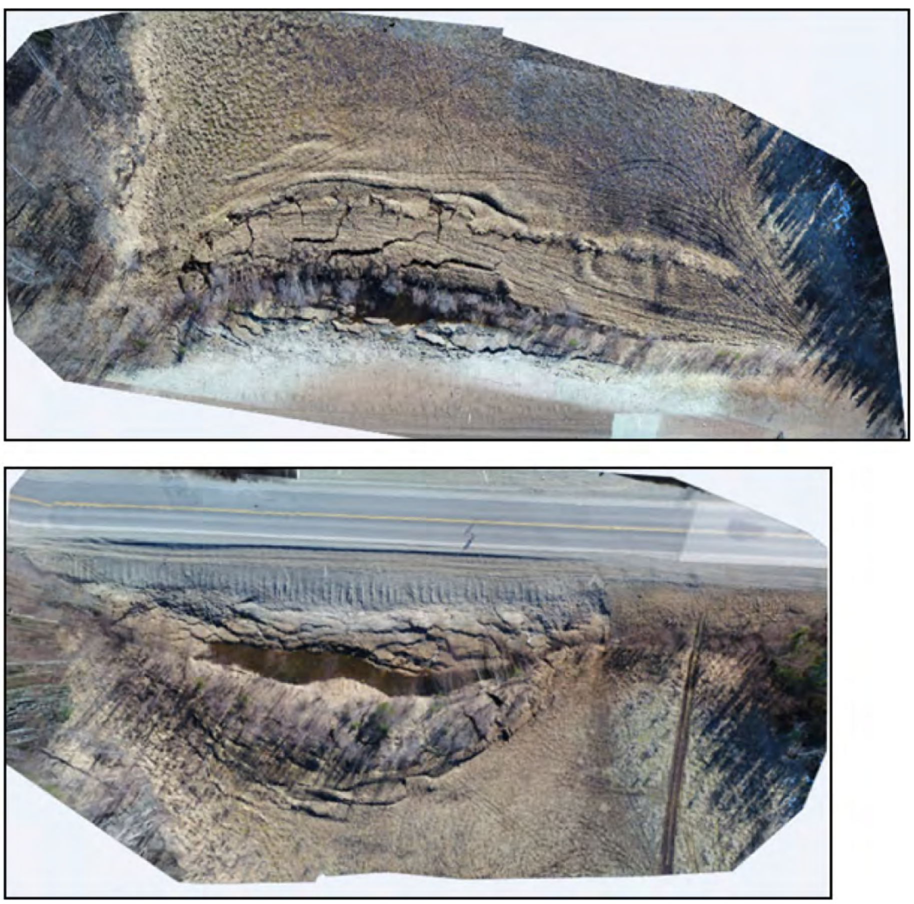

Figure B22. Photogrammetric reconstructions of the road-side failure at the Vine road. (A) east side, and (B) west side.

UMKC Site G - River's Edge Condominium

The UMKC team worked with other team members to visit the River’s Edge Condominium. Many residences at the foothill in this community suffered from ground shaking and settlement. Figure B24 shows a comparison of Google satellite view and the reconstructed 3D map of the north-east corner of the River’s Edge Condominiums.

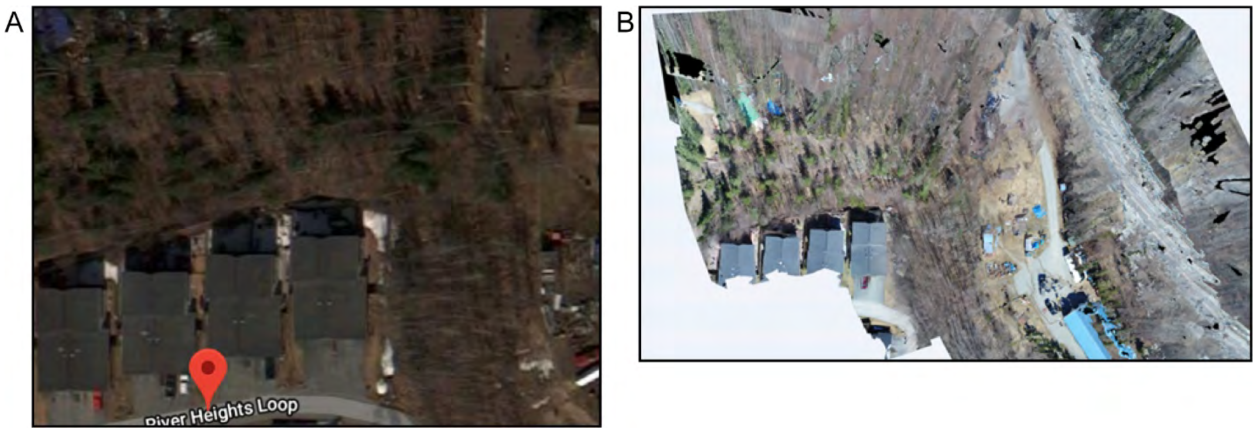

Figure B24. (A) Google satellite view, and (B) the reconstructed 3D view of the north-east corner of the River’s Edge Condominium.

UMKC concluding remarks

With the use of UAVs and mobile technologies, a large volume of imagery datasets were collected, and all data points (images) are geotagged. With the use of modern photogrammetric software (Pix4D), a variety of products were produced, including orthomosaic 3D maps and 3D models. For this report, all products were generated using a low-resolution option. Nonetheless, the products shown in this report signifies the tremendous value of using small UAVs (drones) for rapid site mapping and documentation. Essentially, the UAV imaging and photogrammetric processing are ad-hoc, rapid, and mostly meet the goal of rapid identification of structural damage, ground failure, and potentially quantitative anomaly assessment.

Some future efforts are suggested:

(1) It is necessary to model with the high-resolution option using Pix3D. With this, quantitative validation against LiDAR-based 3D modeling can be evaluated for different types of structural and geotechnical damage.
(2) It is interesting to conduct object-based recognition from these imagery products. One needs to discern that the algorithms should be developed based on UAV-based individual image sequences or based on the reconstructed 3D models.
(3) Optimized or autonomous flying may be further envisioned in future efforts. In the field, the fly protocols have been mostly determined empirically, lacking intelligent decision-making when the drone is in the air. This results in the observed model insufficiency as ‘holes’ due to the insufficient images collected.

Lidar point cloud datasets (University of California, San Diego team)

Lidar point cloud data were collected with a terrestrial lidar scanner from a total of seven earthquake damaged sites in the Anchorage area (UCSD Sites #1-7). All the point cloud data were collected using a Faro Focus 120 LiDAR scanner (40 million points collected for each scan). In addition, still images (taken using DSLR camera and mobile phone) were collected to supplement the LiDAR data. A description of the site location, characteristics, and a summary of the dataset collected at each site are provided below. Examples of the lidar point cloud images are shown in Figures B14-B20. The raw lidar point cloud data are available at: https://www.designsafe-ci.org/data/browser/public/designsafe.storage.published//PRJ-2336/Phase2/LiDARPointClouds/UCSD.

UCSD Site #1: 2100 & 2200 Minerva Way Condominium Buildings

Coordinates: 61.1346, -149.9198

Description: This site consists of a pair of two-story condominium buildings. The two buildings were constructed using similar structural type (wood framing with cripple walls) and are oriented only slightly differently (< 10 degrees). Building 2100 sustained severe structural damage (yellow tagged) as a result of liquefaction-induced differential ground settlement (See Figure B9), whereas Building 2200 remained functional following the earthquake (according to feedback from the residents).

Dataset: A total of **27 scans** were conducted to document the building exterior (all sides). Data were collected in two separate sessions:

– April 25 (2 – 5 pm): 12 scans for Building 2100 (severely damaged).

– April 27(1 – 3 pm): 15 scans for Building 2100 (severely damaged) and Building 2200 (functional).

Figure B25. LiDAR preview – 2100 Minerva Way Condominium Buildings.

UCSD Site #2: 1271 W 82nd Street Single Family House

Coordinates: 61.1481, -149.9031

Site description: This site represents a two-story single-family house. This structure was severely tilted due to ground settlement and/or liquefaction. The building foundation was exposed (with surrounding soil excavated) at the time of the survey.

Dataset: 8 scans were conducted on April 26 (11 am – 1 pm) to document the front and two sides of the building exterior (backside of building not scanned). Note that construction activities were underway (pile drilling with a crane) during the scanning.

Figure B26. LiDAR preview – 1271 W 82nd Street Single Family House (single scan).

UCSD Site #3: Glenn Highway Bridges across Eagle River

Coordinates: 61.3094, -149.5787

Site description: This site consists of three parallel multi-span highway bridges. Due to the site scale and time constraints, LiDAR scanning focused only on the Northbound bridge (the middle one and the longest span). Visible earthquake damage to this bridge involved surface cracks of abutment soil and (centimeter-level) bridge deck movement relative to the abutment walls.

Dataset: A total of 23 scans were conducted in three separate sessions to document the Northbound highway bridge (both super- and sub-structure).
– 12 scans were conducted on April 26 (4 – 6 pm), focusing on the north abutment and north bridge pier group.
– 5 scans conducted on April 28 (5 – 6 pm), focusing on the south and middle bridge pier groups.
–6 scans conducted on April 29 (11 am – 12 pm), focusing on the south abutment, in particular the surface cracks on the abutment soil.

Figure B27. LiDAR preview – northbound Glenn Highway Bridge (single scan).

UCSD Site #4: Rabbit Creek Bluff Landslide

Coordinates: 61.0895, -149.8431

Site description: This site consists of bluff landslide extending several kilometers along the coast line.

Dataset: 10 scans were conducted on April 27 (4:30 – 6:30 pm) to document a 100-meter long segment of the landslide site.

Figure B28. LiDAR preview – Rabbit Creek Bluff Landslide.

UCSD Site #5: Vine Rd, Wasilla

Coordinates: 61.5740, -149.6022

Site description: This site consists of road surface and embankment fill failure (~ 100 meter long). The road pavement was repaired and open to traffic and the time of the survey.

Dataset: 14 scans were conducted on April 27 (12 – 4 pm) to document the east slope of the road embankment.

Figure B29. LiDAR preview – Vine Rd east embankment (single scan).

UCSD Site #6: 9180 Ticia Cir Duplex

Coordinates: 61.1379, -149.9380

Site description: This site consists of a two-story duplex. This structure was severely tilted as a result of ground liquefaction. The garage doors were severely distorted. This building was unoccupied the time of the survey (according to feedback from nearby residents).

Dataset: 5 scans conducted on April 30 (10 – 11 am) to document the front and two sides of the building (back side of building not accessible).

Figure B30. LiDAR preview – 9180 Ticia Cir Duplex.

UCSD Site #7: Aircraft Drive (near Alaska Aviation Museum)

Coordinates: 61.1782, -149.9726

Site description: This site represents a segment of damaged road (~100m meter long). The observed damage involved uneven ground settlement and surface cracks. The damaged road was closed to traffic at the time of survey.

Dataset: 7 scans were conducted on April 30 (12 – 1:30 pm) to document the road damage and surface elevation profile.

Figure B31. LiDAR preview – Aircraft Drive (single scan).

Multi-spectral analysis of surface waves (MASW) (Georgia Tech team)

Multi-Spectral Analysis of Surface Waves (MASW) surveys were performed at a total of 12 sites throughout Anchorage. The approximate survey locations are shown on Figure B32. Details on the survey locations, array types used, and the observed PGA are provided in Table B5. The MASW survey locations were selected based on a combination of observed and/or measured site response at nearby seismic stations, coverage across the city, and knowledge of local conditions, as well as accessibility to the survey sites. Data acquired in the MASW surveys are available at: https://www.designsafe-ci.org/data/browser/public/designsafe.storage.published//PRJ-2403.

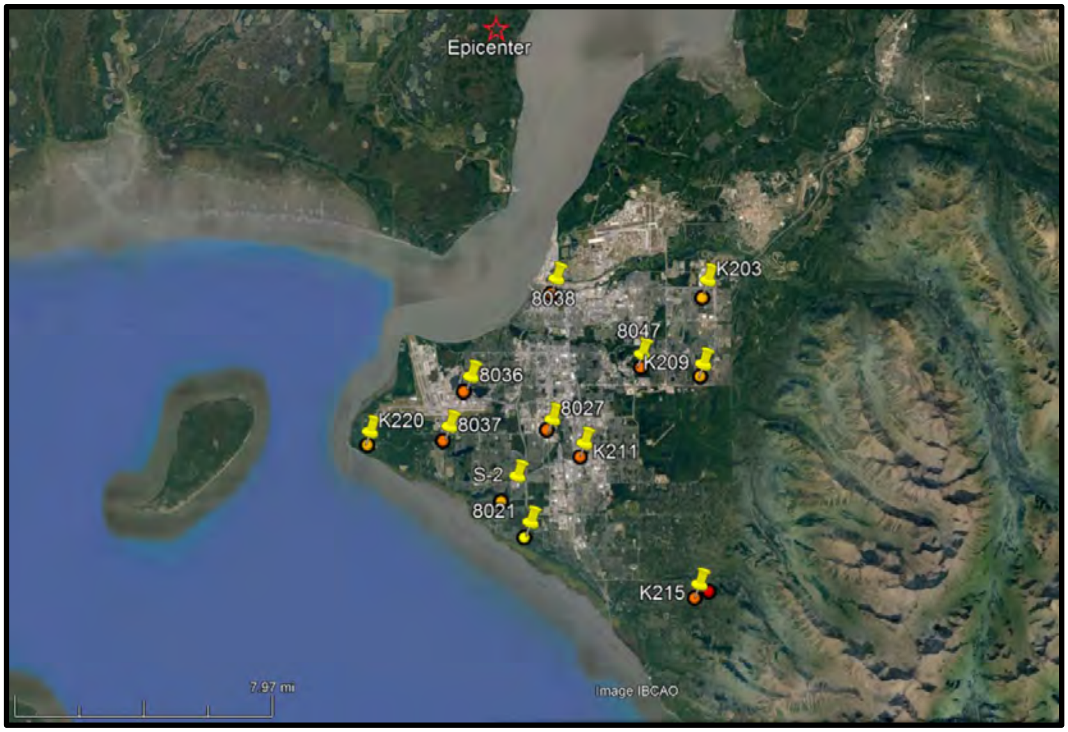

Figure B32. MASW survey locations (yellow pins) and existing seismic stations (colored circles). Earthquake epicenter shown by red star.

The MASW surveys were performed using a Geometrics Atom seismic system. Each Atom acquisition unit (AU) consists of a 2-Hz geophone and a self-contained, one-channel wireless data acquisition system that amplifies, digitizes and buffers the geophone output voltages. While the Atom is primarily a passive seismograph, it can also be used for data collection in active mode for enhanced near-surface seismic data collection.

For passive data collection, 23 Atom AUs were used in either a linear and/or a L-shaped array configuration (depending on availability of space to conduct the surveys). The AU spacing for passive linear arrays was 1.5 to 2.5 m, resulting in a total array length of 33 to 55 m. The spacing for passive L-shaped arrays was 3 to 4.5 m, resulting in a total array length of 33 to 49.5 m.

For active data collection, 23 Atom AUs were used in a linear array configuration, with a spacing of 1.5 m and total array length of 33 m. The first shot locations for the active surveys were at 5 and 10 m away from the nearest geophone, with shots taken at both ends of the array. A 12-lb sledgehammer was used as the energy source. A small square steel plate was used as a strike plate to for energy transfer between the hammer and ground.

In general PGA values at the sites range between a minimum of 0.123g and a maximum of 0.564 g (Table B5). Preliminary analyses of the MASW survey data was performed using the SeisImager software package by Geometrics. Only the passive survey data was used for the preliminary analyses for estimation of Vs30 and seismic site class, and the Vs30 estimates provided in Table B5 are subject to this limitation. Analysis of the data using both the active and passive survey data can provide a more rigorous estimate of the shear wave velocity profiles, especially in the upper 2 to 4 m where the active MASW survey data can provide greater accuracy and better resolution.

Table B5. Summary of MASW survey data including site name, GPS coordinates, PGA results and notes.

Location	GPS Coordinates	Passive Array	Active Array	PGA	Notes	Vs30*
K203	Lat. 61.221869° Long. -149.743655°	L-shaped 23 AUs 4.5 m spacing	Linear 23 AUs 1.5 m spacing	0.295 g	The survey was performed in Turpin Park approximately 250 m from the seismic station location due to site accessibility. A small wetland area was present to the east of the survey location.	211 m/s (Site Class D)
K211	Lat. 61.149049° Long. -149.857792°	L-shaped 23 AUs 3 m spacing	Linear 23 AUs 1.5 m spacing	0.463 g	The survey performed in the unpaved areas to the east and north of Fire Station #12.	331 m/s (Site Class D)
8038	Lat. 61.222460° Long. -149.884135°	Linear 23 AUs 1.5 m spacing & Linear 23 AUs 2.5 m spacing	Linear 23 AUs 1.5 m spacing	0.440 g	The survey was performed in grass area across the street from Comfort Inn – Ship Creek on the south side of the hotel, approximately 75 m from the seismic station.	213 m/s (Site Class D)
8036	Lat. 61.178651° Long. -149.963054°	Linear 23 AUs 1.5 m spacing & L-shaped 23 AUs 4.5 m spacing	Linear 23 AUs 1.5 m spacing	0.412 g	The survey was performed at the Alaska Department of Transportation - Central Region office approximately 175 m from the seismic station location due to site accessibility.	196 - 235 m/s (Site Class D)

Location	GPS Coordinates	Passive Array	Active Array	PGA	Notes	Vs30*
8037	Lat. 61.156356° Long. -149.982810°	Linear 23 AUs 1.5 m spacing & L-shaped 23 AUs 3 m spacing	Linear 23 AUs 1.5 m spacing	0.361 g	The survey was performed in grass area on the east side of the NOAA building.	261- 271 m/s (Site Class D)
8027	Lat. 61.159757° Long. -149.887566°	Linear 23 AUs 1.5 m spacing	Linear 23 AUs 1.5 m spacing	0.474 g	The survey was performed between the bicycle path and Alaska Department of Fish and Game Building at the intersection of Raspberry Road and C Street; the building was undergoing foundation repairs at the time of testing (Figure B33-B35).	274 m/s (Site Class D)
K220	Lat. 61.153843° Long. -150.056462°	Linear 23 AUs 1.5 m spacing	Linear 23 AUs 1.5 m spacing	0.326 g	The survey was performed along the gravel path west - southwest of the Kincaid Park Outdoor Center.	272 m/s (Site Class D)

Location	GPS Coordinates	Passive Array	Active Array	PGA	Notes	Vs30*
S-2	Lat. 61.134276° Long. -149.919790°	Linear 23 AUs 1.5 m spacing	Linear 23 AUs 1.5 m spacing	0.241 g	The survey was performed immediately south of the condo building located at 2100 Minerva Way approximately 850 m from nearest seismic station to the southwest; ground cracking was observed between the eastern exterior wall of the building and the tennis court to the east of the building (Figure B36).	210 m/s (Site Class D)
K215	Lat. 61.086060° Long. -149.751514°	Linear 23 AUs 1.5 m spacing & L-shaped 23 AUs 3 m spacing	Linear 23 AUs 1.5 m spacing	0.564 g	The survey was performed in the northeastern portion of Fire Station #10; there are wetlands to the east of the station.	415 - 436 m/s (Site Class C)
8021	Lat. 61.113722° Long. -149.907564°	Linear 23 AUs 1.5 m spacing	Linear 23 AUs 1.5 m spacing	0.123 g	The survey was performed on Anchorage Klatt Elementary School grounds; the school principal noted that the soils in this area are generally soft.	260 m/s (Site Class D)

Location	GPS Coordinates	Passive Array	Active Array	PGA	Notes	Vs30*
K209	Lat. 61.184446° Long. -149.747853°	Linear 23 AUs 1.5 m spacing & L-shaped 23 AUs 3 m spacing	Linear 23 AUs 1.5 m spacing	0.191 g	The survey was performed in grass area to the west of Scenic Park Bible Church building.	494 m/s (Site Class C)
8047	Lat. 61.188829° Long. -149.804662°	Linear 23 AUs 1.5 m spacing	Linear 23 AUs 1.5 m spacing	0.404 g	The survey was performed in the grass area in front of Alaska Pacific University, Carr-Gottstein Academic Center building; across the street from the USGS building where the seismic station is located.	459 m/s (Site Class C)

* Based on preliminary analysis using only the passive MASW data

Figure B33. Foundation repairs on the southwestern corner of the southern building wall.

Figure B34. Foundation repairs on the southeastern corner of the southern building wall.

Figure B35. Foundation repairs near the middle of the southern exterior building wall.

Figure B36. Ground cracking on the east side of apartment building at 2100 Minerva Way.

Summary

In summary, the GEER Phase II investigation focused on documenting perishable data that was preserved after the winter 2018/2019 snow season. Efforts to document these features in December 2018 was challenging due to active snowfall. Data collected during the Phase II investigation included ground photographs, aerial and hyperspectral imagery acquired by unmanned aerial vehicles (drones), point cloud data acquired by terrestrial lidar scanning, and near surface geophysical data acquired through Multi-Spectral Analysis of Surface Waves (MASW) surveys. In general, the majority of the sites visited exhibited similar characteristics as was observed during the Phase I investigation. Additional settlement or movement along slope failures that occurred during the November 30 earthquake were not observed. The acquired data provide high-resolution images of damaged structures and secondary earthquake effects. The shallow geophysics and hyperspectral images provide the opportunity for future research aimed at better understanding the effects of seismic shaking on the built environment and the effectiveness of hyperspectral imaging in remotely identifying soil characteristics, respectively.

All of the data collected during the Phase II investigation have been archived via NHERI DesignSafe repository to facilitate future research at: https://www.designsafe-ci.org/data/browser/public/designsafe.storage.published//PRJ-2336/Phase2.